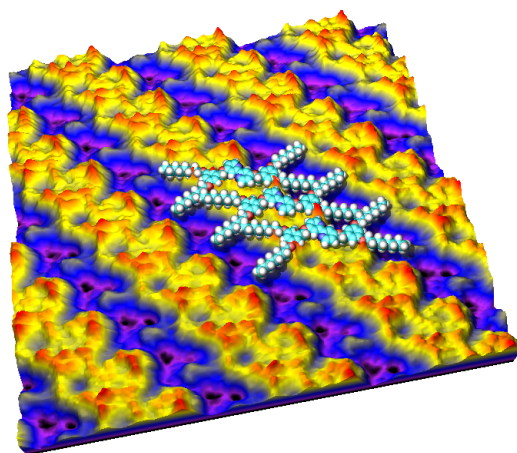


Chemistry at the Nanoscale: Molecular Assemblies probed by Scanning Tunnelling Microscopy



Inauguraldissertation
zur Erlangung der Würde eines Doktors der Philosophie
vorgelegt der
Philosophisch-Naturwissenschaftlichen Fakultät
der Universität Basel

Von
Leo Merz
aus Interlaken (BE)

Basel, 2004

Genehmigt von der Philosophisch-Naturwissenschaftlichen Fakultät auf
Antrag von:

Prof. Dr. E. Constable
Prof. Dr. H.-J. Güntherodt
Prof. Dr. B. Hermann

Basel, den 20. Januar 2004

Prof. Dr. M. Tanner, Dekan

ABSTRACT

The emerging nano-technology raises hopes for a technological revolution. Many manufactured goods can be redesigned to a better advantage, thanks to the access to the nanoscopic dimensions, granted by the scanning probe microscopes. Most molecular nano-technology products will have to rely on self-assembly. Basic research in supramolecular chemistry and nano-science, increases the knowledge of the underlying principles of self-assembly processes.

Several different “assembly motives” for the formation of two-dimensional molecular assemblies are studied in this thesis. Chemisorbed oligopyridine complexes for photovoltaics are studied as single molecules and as molecular layers. Chemisorption can build organised assemblies of molecules with repulsive interactions. For large molecules, the physisorption can become stronger than the chemisorption, if the molecules form only one chemical bond to the substrate. To demonstrate this effect, a fullerene-ligand with a free terpyridine is studied on platinum. Thanks to the strong physisorption, a submolecular resolution is achieved at room temperature in air.

As all molecular assemblies are made from unordered phases, the adsorbed molecules need a certain mobility on the surface, to assemble after adsorption. A short study of the mobility of a phthalocyanine derivative is presented as an example of the capability of STM to study dynamic structures. Single large dendrimers can be physisorbed on gold, interspersed in a chemisorbed monolayer of alkanethiols. The STM is used as a tool for to manipulate single molecules, a large porphyrin dendrimer is moved in a controlled manner with the STM tip.

Alkoxyated Fréchet-dendrons are investigated as a functional group that facilitates self-assembly in two dimensions of various molecules on graphite. Simple preparation from solution yields monolayers. Mainly two phases, lamellar and disk-like, are distinguished, but also patterns of different organisations are studied. At room temperature, in air, a conformational divergency of a bipy dendrimer is analysed with STM. Conformational analysis with the STM allows the investigation of non-periodic patterns in two-dimensions, and the observation of a change of conformation of adsorbed species. Two examples of conformational change of adsorbed species are presented: one, that occurs spontaneously, and one initiated by a treatment with gaseous HCl. A chiral structure, with a pseudo-periodicity with a unit cell of seven achiral molecules, is studied with submolecular resolution. The transition of this, disk-like structure into a highly symmetric lamellar structure is followed with STM. Finally, a short AFM characterisation of polymer vesicles on a mica surface to study their immobilisation properties, that might prove interesting for further applications, is presented.

TABLE OF CONTENTS

<i>Abstract</i>	i
<i>Abbreviations</i>	v
<i>1. Introduction</i>	1
1.1 Supramolecular chemistry	1
1.1.1 Dendrimers	2
1.1.2 Self-assembly	4
1.2 Scanning probe microscopy	6
1.2.1 History and a short overview of the variations of mi- croscopes	6
1.2.2 Aim of this thesis	9
<i>2. Methods and materials</i>	11
2.1 Sample preparation	11
2.1.1 Substrates	11
2.1.2 Dipping	13
2.1.3 “Solution casting”	14
2.2 Mode of operation of an STM	14
2.3 Data processing	17
2.3.1 Correlation averaging	18
2.3.2 3D molecular models and molecular orbital plots	19
2.4 Conformational analysis of adsorbed species	19
<i>3. Self-assembly by strong interactions (chemisorption)</i>	21
3.1 Ru-oligopyridine complexes	24
3.1.1 Results and discussion	26
3.2 C ₆₀ derivative with a free terpyridine	31
3.2.1 Results and discussion	31

4. Mobility and manipulation	35
4.1 Mobility of ZnPcOC ₈	36
4.1.1 Results and discussion	37
4.2 Manipulation of a single macromolecule	40
4.2.1 Results and discussion	42
5. Self-assembly by weak interactions (<i>physisorption</i>)	49
5.1 First generation bipy-dendrimer	51
5.1.1 Results and discussion	52
5.1.1.1 Domains and their internal structures – conformational analysis with STM	52
5.1.1.2 Defects	59
5.1.1.3 Protonation	63
5.2 Variations of the 2 nd generation Fréchet-dendrimer	64
5.2.1 Second generation bipy-dendrimer	66
5.2.1.1 Results and discussion	66
5.2.2 Second generation <i>S,S</i> -DDB-dendrimer	68
5.2.2.1 Results and discussion	68
5.2.3 Aldehyde of the second generation Fréchet-dendron	75
5.2.3.1 Results and discussion	76
5.2.4 Alcohol of the second generation Fréchet-dendron	85
5.2.4.1 Results and discussion	85
6. AFM visualisation of triblock-copolymer vesicles	89
6.0.4.2 Results and discussion	90
7. Conclusions and outlook	93
Appendix	97
A. Short list of other measured molecules	97
A.1 Artifacts and unresolved patterns	99
B. Measurements by collaborators	103
B.1 Oligopyridine complexes on platinum	103
C. List of publications	105
C.1 Papers	105
C.2 Posters	106

References 117

Acknowledgements 119

Abbreviations

2D	two-dimensional
3D	three-dimensional
Å	Ångström (10^{-10} m)
AFM	atomic force microscope
bipy	2,2'-bipyridine ¹
bipyterpy	4'-(2,2'-bipyridin-4-yl)-2,2':6',2''-terpyridine
CVC	critical vesicle concentration
DDB	1,4-bis(dimethylamino)-2,3-dimethoxybutane
ESR	electron spin resonance [spectrometry]
Fréchet-dendrimer	3,5-dihydroxybenzyl alcohol dendrimer
HDT	1-hexadecanethiol
HOMO	highest occupied molecular orbital(s)
HOPG	highly oriented pyrolytic graphite
HtBDC	hexa-di- <i>t</i> -butyl decacyclene
IETS	inelastic electron tunnelling spectroscopy
IUPAC	international union of pure and applied chemistry
LUMO	lowest unoccupied molecular orbital(s)
nm	nanometre (10^{-9} m)
NMR	nuclear magnetic resonance
NSC	nanostructured solar cell
pA	picoampère (10^{-12} A)
PAMAM	poly(amidoamine) [dendrimer]
Pc	phthalocyanine
PEO	poly(ethylene oxide)
PMOXA-PDMS- PMOXA	poly(2-methyloxazoline)-b-poly (dimethylsiloxane)-b-poly(2-methyl-oxazoline)
PVBA	4-trans-2-(pyrid-4-yl-vinyl) benzoic acid
room temperature	22 – 30°C
RT	see <i>room temperature</i>
sec	second(s)
SFM	scanning force microscope
STM	scanning tunnelling microscope
TBPP	tetra-[3,5 di- <i>t</i> -butylphenyl]porphyrin

terpy	2,2':6',2''-terpyridine ¹
terpy	4'-(4-Pyridyl)-2,2':6',2''-terpyridine
TΩ	teraohm ($10^{12}\Omega$)
TOF-MS	time of flight mass spectrometry
UHV	ultra high vacuum
ZnPcOC ₈	Zinc 2,3,9,10,16,17,23,24-octakis(octyloxy) phthalocyanine

¹ The old forms *bipy* and *terpy* are used for better readability throughout this thesis, instead of the modern *bpy* and *tpy*

1. INTRODUCTION

In the year 1990 D. Seebach published the seminal review: “Organic Synthesis – where next?” [1]. He concludes over 25 years of organic synthesis, analyses the current trends, and gives indications on which directions the organic synthesis could take in the future: organic synthesis is at a turning point. Chemistry has now a wonderful “basic vocabulary”, or as H. Primas is cited in [1]: “*Das molekulare Programm der Chemie ist erfolgreich abgeschlossen.*” Chemists achieved a very extensive knowledge of covalently formed molecules. With all this knowledge available, we are ready to advance to the next level of complexity, namely macro-molecules, secondary structures, intermolecular interactions, and biological systems.

1.1 Supramolecular chemistry

The term *supramolecular chemistry* was introduced by J.-M. Lehn¹ [2, 3] in 1978: “*Just as there is a field of molecular chemistry based on the covalent bond, there is a field of supramolecular chemistry, the chemistry of molecular assemblies and of the intermolecular bond.*” Supramolecular chemistry can be regarded as a generalisation of A. Werner’s² coordination chemistry presented 110 years ago [4], concerning the fact that he already studied and explained interactions between noncovalently bonded entities. J.-M. Lehn offers another explanation of the term by drawing a parallel between natural language and supramolecular chemistry [5]: “*... one might say that the atom, the molecule, the supermolecule would be the letter, the word and the sentence in the language of chemistry [...] the polymolecular, supramolecular entity would be the book.*” Following this analogy, this thesis is about type-setting

¹ J.-M. Lehn was awarded 1/3 of the Nobel prize in chemistry 1987 “for their [D. J. Cram, J.-M. Lehn and C. J. Pedersen] development and use of molecules with structure-specific interactions of high selectivity”.

² A. Werner was awarded the Nobel prize in chemistry 1913 “in recognition of his work on the linkage of atoms in molecules by which he has thrown new light on earlier investigations and opened up new fields of research especially in inorganic chemistry”.

and layout of books and high-gloss brochures. In the last decade, an increasing number of scientists have entered the field. Chemistry is one of the first natural sciences that dares to take the step towards larger systems and weaker interactions, where the objects and goals change from structures and properties towards systems and functions [5]. In biology, right now a similar course of redefining the whole field from 'research' to 'basic vocabulary' can be observed: larger systems and their interactions are being studied, e. g. in Basel, there is a new institute planned for *system biology*. Another beautiful example is P. R. Selvin's studies of the transformation from chemical, molecular energy (ATP) into mechanical, supramolecular energy. His group studies the molecular motors myosin V (moving on actin), kinesin, and dynasin, their movements and stepsizes at the level of single molecules [6].

As supramolecular chemistry is mostly concerned about function, dendrimers (see below) are often regarded as a topic of supramolecular chemistry. Strictly speaking, the synthesis of dendrimers is molecular chemistry, but what they are made for is usually supramolecular chemistry.

1.1.1 Dendrimers

One of the first steps in the direction of exactly controlled (low polydispersity) macromolecules was the "invention" of dendrimers. The three known polymer classes, *linear*, *branched*, and *cross-linked* were complemented with a fourth: *dendritic* polymers. Dendrimers are made of branched monomer-units that are repetitively linked to identical units around a central core, as sketched in figure 1.1. The IUPAC defines a *polymer* as "A substance composed of macromolecules" and *macromolecules (polymer molecules)* as "A molecule of high relative molecular mass, the structure of which essentially comprises the multiple repetition of units derived, actually or conceptually, from molecules of low relative molecular mass" [7]. Large dendrimers can be considered polymeric molecules, but a dendrimer is not per se a polymer. To synthesise a host macromolecule with a large cavity, E. Buhleier et al. (group of F. Vögtle) took up the theoretically known concept of dendrimer synthesis. They synthesised a hyperbranched polyamine ("cascade molecules") to study host-guest systems [8]. The term *dendrimer* (from greek *δενδρον* for tree and *μερος* for part) was introduced by D. Tomalia et al. in 1985 [9]. Two different concepts of dendrimer synthesis are known:

Divergent synthesis: the branched units are connected to the core, and each generation is added to the dendrimer. As the last step, the peripheral

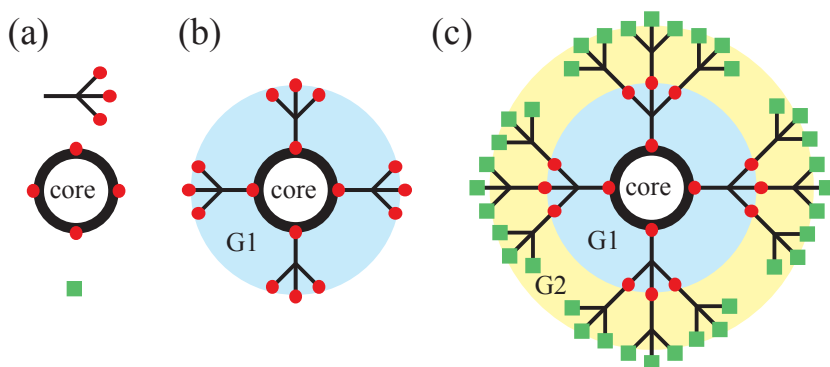


Figure 1.1: (a) Dendrimers are built from branched monomers, a core and peripheral units. (b) and (c) The branches are linked repetitively to a central core. The layers of monomers are called *generations*, denoted G1 (blue) and G2 (yellow). The peripheral groups can be functionalised (green squares).

groups may be functionalised. Divergent synthesis is the easier method, due to the usually smaller reactive parts, that also react faster. It is therefore the cheaper method to manufacture dendritic macromolecules, although with a relatively high polydispersity. Even very high generations can be obtained. D. Tomalia synthesised up to the 10th generation of a poly(amidoamine) (PAMAM) dendrimer. P.-G. de Gennes³ calculated the highest possible generations for PAMAM dendrimers. Between generation ten and eleven, the branches are packed so tightly, that it becomes impossible to attach another branch to each of them. Usually, the higher the generation, the more polydisperse the dendrimers become. And it is almost impossible to separate the reaction products from “incomplete” dendrimers, that are (still) missing a few branches, because the physical properties do not differ much.

Convergent synthesis: is the alternative synthesis strategy C. Hawker and J. Fréchet presented in 1990 [10]. In this approach, the dendrimer is synthesised from the peripheral units towards the core. First, the outermost branches are connected to the next branches, then these dendritic branches, or *dendrons*, are connected, and finally, they are attached to a core. In

³ P.-G. de Gennes was awarded the Nobel prize in chemistry 1991 “for discovering that methods developed for studying order phenomena in simple systems can be generalised to more complex forms of matter, in particular to liquid crystals and polymers”.

this way, the reaction products are always of two or three times the size of the educts and therefore easier to separate. Convergent synthesis yields dendrimers with very low polydispersity, but it is challenging to get higher generations. C. Hawker and J. Fréchet synthesised up to the 6th generation of their 3,5-dihydroxybenzyl-alcohol dendrimers, that are commonly called *Fréchet-dendrimers* [11].

Higher generation dendrimers have a very high surface-to-volume ratio. A closed shell of peripheral groups is held together by few inner branches. The density at the periphery is so high compared to the centre, that dendrimers can be used as containers. Dendrimers are studied and used as reaction containers [12], as catalyst carriers (at the core as well as at the surface) [13, 14], as biomimetics (e. g. models for globular, catalytic enzymes) [15], as drug carriers in diagnostics and therapy [16], containers for NMR contrast agents [17], as resists for scanning probe lithography [18], as fluorescent sensors [19], and the number of applications is still increasing. Another topic of supramolecular chemistry, which has been studied intensively in the last two decades in chemistry, physics, and biology, is self-assembly.

1.1.2 Self-assembly

The term *self-assembly* is overused, and not well defined. Scientists are fascinated by the local creation of order out of disorder without their direct interaction. A very broad spectrum of processes have been called self-assembly. Living matter in general relies on the concept of self-assembly as one of its main construction elements. Some scientists have attempted to define *self-assembly* and related terms in their fields:

T. Misteli distinguishes between *self-assembly* and *self-organisation* in biology [20]: “*Self-assembly is the physical association of molecules into a (thermodynamic) equilibrium structure, whereas self-organisation describes a set of components in a steady-state, dynamic structure.*”

G. Whitesides defines the term *self-assembly* in [21] as “*processes that involve pre-existing components (separate or distinct parts of a disordered structure), are reversible, and can be controlled by proper design of the components.*” He further distinguishes four variants: “*static self-assembly involves systems that are at global or local equilibrium and do not dissipate energy. [...] In dynamic self-assembly the interactions responsible for the formation of structures of patterns between components only occur if the*

system is dissipating energy. [...] In templated self-assembly interactions between the components and regular features in their environment determine the structures that form. [...] The characteristic of biological self-assembly is the variety and complexity of the functions that it produces.”

J.-M. Lehn wrote the following in [5]: “Self-assembly is the broader term. It can be taken to designate the evolution towards spatial confinement through spontaneous connection of a few/many components, resulting in the formation of discrete/extended entities at either the molecular, covalent or the supramolecular, non-covalent level. [...] Supramolecular self-assembly concerns the spontaneous association of either a few or many components resulting in the generation of either discrete oligomeric supermolecules of extended polymolecular assemblies such as molecular layers, films, membranes, etc. The formation of supermolecules results from the recognition-directed spontaneous association of a well-defined and limited number of molecular components under the intermolecular control of the non-covalent interactions that hold them together. The name tecton (from $\tau\epsilon\kappa\tau\omega\nu$: builder) has been proposed for designating the components that undergo self-assembly.”

In analogy to the term *crystal*, these terms are not crystal clear [22].

As there is no consensus for a clear distinction between ordered self-assembly and self-organisation, throughout this thesis the term *self-assembly* will be used as an expression including various forms of phenomena, describing molecular systems, that organise without further human intervention into regular layers. Dynamic and static forms of self-assembled layers shall be included, as well as those dominated by intermolecular interactions or molecule-substrate interactions. The term *self-organisation* will be used to emphasise the ordering of a self-assembled layer.

While the chemists were studying larger and larger molecules (what is *macro* to them), the physicists were approaching the neglected region of sizes from the other side. Electronics especially, with “Moore’s law” asking for smaller and smaller structures, pushed towards *nano*-technology. Amazingly, what is *nano* to the physicists is usually *macro* to the chemists. But both sciences are only recently approaching the regime of a few nanometres. Many fundamental research projects have used the term *molecular electronics* as a catching phrase. On one hand, many new insights and interesting visions were developed [23], but on the other hand some scientists were over-enthusiastic, as is often the case in new evolving fields. Some considerations about not reaching the market are described by R. Service in his article *Next-Generation Technology Hits an Early Midlife Crisis* [24].

The main access to the dimension of a few nanometres was granted by the invention of the scanning tunnelling microscope in the early 1980s.

1.2 Scanning probe microscopy

Scanning probe microscopy (SPM) is based on short range interactions between a sample and a sharp tip (sensor), which is scanned over the sample with sub-Å precision by use of piezoelectric actuators. Scanning tunnelling microscopy (STM) makes use of the quantum mechanical phenomenon of electron tunnelling, a current that flows between two electrodes at distances below a nanometre. The tunnelling effect has been known since the 1930s, but the experimental observation has been achieved much later (for an overview see [25]). The whole field of scanning probe microscopy relies on piezoelectric materials (commonly called piezos). Piezos allow sub-Å precise movements of the scanning tips. An electric field is applied to the material to cause a change in size (or vice versa), which is called piezoelectric effect. For further details, see section 2.2.

1.2.1 History and a short overview of the variations of microscopes

Many different short-range interactions can be used to build a scanning probe microscope, for instance electron tunnelling (STM), electromagnetic fields of an optical near field (scanning near-field optical microscope SNOM), different kinds of short-range forces (from magnetic forces to covalent bonds; SFM), and the electrochemical response in electrolyte (EC-STM).

STM The first of the scanning probe microscopes, the scanning tunnelling microscope, was invented by G. Binnig and H. Rohrer⁴ at the IBM research laboratories in Rüschlikon and first published in July 1982 [26, 27]. With the STM it was finally possible to answer questions about metal or semiconductor surface reconstructions, because it became suddenly possible to “look at” the surface in real space [28]. It was possible to study single atomic defects, non-equilibrium, and non-periodic structures without averaging over large areas and billions of atoms/molecules. The brilliance of this new microscope was soon recognised, and other groups started to build their own STMs. The group of H.-J. Güntherodt at the University of Basel started on April 26th

⁴ G. Binnig and H. Rohrer were awarded half of the Nobel prize in physics 1986 “for their design of the scanning tunnelling microscope”.

of 1982⁵. Early results about nano-lithography with the STM were soon published [29, 30].

It has been observed before, that with new microscopy techniques available, many scientific fields advance with big steps. The invention of the optical microscope set free entire fields of observations and knowledge. As examples, M. Leewenhoek's observations of all that is too small to be seen with the naked eye [31, 32] and L. Pasteur's entire work on microorganisms [33] are given.

Further uses of the STM The STM does not measure the “real topography”, but a surface of constant density of states near the Fermi level. This surface can correspond directly to the geometric surface. In other cases, e. g. with organic molecules on a metallic surface, it does often *not* correspond to the topography. For instance, benzene on on Pt(111) looks different, depending on the adsorption site [34, 35], and interestingly carbon atoms adsorbed on Ni(100) are imaged as depressions [36].

D. Eigler et al. used this peculiarity of the STM to image standing electron waves on a copper surface, confined by a corral of deposited iron atoms [37, 38]. Actually, the STM can do much more than image surfaces. Objects, namely molecules, that are located in the tunnelling gap between tip and surface can be characterised spectroscopically. Inelastic electron tunnelling spectroscopy (IETS) maps electronic properties in space and energy. The tip is fixed at a certain position above the sample, a voltage of interest is ramped, and the current is recorded. The first derivative of the current dI/dV is proportional to the density of states and the second derivative d^2I/dV^2 can directly map the electronic levels of an adsorbed molecule. B. Stipe, M. Rezaei, and W. Ho successfully resolved vibrational levels of the electronic spectra of single acetylene molecules [39]. X. Qiu, G. Nazin and W. Ho measured vibrationally resolved fluorescence from component parts of adsorbed molecules [40]. Other variations of STM-spectroscopy were developed, like the current-distance spectroscopy, that can give the barrier heights as a slope of the $I(z)$ curve [27]. W. Ho wrote a very good review about single molecule chemistry in 2002 [41]. An STM can be employed in various media. In ambient air, in UHV, under special atmospheres, at the solid-liquid interface, and at

⁵ After a talk by G. Binnig (Topic: “Vakuum Tunnel-Mikroskop”) on the evening of Friday 23rd, the decision to build such an instrument in Basel was made. The next Monday morning D. Holliger, H. R. Hidber and M. Ringger, started the construction of the first non-IBM STM!

the liquid-liquid interface⁶, but it is restricted to (electrically) conducting materials. Electrochemical STM (EC-STM) measures the electrochemical response of a sample at an electrolyte-metal interface.

AFM The scanning force microscope, often called atomic force microscope (AFM), was invented by G. Binnig, C. Quate, and Ch. Gerber in 1986 as a further family of scanning probe microscopes [44]. In AFM a tip mounted on a small cantilever spring is scanned across the sample. The forces acting on the tip bend the lever, whose movements are detected in many different ways. The first method to detect it, was an STM tip above the lever that recorded the changes in the distance between lever and tip and so the bending of the former. A breakthrough was achieved when G. Meyer and N. M. Amer invented the beam deflection technique for AFM [45], which uses the backside of the cantilever as mirror for a laser beam. The beam deflection amplifies the movements of the cantilever to dimensions that can be measured with a position sensitive photodiode. Today, beam deflection is used in most scanning force microscopes, whereas other methods like interferometry are in use in high-end research microscopes. Two standard modes of operation for AFM are known: (a) the *contact mode*, where the tip is in contact with the sample and measures repulsive forces, and (b) the *non-contact* or *dynamic mode*⁷, where the tip oscillates at high frequencies and attractive as well as repulsive forces can be measured. None of the many other existing modes shall be discussed here, but are well described in the literature [25]. In the dynamic mode, the cantilever is oscillated near its resonance frequency and forces that act on the tip are detected by a change of the frequency (or a phase shift). The AFM allows measurements of insulating samples, friction forces, or even the forces involved in forming and rupturing a single chemical bond [25].

SNOM and many other scanning probe microscopes were soon developed. To combine the advantages of optical microscopy (chemical sensitivity, tunable interaction energy, etc.) with the high resolution of a scanning probe, D. Pohl et al. developed the scanning near-field optical microscope SNOM [46]. In the same time, A. Lewis developed independently the similar technique called NSOM [47]. To circumvent the classical resolution limit of $\lambda/2$

⁶ Langmuir-Blodgett films on a liquid mercury droplet can be expanded/compressed easily [42] but other difficulties reduce the use of liquid mercury as substrate [43].

⁷ often referred to as *tapping mode* which is a registered name of Digital Instruments

in optical microscopy, an optical near-field is used. Two basic modes of operation are known. In the first one, an optical fibre is coated with an opaque medium, into which a hole of sub-wavelength diameter is opened. At this hole a non-propagating near-field is generated by illumination by a laser. The tip is brought into close proximity of a sample, so that the near-field and e. g. the adsorbed molecules of interest interact. This interaction can be detected in various ways, such as scattering, transmission, absorption, fluorescence, etc. In the second mode of operation, the sample is illuminated from below in a regime of total internal reflection, to generate an evanescent field on the sample, that can be picked up with a very sharp dielectric at the end of a fibre. For further details see [46, 25].

In general, every interaction that decays on a very short distance can be used and probed locally. Currently single molecule ESR and NMR are being developed on the base of scanning probes. Also many combinations of techniques are being created, like AFM-TOF-MS, to get a chemical sensitivity with a scanning probe. All these fascinating technologies shall not be discussed here any further, because they were not used for this thesis.

Not only the solid-gas interface is accessible with the various scanning probe microscopes, but also the solid-liquid interface, which is of vital importance for many biological investigations or electrochemical measurements. These amazing new developed tools were soon applied to the scientific field which has always been working at exactly this scale, but without the possibility of looking at single entities: chemistry. *“While femtosecond lasers have made it possible to study chemistry at the temporal limit, the STM provides an understanding of chemistry at the spatial limit”* (W. Ho in [41]).

1.2.2 Aim of this thesis

Standing between the fields described above: supramolecular chemistry, condensed matter physics, and nanoscience, this thesis attempts to get new insights into intermolecular interactions on surfaces. This shall be achieved by studying molecular assemblies of different self-organisation motives: assembly by strong interactions (e. g. chemisorption, chapter 3), assembly by weak interactions (e. g. physisorption, chapters 4, 5), organisation through embedding in heterogeneous molecular layers (chapter 4). Further information about self-assembly processes shall be found through studies of the mobility of molecules on a surface (chapter 4). Finally, chemical questions, such as conformational analysis of adsorbed species shall be addressed, together with the study of a delayed reorganisation phenomenon, accompanied

by a huge loss of entropy (chapter 5). Changes of the conformation of adsorbed species are detected by STM. The last chapter will present a short study of polymer vesicles on a surface.

2. METHODS AND MATERIALS

This chapter gives experimental details of the sample preparation, the measurements, and the data processing.

2.1 *Sample preparation*

This section explains the substrates and the preparation methods used in this thesis. Despite the well established preparation methods, the substrates had to be examined carefully before any molecular deposition, to assure a clean and suitable sample.

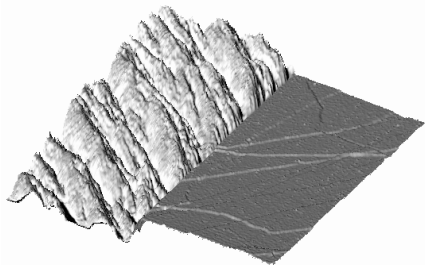
2.1.1 *Substrates*

Substrate in STM denotes the surface onto which the molecule of interest is placed, as opposed to *substrate* in (supramolecular) chemistry, which is the, usually smaller, molecule that is bound to the receptor and (eventually) processed.

For STM measurements, the substrates have to be conductive and atomically flat as well as clean. Measurements in ambient air demand additionally an inertness, that is only found in noble metals and e. g. graphite. Less noble metals like copper, are oxidised too fast, and can therefore only be used in UHV.

Platinum Pure, commercial platinum wire was rolled, polished, and annealed to give crystalline surfaces. The crystal faces seen in the STM images were previously correlated using x-ray diffraction [48]. Figure 2.1 shows a domain boundary between the two crystal faces that are dominantly found with this preparation: Pt(110) (the rough region) and Pt(100) (the flat region). Only the flat Pt(100) domains can be used to measure molecules on platinum. Even though platinum in air is covered with adsorbed species of almost everything that is found in air, a suitable molecule (preferably chemisorbed) can expel this layer of impurities.

Figure 2.1: A domain boundary between the rough Pt(110) (left) and the flat Pt(100) (right). The right domain is atomically flat (apart from monoatomic steps) over a large area. Parameters: room temperature in air. $U_{bias} = 100$ mV; $I_t = 1000$ pA; size = 393 nm \times 393 nm; z-scale ≈ 20 nm. For an definition of the parameters, see section 2.2



Graphite Commercially available, highly oriented pyrolytic graphite (HOPG) was used. The main advantage of HOPG is its easy preparation. A few layers are cleaved off with adhesive tape shortly before the measurements. This results in clean, atomically-flat terraces. HOPG is built from aromatic honeycombed layers. The layers are stacked in an ABA pattern: every second atom has a nearest neighbour in the layer below, and every other has one in the layer above. When the graphite is cleaved, the topmost layer shows two sorts of atoms: those with direct neighbours below, and those which “miss” their previous neighbours above. This is clearly visible in STM, only three atoms (out of a hexagon) are visible [49, 50, 51]. Therefore, the graphite surface has a *threefold* symmetry, not a six-fold as expected from a single layer. This often results in three symmetrical arrangements of domains of organic monolayers, as seen in [52, 53] or chapter 5. Graphite is the easiest substrate to handle, but the most dangerous in respect of artifacts and mis-interpretation of results. Quite often Moiré-patterns, such as those, shown in figure 2.2, are found. Various sizes were observed during the measurements of this thesis. Even Moiré-patterns with abrupt ends (with a very bright last row) were observed (see also [54] and appendix A.1).

Gold Pure gold was evaporated on cleaved, evacuated mica. Two different methods were employed. In one case, a glass plate was glued on top of the gold film and the gold-mica interface was cleaved prior to use. This allows the preparation of substrates in advance. In the second case, the gold film on mica was annealed, and the gold-air interface was used [55, 56]. Both preparation methods yield atomically flat terraces of different sizes.

Mica For the scanning force microscopy examinations, commercial mica sheets were used as substrate. Immediately before use, the mica was cleaved

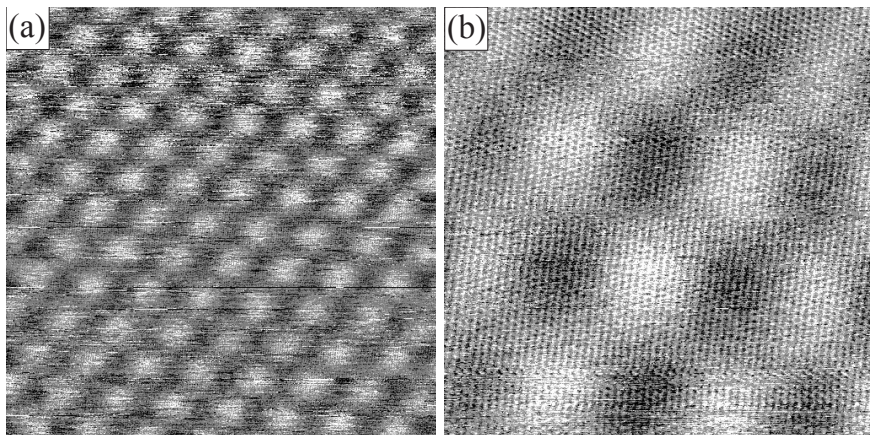


Figure 2.2: Two images of a large Moiré-pattern on graphite. The periodic pattern of the left image is resolved into brighter and darker atoms on a smaller scale (right).

(a) Parameters: $U_{bias} = -1700$ mV; $I_t = 5$ pA; size= 30 nm \times 30 nm; z-scale \approx 0.2 nm (b) Parameters: $U_{bias} = -533$ mV; $I_t = 30$ pA; size= 10 nm \times 10 nm; z-scale \approx 0.15 nm

with adhesive tape, similar to the graphite. This yields atomically-flat and clean surfaces.

Each measurement technique requires specific substrates and preparation methods. Two different methods of preparation were used in this thesis to get molecular assemblies on the substrates.

2.1.2 Dipping

A freshly prepared and characterised substrate is immersed into a dilute solution of the molecules for a definite time. The samples are (usually) rinsed with the solvent before use. This is a rather “thermodynamic” method of preparation, as the equilibrium structure on the surface is reached in most cases, due to the long deposition times. The surface coverage depends directly on the concentration of the used solution and has to be optimised for the desired coverage. This technique has the major advantage of direct control of most of the parameters, such as concentration, time, temperature, chemical composition of the solution. And it is probably the most “natural” way, as nature assembles most of its beautiful structures in or from water (biological membranes, crystals, ...). This technique has some drawbacks, for example, it is slow to optimise all parameters. Another drawback is, that

it takes larger amounts of molecules compared to the preparation described below. And the interaction between sample and substrate has to be much larger than the solvent-sample interaction (but still allowing solubility).

2.1.3 “Solution casting”

A dilute solution of the molecules is freshly prepared, one or a few droplets are placed onto the substrate, and the solvent is evaporated. This is more the “kinetic” way to prepare samples, because the equilibrium is only reached when its very fast, or the mobility on the “dry” surface is high enough to allow a rearrangement of the molecules. At first, it seems a dirty method with difficult reproduction. So, why solution casting? Self-assembly has the great advantage that it expels ambient impurities, that do not match the assembly motif. Another reason to use this technique, is the low amount of substance required to test a large range of concentrations. As a consequence of the gradual evaporation of the droplet, the concentration increases and a gradient of concentrations is formed on the surface. As the STM probes only a few hundred nanometres at a time, the concentration in one measurement is constant, but all the concentrations are accessible macroscopically. Some other advantages are, that it is really fast to prepare samples, that it requires very little substance, and that the molecules have the possibility to pre-assemble at the solid-liquid interface, as opposed to vapour phase deposition, where the molecules arrive “randomly collapsed”. It may be added, that it will make potential applications much cheaper in the production and protection, if they can be made from solutions in ambient air. The major drawback is, that it is difficult to control all parameters and to vary only one. Temperature, solvent, quality of the air (including its humidity), concentration, number of droplets, form of the evaporation and position of the STM tip in the gradient of concentration are not controllable as independent parameters.

2.2 *Mode of operation of an STM*

The main parts of an STM system are a sample, a tip on a piezo-actuator, electronics to apply a potential and to control the piezo-voltage by a feedback, and a computer to record the data. Figure 2.3 shows a schematic representation of these components. The necessary characteristics of the sample (S) are described above in the section 2.1. The tip (T) must meet

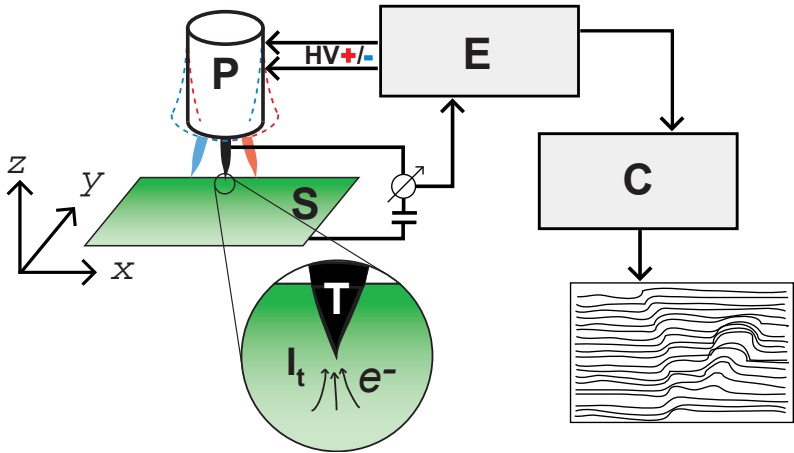


Figure 2.3: Scheme of the main parts of an STM: (S) sample, (T) metal tip (in the enlargement), (P) piezo-scanner, (E) electronics controlling the potential applied between sample and tip, the scanning movements (red and blue) and the feedback to control the z -position of the scanner, and (C) a computer to record and display the data.

some requirements. It has to be conducting, it should have as little electronic structure around the Fermi-level as possible, and it has to be atomically sharp. All the tips used in this thesis were made of mechanically cut platinum iridium wire (90%:10%). The shape of the tip is not that critical, because the tunnelling current I_t decays exponentially with the distance d between tip and sample:

$$I_t(U_{bias}) \propto U_{bias} * e^{-\frac{d}{\hbar} \sqrt{2m_e \phi}} \quad (2.1)$$

where U_{bias} is the voltage applied between the tip and the sample, m_e is the mass of the electron, ϕ is the tunnelling barrier, $\hbar = h/2\pi$, and h is Planck's constant¹ This involves two things. First, it enables atomic resolution, even with a relatively blunt tip, because the tunnelling current flows mainly through the atom at the very end of the tip and no long-range background noise is observed. Second, it becomes necessary to position the tip at sub-Å precision in the z -direction. This leads to the heart of every scanning

¹ Some approximations are made to get to this equation. For more exact descriptions, the interested reader should refer to [57, 58, 59].

probe microscope: the piezoelectric scanner (P). Piezoelectricity is a complicated phenomenon, that distorts a crystal when an electrical potential is applied and vice versa forms a potential when the crystal is distorted. Two of the best known examples of applications, that make use of piezoelectricity, are quartz-resonators as frequency generators (in watches and computers) and the lighters without flint (a spark is generated upon strong distortion of a piezo). For further details, see [60, 25]. In STM, the piezos are used as actuators to position the tip in close vicinity of the sample. A constant bias voltage is applied between the tip and the sample (see fig. 2.3) and the tip is scanned over the surface in x and y directions. Two basic modes of operation are known. The so-called *constant height*² mode, in which the tip is scanned at a fixed height above the surface and the variations in the current (resulting from changes in surface topography and/or electrical properties of the sample) are recorded. (b) In the so-called *constant current* mode, an electronic feedback loop (in E) controls the distance between the tip and the sample to keep the current constant. The output voltage of the feedback loop is recorded as the “topographical” data. All results presented in this thesis are recorded in the constant current mode. The measured current and the potential applied to the z -axis of the piezo are recorded by a computer (C) at discrete x and y positions of the scanner. The z -potential can be directly converted into distances in z -direction by a fine calibration. This is referred to as topography, even though many effects other than the real topography of the sample influence this measurement, such as electronic properties of the sample, properties of the surrounding tunnelling media (vacuum, air), etc. At nanoscopic dimensions, thermal drift and piezo-creep (resulting from hysteresis) can be a problem. Low temperature measurements can eliminate thermal drift. Whereas piezo-creep can be partially compensated by nonlinear calibration factors. Another crucial part for successful scanning probe measurements is a good vibration damping system. Commercial microscopes use air-damped tables, actively damped systems, bungy-cords, rubber pads, or combinations thereof. High-end devices usually have an eddy-current damping.

Conventionally, the *fast scanning direction*³ (along one scan line) is defined as x , the *slow scanning direction* as y , and the measured data as z (see fig. 2.3). These three dimensional images are usually represented as so-called *topview* images, two-dimensional x - y images with colour-coded z -values. By

² The constant height mode is often used in measurements at the solid liquid interface, in spin polarised tunnelling experiments or in video-STM, where the feedback would be too slow.

³ Feedback artifacts can only be seen along the fast scanning direction.

convention, bright colours are used to image elevations and darker colours refer to lower z . While the first STM images were recorded analogically and plotted line for line, today all measurements are recorded digitally. Digital processing of the data enables a better presentation of the recorded data in an appealing way⁴. In the constant current mode, usually (at least) two measurements are recorded simultaneously: the movements of the tip (topography) and the current (which would be constant with a perfect feedback mechanism). While the current can be regarded as “error-signal”, the “topography” contains much more information. It is the sum of various effects, ranging from “real” topography to differences in the electronic properties of tip and sample. Also the forces that act between tip and sample can influence the measurement or even change the tip and/or the sample. STM does not always show locations of atom centres, as is discussed e. g. in [61]. One of the advantages of STM is at the same time one of its difficulties: the so-called topography (which maps the position of the tip above the surface) is not a real topography of the sample, but always a mixture of topography and electronic structure. Measurements of adsorbed molecules always show characteristics of the molecular frontier orbitals and not the atom-centres (as shown in chapter 5, or [62]). That the STM maps a constant density of states, was also beautifully illustrated with the famous images by the group of D. Eigler, showing patterns of standing electron waves on a copper surface [38].

The STM and AFM measurements in this thesis were all measured either with a homebuilt low temperature STM, or a commercial Nanoscope III (Digital Instruments) equipped with a low-current converter, that is capable of measuring currents below 1 pA. This means, that only about 100 electrons were used per pixel of the resulting data.⁵

2.3 Data processing

Most data processing in this thesis was done with the program SXM-Shell, that was designed and written at the Institute for Physics of the University of Basel. Thanks to its open structure, it can easily be expanded by user-programmed functions and procedures. Some processing was done with

⁴ Early attempts of 3D representations were done by plotting on thick cardboard, cutting along the scan-line, stacking in the slow scanning direction and photographing from a bird-view perspective.

⁵ This is a rough estimation for $U_{bias} = 1$ V, $I_t = 1$ pA and a typical sample period of 16 μ sec.

the Nanoscope software (Digital Instruments), SPIP (Image Metrology) or WSxM (Nanotec Electronica). A few basic manipulations shall be explained here:

plane subtraction Usually STM images are tens of nanometres wide but only Ångströms high. This makes it necessary to tilt the data, so that the fine differences in z are visible in a colour-scale. A plane is fitted to the measurement and subtracted.

flatten It denotes a procedure which fits a polynom (of a chosen degree) to every scanline and subtracts it, to remove tilt and contortion. Most images presented in this thesis were flattened.

topview It is the 2D representation with a colour-coded z -dimension, often from black to white (“viewed from the top”).

colour STM images are three dimensional data with a scale of Volts (applied to the piezo). These are converted into nanometres, by use of a fine-calibration and often displayed in two dimensions. The third dimension is usually coded in colours. By convention dark colours (black) stand for low z -values and bright colours (white) represent high z -values, sometimes more fancy colourings are used to guide the reader.

pseudo 3D To further increase the “readability” of the STM images, a perspective view of a three dimensional representation is often used. These plots can additionally be coloured to enhance the impression of three dimensions. Often a colour-scale in z is used, similar to a topview representation. Sometimes a derivative or the error-signal from the scanning is used to mimic a light, shining from the side onto the surface.

linescan A cut along a straight line through the measurement is called a linescan. This can be along x , y or any mixture thereof and is displayed in a x - z plot.

2.3.1 Correlation averaging

An interactive correlation averaging procedure for the SXM-Shell was programmed by R. Hoffmann, and modified by L. Ramoino and L. Merz with a lot of help from R. Hofer. The procedure allows one to select a part of the image, that is then used as a reference. In a cross-correlation of the selection and the original image, the positions of the best fit are selected. In

all these positions, a sub-image with the size of the selection is cut. These sub-images are then averaged. Single locations (e. g. with scratches or noise) can be excluded manually from the averaging procedure.

2.3.2 3D molecular models and molecular orbital plots

The three dimensional models were generated by minimising the energy with a MM+ forcefield (using “Polak-Ribiere” and “steepest-descent” methods) in either HyperChem (Hypercube Inc.) or Chem3D (CambridgeSoft), carefully keeping the molecules in a flat conformation where needed. The molecular orbitals were calculated with HyperChem, using a semi-empirical PM3 method. Purple and green were used to distinguish positive and negative signs of the wavefunction. All models were either exported as two-dimensional bitmaps or as three-dimensional POV-Ray (copyrighted freeware, see www.povray.org) files.

These models were then placed on top of some depicted measurements using either Photoshop (Adobe) for topview images or POV-Ray for perspective three-dimensional images, to envisage the observed molecular ordering (see chapter 5).

2.4 Conformational analysis of adsorbed species

The analysis used in chapter 5 was done by a time-consuming, but reliable method. The measurements of interest were all printed at the same scale as topview images. Often, a single measurement had to be printed in different variations, like high-contrast images or with overlaid contour lines. Only pairs of images with opposed slow scanning direction, that were recorded in sequence and with the same parameters, were used. Then line-formulas of all conformers of interest were printed on transparencies. The formulas so obtained were used on both sides, if necessary. The molecules were tested systematically on the measurements, under the assumptions that the molecules do not overlap (at least not the aromatic parts, that form π - π bonds with the HOPG) and that the benzylic rings, or rather the position of the frontier orbitals, give the highest contrast. The alkyl-chains were nearly neglected in this procedure. They are assumed to lie interdigitating with the neighbouring molecules, in a conformation as straightened (all-*trans*) as possible. This remains an assumption, since the alkyl-chains were rarely resolved with the applied parameters. Nevertheless, the assumption was justified by the fact, that the distance between the molecules in the found

arrangements always had exactly the space to fit in an all-*trans* chain. Many arrangement that “jump to the eye” had to be excluded because of overlap with the neighbouring molecule (section 5.1). A few measurements were not well enough resolved to be assigned an arrangement. An alternative method was employed for some molecules, in which 3D-representations of the different conformations were placed in a 3D image of the measurement, using the program POV-Ray.

3. SELF-ASSEMBLY BY STRONG INTERACTIONS (CHEMISORPTION)

With the STM, physicists and nano-scientists are capable of imaging molecular layers at the single molecule level. This allows one to investigate “molecular electronics”, which could eventually replace the “classic” semiconductor-electronics. So far, the semiconductor industries were roughly able to follow “Moore’s law”, that the computational power is doubled and the price halved every couple of years. In the near future, the miniaturisation of semiconductor electronics will reach some fundamental limits of the construction, because it is based on solid-state bulk theories. Soon, the size of the structures is in a range, where quantum-mechanics rule. As soon as insulators start to be conducting, because of electron-tunnelling, the whole technique breaks down. Molecular electronics are expected to be one possible solution to the problem. A major advantage of this so-called *bottom-up approach* will be, that the parts of the system are expected to assemble themselves into the final structure – self-assembly is one of the studied phenomena, that have to be mastered before applications can be built. In this chapter several large molecules are investigated: oligopyridine complexes as well as a fullerene-ligand. Single molecules are compared to molecules in monolayers. Parts of this chapter have been published in [63, 64] and will be published in [65]. These studies were done in close collaboration with D. Ammann (measurements, Semesterarbeit [66]) in the laboratory of B. Hermann in the group of H.-J. Güntherodt; Y. Zimmermann (synthesis of the oligopyridines [64]) and E. Figgmeier (measurement of the electrochemistry [63]) in the group of E. Constable and C. Housecroft; D. Joester (synthesis) in the group of F. Diederich.

Up to now, a vast majority of the studies of molecular electronics and supramolecular assemblies were conducted with chemisorbed monolayers. Chemisorption is the easiest way to immobilise molecules at a certain position to image them. It is also the simplest way to contact them electrically. Most of these experiments were done with (alkane) thiols on crystalline gold

surfaces. In consequence, the knowledge about these layers, that are grown either from vapour phase or solution, is quite advanced ([67] and references therein). The chemisorption enthalpy E_{chem} for alkanethiols on gold (in UHV) is known to be 126 ± 2 kJ/mol. The corresponding physisorption energies E_{phys} , are

$$E_{phys}^{alkanethiol} = [6.08(\pm 0.74)n + 43.5(\pm 5)] \text{ kJ/mol}, \quad (3.1)$$

$$E_{phys}^{alkane} = [6.16(\pm 0.16)n + 19.4(\pm 1.4)] \text{ kJ/mol} \quad (3.2)$$

where n is the number of carbon atoms. Each CH_2 group in a linear chain, contributes therefore $E_{phys}^{\text{CH}_2} = 6.2 \pm 0.2$ kJ/mol (acc. to [67, 68]). Detailed studies were also conducted on Cu(100) and Pt(111). For further details see [67, 68, 69, 70]. All of the above values were measured in UHV. The physisorption and chemisorption energies will be the same in air or in contact with a solution. But the *difference in energy* between the adsorbed and the solvated state is less in solution or air than in vacuum. G. Poirier and E. Pylant could show, that linear alkanethiols form a lattice-gas on gold at low surface coverages. The molecules are lying flat on the surface, and have a high lateral mobility, as sketched in figure 3.1 (a). At higher coverages, the alkanethiols form stripes of flat-lying molecules, that are in equilibrium with a mobile gas-phase (b). With further increased coverage, the stripes form an equilibrium with upright standing domains (c), until, at the saturation density, all alkanethiols stand upright (with an angle of approximately 30° from the surface-normal) [69]. While all these details are known for alkanethiols, the studies of larger, more complicated molecules are still few.

For large molecules, which form only one chemical bond to the substrate, the physisorption energy can be larger than the chemisorption. For linear alkanethiols on gold, this happens at a chain length of about 14 CH_2 units. A rough sketch of chemisorption and physisorption potentials is shown in figure 3.2. When a molecule approaches the surface, it first physisorbs because the physisorption potential is lower for larger distances r . When the molecule approaches further, it chemisorbs if a covalent bond can be formed. Physisorption, which sums up all the weaker and long-ranged forces, such as van der Waals forces, is observed with all molecules. Chemisorption, on the other hand, depends on the possibility of a “chemical bond” (namely covalent) being formed.

Another application, which was a part of classic semiconductor physics and is now approached from the chemical side (bottom-up) is *photovoltaics*. M. Grätzel described photovoltaics as „*Photovoltaic devices are based on*

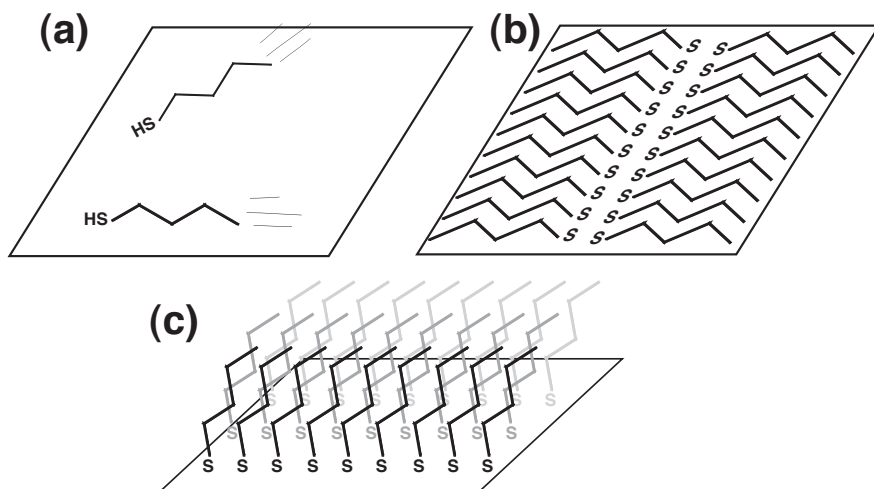


Figure 3.1: Scheme of the different adsorption modi of linear alkanethiols. (a) At low coverage, single molecules move rapidly in a molecular gas-phase on the surface. (b) With increased coverage, the flat-lying molecules form ordered domains of stripes. (c) At the saturation coverage the alkanethiols stand upright with an angle of approximately 30° from the surface normal. Adapted from [69].

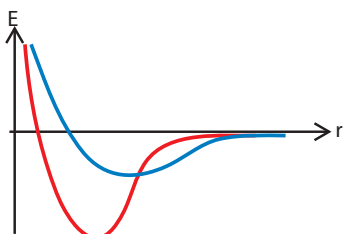


Figure 3.2: A qualitative sketch of a chemisorption (red) and a physisorption (blue) potential versus the distance from the surface (r) for small molecules. All molecules approaching the surface first physisorb, and then chemisorb.

the concept of charge separation at an interface of two materials of different conduction mechanism, normally between solid-state materials, either n- and p-type regions with electron and hole majority carriers in a single semiconductor material, hetero-junctions between different semiconductors, or semiconductor-metal (Schottky) junctions. [...] A breakthrough represented by the separation of the optical absorption and the charge separation processes in photo-electrochemistry, was realised by the association of a redox dye as light-absorbing material with the wide band gap semiconductor.” in [71]. One of the most prominent ways to achieve this separation of the optical absorption and the charge separation, is by use of oligopyridine complexes on surfaces.

3.1 Ru-oligopyridine complexes

Oligopyridines and their complexes have been known for a long time as dyes for various applications, ranging from textile colour to fluorescent marker groups in biological studies. The coordination chemistry of oligopyridines is well known; as chelates, they form very stable complexes. Because pyridine is a strong field ligand, it stabilises low oxidation states like Fe^{II} or Co^{II} . Their main applications are as dyes, in optoelectronics like light-harvesting¹, as building blocks for modular chemistry, or in metal ion directed assembly of complex architectures [72, 73]. Innumerable varieties of oligopyridine molecules are synthetically obtainable [74]. Currently, they receive much interest as candidates for molecular electronics, especially photovoltaics [75, 76, 77]. Already in 1979, S. Anderson et al. reported that a single-crystal n-type TiO_2 electrode can be chemically modified by attaching a monolayer of $[\text{Ru}(\text{bipy})_3]^{3+}$ to produce significant anodic photocurrents (when irradiated with visible light) in the absence of a supersensitiser [78]. This was one of the starting points for photo-electrochemical applications, such as the dye-sensitised nanocrystalline solar cells. For many electrochemical applications it is necessary to have a monolayer of molecules on an electrode surface. To study self-assembled monolayers of redox active species, several oligopyridine complexes were synthesised by Y. Zimmermann and studied electrochemically by E. Figgemeier [64, 63] (see also appendix B). Two mono-ruthenium complexes with different “anchors” (to the substrate) and one bimetallic complex were studied with STM in this thesis (see figure 3.3).

¹ light can move an electron from the metal to the ligand, and from there onto an electrode

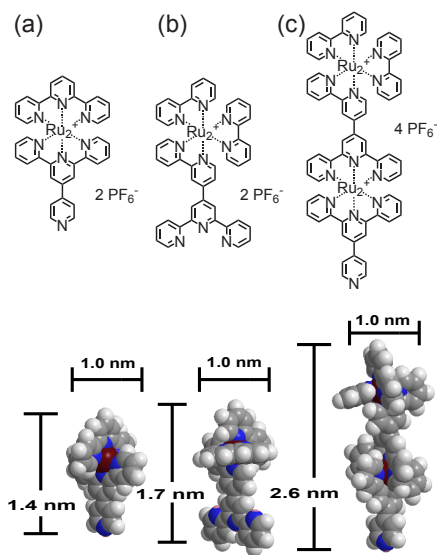


Figure 3.3: Formulae of the three studied ruthenium complexes. And space-filling representations with estimated sizes, see also footnote³. (a) Terpyridine complex with a free pyridine, (b) bipyridine complex with a free terpyridine, and (c) a bimetallic complex with a free pyridine.

These molecules are best adsorbed on platinum, because a strong bond to the substrate is expected to be formed between the nitrogen and the platinum [79, 80]. These complexes are the simplest version of redox active ruthenium oligo-pyridine complexes, which have an aromatic system, that can be chemisorbed directly onto an electrode. In detail, the mechanism is not well known, yet it is debated, if these molecules bind only with the nitrogen, if π -complexes are formed, if an α -dehydrogenation occurs², or if the molecules are even further degraded on the reactive platinum surface. A bipyridine (bipy) complex with a free terpyridine (terpy) (fig. 3.1(b)) to attach the molecule on the substrate, and a terpy-complex with a free pyridine group (a) as “anchor” were studied. As a preliminary study, also a bimetallic complex with a free bipy (c) was examined. Figure 3.3 shows also space-filling representations of the complexes with estimated dimensions³.

$[\text{Ru}(\text{bipy})_2(\text{bipyterpy})][\text{PF}_6]_2$: bipy-complex⁴ with a free terpy (b). As a precursor molecule for larger complexes, a (mono) ruthenium complex with

² as has been observed for pyridine itself [79, 80]

³ All “expected sizes” given in this thesis are measured in Chem3D after an energy minimisation with an MM2 forcefield.

⁴ For systematic names, see the list of abbreviations on page v.

a terpy “anchor” was studied on platinum. The free terpy offers a highly selective binding site, that can be easily attached to a suitable metal centre.

$[(\text{terpy})\text{Ru}(\text{terpy})][\text{PF}_6]_2$: terpy-complex with a free pyridine (a). The ruthenium terpy complex with a pyridine “anchor” was studied electrochemically on polished and etched Pt electrodes by E. Figgemeier (see also appendix B and [63]).

$[(\text{bipy})_2\text{Ru}(\text{bipyterpy})\text{Ru}(\text{terpy})][\text{PF}_6]_4$: “dimer” with a free pyridine (c). Using two redox-addressable metals, e. g. Ru/Ru or Ru/Os, the electrochemistry gets more interesting and the surface characterisation more difficult. More complex molecules (up to dendrimers) consisting of oligo-pyridine ruthenium/osmium complexes might find an application as light harvesting coatings, building blocks for molecular electronic, &c [74, 81].

Because a strong bond to the substrate is formed, the samples can be prepared by dipping the substrates in diluted solutions (2% acetone in water, see also the experimental section 2.1 on page 11). The molecules will replace adsorbed “dirt” and solvent molecules. With the right dilution and immersion time, it is possible to get sub-monolayer to monolayer coverages of the complexes on platinum surfaces.

3.1.1 Results and discussion

At concentrations of about 0.1 mM, immersion times between minutes and days were used to get different coverages. The bipy complex with a free terpy was imaged at a sub-monolayer coverage. Figure 3.4 shows an STM image of single complexes distributed randomly on a platinum surface and a single scan-line in a x-z view. The position of the line scan is indicated with a white line in the 2D image.

Individual molecules can be clearly distinguished and measured. The molecules are imaged with a width⁵ of about 0.85 nm (at $U_b = -90$ mV) and an apparent height of 0.19 nm. As explained in section 1.2.1 (page 7), the measured height does not correspond directly to the topographical height of the molecules, but rather to the difference in conductance between the molecule and the surrounding tunnelling media, which is ambient air in this case.

Terpyridine does not have the ideal geometry for adsorption on a flat surface. Nonetheless, the complex with a terpy “anchor” adsorbs and binds

⁵ All lateral molecular sizes in this thesis are measured as full width at half height.

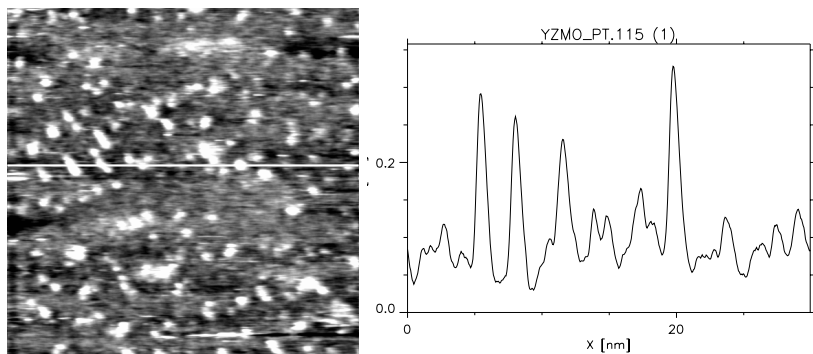


Figure 3.4: A lowpass filtered STM image of the bipy complex with a free terpyridine group as “anchor” to the platinum. One scan line (indicated in white) is shown on the right. Parameters: room temperature in air, $U_{bias} = -90$ mV; $I_t = 0.8$ pA; size= 30 nm \times 30 nm; z-scale \approx 0.4 nm.

strongly enough to be imaged by STM. Terpyridine was used, because it could be attached even more strongly to an STM tip, or bound specifically to other molecules in further studies. At the same time, this explains one of the experienced difficulties. The molecule, which is adsorbed to the surface, does also bind to the STM tip (which is a 90:10 Pt/Ir alloy) with at least an equal interaction energy, probably a higher one, because the curved geometry of a tip with its steps and edges is better adapted to the form of terpyridine. It is therefore very important to approach and scan very carefully, to prevent any contact with the molecular layer, in order to keep the tip clean.

A sub-monolayer coverage of the “dimer” complex (c) was imaged on platinum. In figure 3.5 a narrow stretch of flat Pt(100) between two domains of rough Pt(110) (compare the experimental section on page 11) is seen. On this flat part, single dimers can be seen.

The image also shows, why rough surfaces like Pt(110) cannot be used to study the molecules with STM. The molecules can be recognised, but no clear measurement is possible. The elongated form of the molecules is most probably caused by thermal drift, and not by the elongated form of the molecule. – There is no known reason, why the molecules should align on only one of three identical axes of the substrate. The size of single dimers was measured, with averages of 2.34 nm in diameter and 0.94 nm in height. In electrochemical measurements of monolayers, the dimeric complexes were found to take up a little more space than the monomers. This is attributed

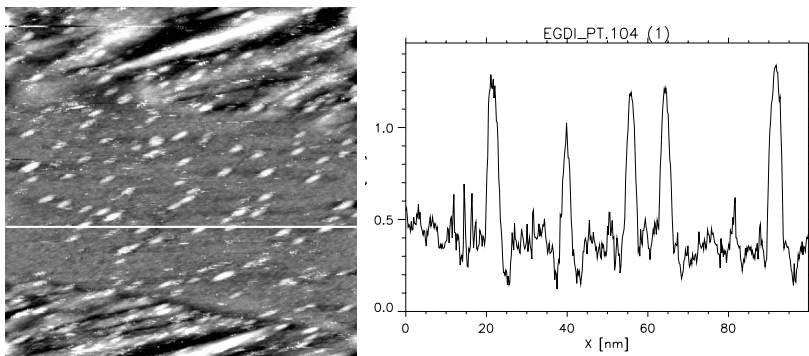


Figure 3.5: Single dimer-complexes on a flat stretch of Pt(100) between two domains of Pt(110). The image is filtered to reduce noise. The single scan line marked in white is shown on the right. Parameters: RT in air $U_{bias} = 1200$ mV; $I_t = 0.8$ pA; size = $100 \text{ nm} \times 100 \text{ nm}$; z-scale ≈ 4 nm, lowpass filtered.

to a complex standing upright but tilted from the surface normal [82].

A next step consisted of tuning the preparation parameters to get a complete monolayer coverage. Figure 3.6 shows two lowpass filtered images of a monolayer of the terpy complex with a pyridine “anchor” (a). The molecules seem only loosely packed. The lattice constant of about 2.9 nm is much larger than the estimated size of the molecule (compare figure 3.3) or the measured width of a single (bipy) complex (see above). The hexagonal arrangement was measured, and the surface coverage was calculated to be $\Gamma_{STM} = 2.2 \cdot 10^{-7} \text{ mol/m}^2$.

The electrochemical measurements conducted by E. Figgemeier showed a monolayer with strong repulsive forces between the terpy complexes, that form an arrangement with six nearest neighbours. The coverage Γ_{CV} , calculated from cyclic voltammetry is $2.5 \pm 0.2 \cdot 10^{-7} \text{ mol/m}^2$ [63]. A representative voltammogram is reproduced in appendix B on page 103. The two employed complementary methods, cyclic voltammetry and STM, give comparable results. Even though the preparation of the platinum surface/electrode is different, and the cyclic voltammetry averages over polycrystalline facets. In the near future, both, the STM and the electrodes will be adapted to allow an STM measurement of an electrode, for a direct comparison of the samples.

The observed shape of a molecule in the monolayer is round, and larger

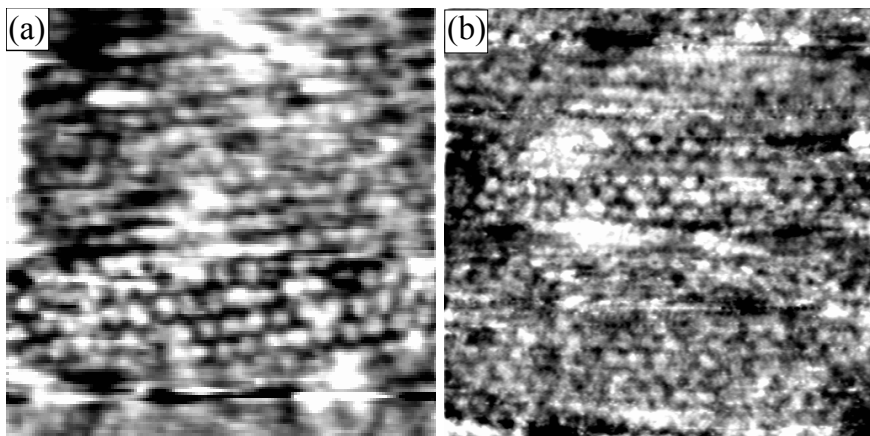


Figure 3.6: A monolayer of the terpy complex with a free pyridine. Each round protrusion is one molecule. Parameters: RT in air (a) $U_{bias} = 200$ mV; $I_t = 5$ pA; size= $80 \text{ nm} \times 80 \text{ nm}$; z -scale ≈ 0.8 nm; (b) $U_{bias} = 200$ mV; $I_t = 30$ pA; size= $60 \text{ nm} \times 60 \text{ nm}$; z -scale ≈ 0.6 nm; lowpass filtered.

than expected. This seems to be caused by a high flexibility and a rotational freedom of the molecule around the chemisorbed pyridine “anchor”. The molecules move faster around the pyridine than the scanning (time-) resolution – therefore the molecules appear “smeared out” over a circular area. A similar hindered mobility has been described for similar molecules (osmium bipy complexes) by J. Hudson and H. Abruña [83]. The regularity of the hexagonal array and the absence of a mobile phase suggest that this is in fact the tightest possible packing. Most molecular studies on surfaces have shown domains of close-packed molecules, and eventually, a mobile phase in two dimensions. It is therefore assumed, that this loose packing in a hexagonal array is the most dense monolayer possible, otherwise a denser packing together with a mobile phase should be observed at this surface coverage. This absence indicates that indeed strong repulsive forces between the molecules are present, as also found with the electrochemical studies. The equilibrium distance of 2.9 nm is very large for a monolayer, which has fixed lattice spaces for the molecules. If this low coverage would be a sub-monolayer coverage, the molecules would move around freely and would be imaged as gas in two dimensions, as described in section 4.1. The complexes themselves are positively charged, which explains a strong repulsion at long range. The counter-ions were not imaged. It is not clear, whether they give

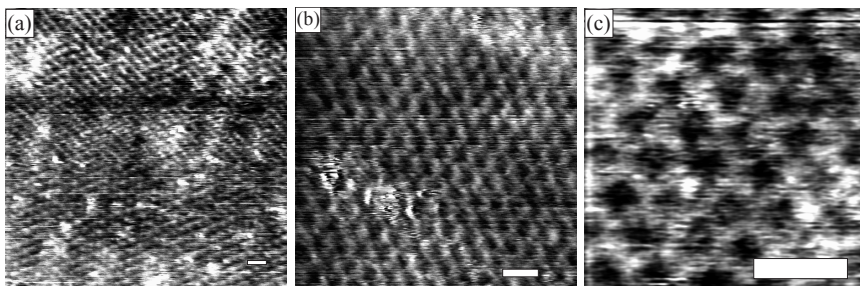


Figure 3.7: Partially decomposed complexes: when “hard” tunnelling parameters are applied for some time, the molecules appear broken. Periodic patterns, similar to benzene on Pt, could be seen for all measured oligopyridine complexes. The example shown, is the dimer at different scales: the scale bar is 1 nm in all three images. Parameters: RT in air (a) $U_{bias} = 50$ mV; $I_t = 500$ pA; size= 15 nm \times 15 nm; z -scale ≈ 0.6 nm; (b) $U_{bias} = 24$ mV; $I_t = 2140$ pA; size= 8 nm \times 8 nm; z -scale ≈ 0.5 nm; (c) $U_{bias} = -25$ mV; $I_t = 600$ pA; size= 3 nm \times 3 nm; z -scale ≈ 0.3 nm.

no contrast, they are too mobile, or they are not in contact with the surface. The loose packing can be explained to some extent with the charge of the molecules. Even if the counter-ions are closely associated with the complex (which is expected), they will take up some space on the surface. The packaging looks “loose” if only the complexes are seen, even though the counter-ions are interspersed. The calculations in [63] would describe this as strong repulsive force.

Decomposition of the molecules on the active platinum surface. When “hard” scanning parameters (e. g. a low tunnelling resistance) are applied for too long, the molecules form periodic patterns like those shown in figure 3.7. It is assumed, that these patterns are organic material similar to graphite-like carbon formations in catalyst-poisoning in heterogeneous catalysis. These measurements resemble the images by U. Hubler of pure benzene on platinum. However, it is not yet understood what exactly happens at the molecular level. The examination of these phenomena is beyond the range of this thesis.

3.2 C₆₀ derivative with a free terpyridine

Fullerenes were the first large molecules that were measured with STM in 1990 [84]. Submolecular resolution on Cu(100) was achieved one year later [85]. To freeze the very fast rotation of C₆₀ on gold, low temperature techniques had to be used, to obtain submolecular resolution [86]. C₆₀ is one of the most intensively studied molecules in the area of nanoscience (for an overview see [87] or [88]). Even today, fullerenes are still very much “en vogue” in the SPM community: mixed molecular layers [89], supramolecular assemblies [90], etc. are being measured.

Another way to immobilise C₆₀ on a surface or a metal tip, is to attach an “anchor” to the C₆₀, that chemisorbs onto the surface. Therefore, a C₆₀ fullerene attached to terpyridine with a ethylene oxide spacer (see figure 3.8) was synthesised by Y. Zimmermann [91, 92] and studied with STM. These “bucky-ligands” (for simplicity reasons called C₆₀-terpy) offer a coupled redox and photosystem, that could be used in light-harvesting devices, or as single electron shuttles (pendulum-like) in molecular electronics, etc.

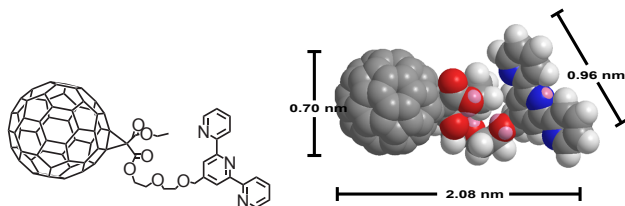


Figure 3.8: Formula and a space-filling representation of C₆₀-terpy with estimated sizes.

A droplet of a 1 mM solution of C₆₀-terpy in chloroform was placed on a freshly prepared platinum substrate and annealed for 40 h at 35°C in a solvent saturated atmosphere.

3.2.1 Results and discussion

Samples prepared as described above, were measured with STM at room temperature in air. This preparation yielded monolayers with a close-packed structure, as seen in figure 3.9. The lattice spacing was 2.07 nm which is almost exactly the estimated size for the long axes of the molecule. It has to be noted, that the molecule (apart from the stiff C₆₀) is very flexible and can

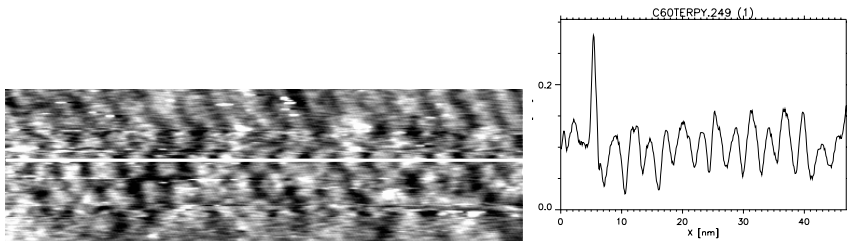


Figure 3.9: A monolayer of C_{60} -terpy on platinum. The image measures $47 \text{ nm} \times 14 \text{ nm}$. The single scan line was taken along the white line. Parameters: RT in air ($U_{\text{bias}} = -35 \text{ mV}$, $I_t = 5 \text{ pA}$, $x = 47 \text{ nm}$, $y = 14 \text{ nm}$, $z \approx 0.3 \text{ nm}$) lowpass filtered.

stretch from about 1.5 nm to 3 nm length. Most STM studies that show sub-molecular resolution were made with flat and stiff molecules like porphyrin or phthalocyanine. The C_{60} -terpy ligands studied here are very flexible, and chemisorption occurs only at one end. A mobility around the chemisorbed terpy, similar to the one of the ruthenium complex shown above, might be expected. Contrary to these speculations, a substructure was recognisable on images of a smaller scale. In the pseudo-3D representation of figure 3.10, each single molecule (indicated with the orange ellipse) of the layer shows a fine periodic pattern. As described above, the physisorption energy can surpass the chemisorption energy for large molecules. It is therefore expected, that the “bucky ligand” is fixed stronger than just with one chemical bond, as is the monomer complex described above.

The substructure could be measured in the single scan line displayed in figure 3.11. The periodicity of the fine pattern was found to be 0.5 nm. No surface-reconstruction of platinum (in air or otherwise) was found in literature, that could explain this pattern. It is therefore assumed, that it is formed by the molecular layer. This molecular pattern indeed resembles the substructure of C_{60} found by S. Behler et al. ten years ago in the same laboratory [86].

This system was not further studied, due to lack of time, and in favour of the fascinating studies which are shown in the chapters 4 and 5.

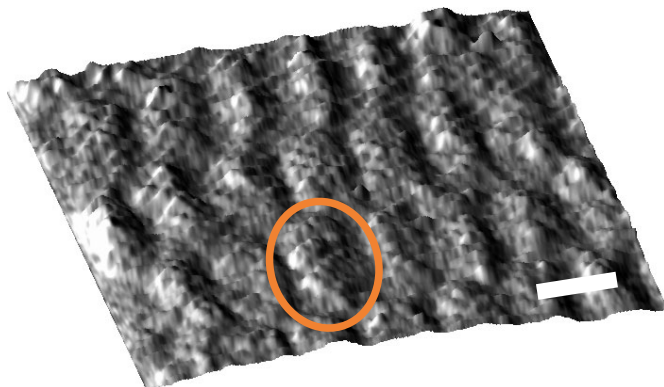


Figure 3.10: Pseudo-3D representation of a monolayer of C_{60} terpy on platinum. The orange ellipse indicates a single molecule. The scale bar is 3 nm long. Parameters: RT in air $U_{bias} = -35$ mV; $I_t = 5$ pA; size= 21.3 nm \times 21.3 nm; z-scale \approx 0.3 nm.

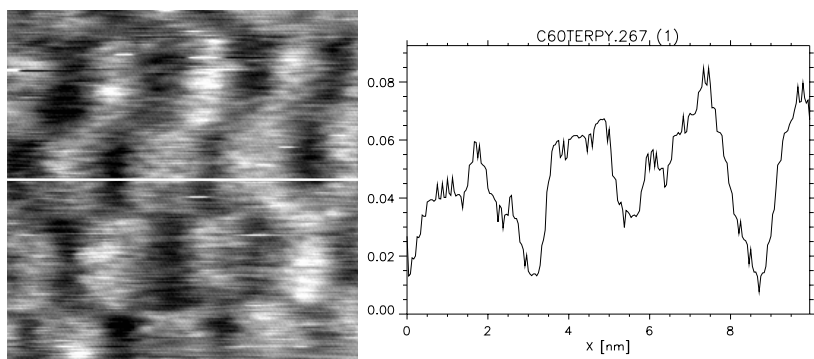


Figure 3.11: A 10 nm \times 10 nm image of C_{60} terpy with a single scan line (measured along the white line). Despite the noise, the fine pattern of 0.5 nm can be seen. Parameters: RT in air $U_{bias} = -35$ mV; $I_t = 5$ pA; size= 10 nm \times 10 nm; z-scale \approx 0.3 nm lowpass filtered.

4. MOBILITY AND MANIPULATION

The physisorption of small adsorbates is rather weak. Only for large molecules with one chemical bond to the substrate, can their collective physisorption be larger than the chemisorption itself. As explained in chapter 3 and figure 3.2 (on page 23), the physisorption has a longer range, compared to the chemisorption of the same molecule. This has an interesting consequence. When a molecule approaches the surface, it first physisorbs, because the energy minimum of physisorption is at a large distance from the surface, and then it chemisorbs, if it is able to form a bond to the substrate. This process is of fundamental importance for forming ordered structures, and ordered structures will be needed in *every* form of molecular nano-technology. Molecules deposited from solution adsorb directly on their space of the surface arrangement. On the contrary, deposition from the gas-phase, by evaporation or sublimation, results in randomly “landed” molecules which have to “find” their lattice space after adsorption. Thus, understanding and controlling the mobility of adsorbates are of great importance for future applications in molecular nano-technology. To get ordered layers, it is therefore of crucial importance that the molecules have a surface-mobility, that is high enough to allow the assembly after adsorption. STM studies can give insights in the mobility and dynamics of adsorbed species, either by observation of mobile arrangements, or by active manipulation experiments.

This chapter investigates the mobility of adsorbates, and shows, how the STM can be used to observe and initiate movements of adsorbates. Parts of this chapter have been published in [93, 94, 66] and will be published in [65, 95]. These studies were done in close collaboration with D. Ammann (measurements, Semesterarbeit [66]) and I. Widmer (measurements, Diplomarbeit [94]) in the laboratory of B. Hermann in the group of H.-J. Güntherodt; P. Weyermann (synthesis of the porphyrin dendrimer [96]) in the group of F. Diederich.

4.1 Mobility of ZnPcOC₈

Octyloxy-substituted zinc-phthalocyanine (ZnPcOC₈¹) on graphite is a model system to study the mobility of adsorbed molecules of intermediate size. The formula of ZnPcOC₈ and its dimensions are shown in figure 4.1. ZnPcOC₈ exhibits strong physisorption but remains very mobile laterally, as long as it is not embedded in a monolayer. It has two “binding motives” to build self-organised layers on graphite. It has a large aromatic centre, that interacts with the graphitic π orbitals, and it has eight octyl chains, that physisorb on graphite as well as pack in two-dimensional lattices. The

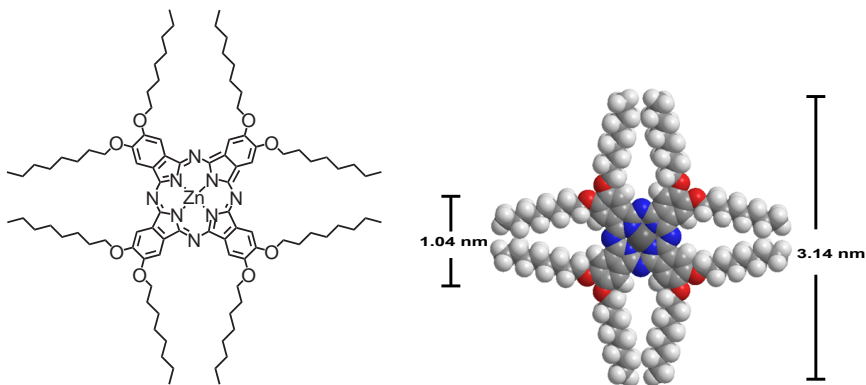


Figure 4.1: Formula and the expected dimensions of ZnPcOC₈.

π -system alone is not able to assemble phthalocyanine (Pc) on graphite. Four methods were used to circumvent this. By either assembling the Pc on top of an alkane layer [97], or embedding it in a layer of alkoxy-substituted molecules [98], Pc could be imaged on graphite. The other two methods used functionalisation with groups that increase both, the intermolecular and the molecule-substrate interactions. The functionalisation with carboxylic acid groups, was successfully used to form two-dimensional, hydrogen-bonded networks [99, 100]. Attaching alkyl chains to a molecule is an elegant way to increase the adsorption and the two-dimensional crystallisation energy, without disturbing the electronic properties (namely the frontier orbitals) of the molecules [62, 101]. An additional method would be to use chemisorption. Unfortunately, chemisorption to a conducting substrate induces major

¹ The systematic name is written in the list of abbreviations, page v

changes to the electronic properties of a molecule. Therefore, the method chosen for the following study was the attachment of alkanes. By attaching alkanes, the phthalocyanines (or other molecules of interest) are separated by an insulating spacer, that also minimises the (unwanted) *electronic* interaction between neighbouring molecules. This can be of great importance in molecular electronics.

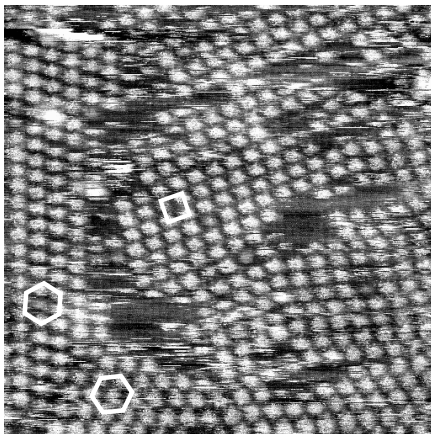
A high resolution image of ZnPcOC₈ on graphite was achieved by X. Qiu et al. [62]. The first step in STM studies is often to seek high resolution, in order to understand which parts of the molecules cause which contrast. It was clearly shown, that the aromatic moiety, which forms the frontier orbitals, is seen as protrusions and the alkyl chains are imaged with much less contrast. As a second step, the mobility of the molecules can be studied, which comprises a completely different approach. The preparation has to be fine tuned to give *sub*-monolayers and the scanning parameters have to be kept very “soft”, meaning very high tunnelling resistances and moderate voltages have to be applied, in order to keep the interaction between the tip and the sample low. The tunnelling resistance for the mobility studies of ZnPcOC₈ was about 2.5 orders of magnitude larger than for the high-resolution images. On the one hand, it is easily possible to wipe away a part of a second monolayer on top of a first one, by scanning with more than 1 pA for a few scans (at about 700 mV). On the other hand, a constructive influence of the scanning tip on the physisorbed layers is visible, even below 1 pA. Molecules in a sub-monolayer can be assembled by scanning repeatedly over the same area. Anyhow, a vast majority of the studied layers was prepared by self-assembly without the interaction of the scanning process. The commercially available ZnPcOC₈² was dissolved in toluene to give solutions of 0.1%. A droplet of these dark green solutions was put onto a freshly cleaved HOPG substrate. After the evaporation of the solvent, the samples were mounted in the STM.

4.1.1 Results and discussion

Figure 4.2 shows a representative STM-image of a sample with almost a monolayer of ZnPcOC₈ on graphite. Two different arrangements can be observed, one trigonal and one squared. In these measurements at room temperature, the arrangements do not appear exactly quadratic or trigonal, but are stretched or compressed in one dimension, because of thermal drift. By

² Purchased from Aldrich

Figure 4.2: ZnPcOC_8 at a sub-monolayer coverage on graphite. Each protrusion represents one molecule. A squared arrangement, dominated by the four-fold symmetry of the molecule and a trigonal arrangement arising from the three-fold symmetry of the graphite can be seen. The white square and hexagons mark these lattices and two orientations of the trigonal arrangement. Parameters: $U_{bias} = -700$ mV; $I_t = 2$ pA; size= 40 nm \times 40 nm; z-scale ≈ 0.3 nm



measuring two images with opposed slow scanning directions, the real orientation can be measured, if the drift remains constant. Both of the arrangements were found in three orientations each, because the graphite surface has a three-fold symmetry (see also section 2.1.1). The quadratic arrangement is obviously induced by the four-fold symmetry of the molecule, while the trigonal arrangement shows more influence of the graphite. At room temperature in air, neither proved to be more stable than the other. This shows, that the interplay between intermolecular and molecule-substrate interactions is exactly balanced at the conditions of our measurements, so that neither dominates the other globally. This is desirable, because it allows the study of dynamics of all the different arrangements.

Figure 4.3 (a) shows a large domain with many defects and borders. Several molecules at the border of the domain look like “half” molecules. They are only present in their location for several scan lines, and they either arrive at their place, or they leave the place during the imaging process. In figure 4.3 (b) a few of these are indicated with arrows. Some molecules (indicated with circles) are only absent for a few scan lines and either present again or replaced by another (these two processes can not be distinguished), or vice versa. Between the ordered layers, the bare graphite surface, littered with many bright streaks can be seen. These streaks are of about the same height as the molecules in the layer. A two-dimensional analogue to a molecular gas is present. The molecules move randomly on the surface with a speed that is higher than the imaging speed of the STM, and therefore,

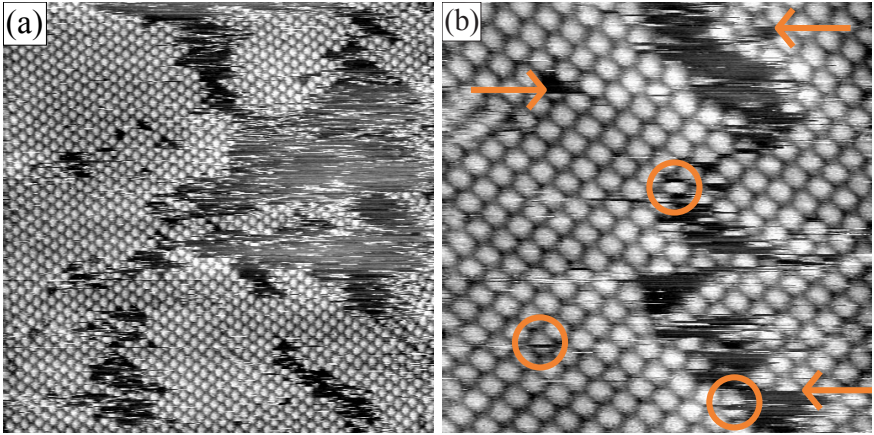


Figure 4.3: Two images of a sub-monolayer of ZnPcOC₈ on graphite. (a) A large domain with many borders and defects. (b) An image at a smaller scale, displaying mobile molecules. The arrows point to “half” molecules, that were only present for some scan lines and absent afterwards. The circles show three examples of molecules that were absent for only a few scan lines and then either back in place or replaced by another. Parameters: (a) $U_{bias} = -886$ mV; $I_t = 5$ pA; size= 100 nm × 100 nm; z-scale ≈ 0.3 nm, (b) $U_{bias} = -886$ mV; $I_t = 10$ pA; size= 35 nm × 35 nm; z-scale ≈ 0.25 nm.

they are only imaged on one (sometimes several) scan lines. Many streaks are longer than the width of a single molecule. This indicates, that the molecules move only a little faster than the STM tip, which was scanned with approximately 160 nm/sec. When a molecule “accompanies” the scanning tip, that is to say, when it moves with a component parallel to the tip movements, it is imaged for a longer time and longer width than an immobile molecule. Therefore, streaks longer than the width of a molecule, are produced. It can not be determined, if the molecules move only along straight lines. Otherwise, the speed of the molecules could be estimated by a statistical analysis of the length of the streaks. Figure 4.4 shows two subsequent scans. Each domain is constantly growing and shrinking, so that a sort of a dynamic equilibrium is observed. The relative proportions of ordered domains and mobile phase remained roughly constant over the measured times. The defects are hopping from one position to another, and the domain borders are constantly shifting. It is not known, if the defect hopping happens through movement of one single molecule, or if all the molecules between the old and new position of the defect are relocated.

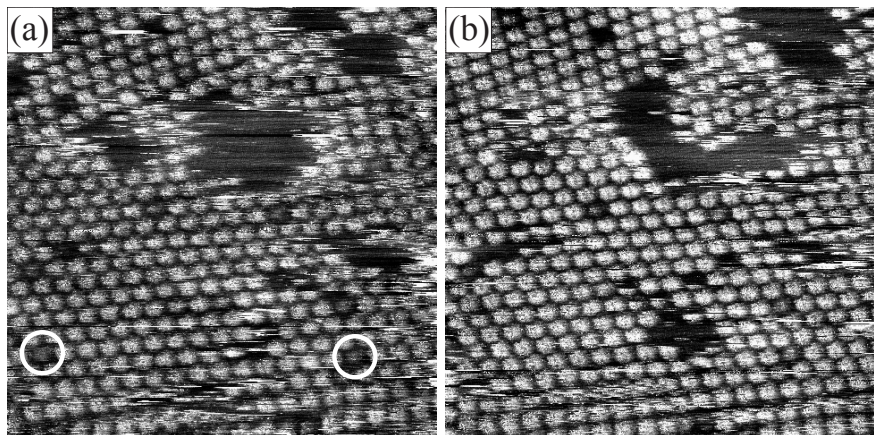


Figure 4.4: Two subsequent images of a sub-monolayer of ZnPcOC_8 on graphite. Rearrangements of large parts of the domains are recognisable. Single molecular defects appear and disappear. And some molecules of half the usual height (white circles) are seen. Parameters: $U_{bias} = -700$ mV; $I_t = 2$ pA; size = $37.66 \text{ nm} \times 37.66 \text{ nm}$; z -scale $\approx 0.2 \text{ nm}$

Some molecules are imaged with approximately half the height of the others. Two of these are marked with white circles in figure 4.4. These molecules of only half the usual height, are a phenomenon, that has been observed with different molecules on different substrates. It seems to be a feature of many STM studies, that nobody can explain consistently for all molecules [102].

As stated above, the influence of the tip on the molecular assembly is noticeable, but uncontrolled. It was not possible to interact selectively with a single or a few molecules. It was possible to image the ZnPcOC_8 layers in UHV, but it proved impossible to image them at low temperature, which is not surprising, because almost no alkoxyated molecules were studied successfully at low temperatures. The usual explanation is, that the layers undergo some phase changes, similar to liquid crystalline materials. To manipulate single molecules, low temperature, and therefore different kinds of molecules are needed.

4.2 Manipulation of a single macromolecule

Since the beginning, STM has not only been used to observe, but also to manipulate at the nanometre scale [29]. Soon, single atoms and molecules

were manipulated. D. Eigler and E. Schweizer wrote their famous 'IBM'-logo with single xenon atoms on a copper surface [103], G. Meyer, B. Neu and K.-H. Rieder wrote 'FU' using CO on copper [104], and J. K. Gimzewski et al. manipulated in- and external degrees of freedom of tetra-[3,5 di-*t*-butylphenyl] porphyrin (TBPP) on copper [105, 106]. S.-W. Hla et al. even induced all steps of a chemical reaction³ on a surface with an STM tip [107]. Nowadays, some groups control the manipulation of small molecules very well. A. J. Heinrich et al. built molecular cascades from CO, that even include logical functions. They constructed, triggered, and observed molecular domino rows with STM [108]. However, large and flexible molecules are rarely used in STM studies, and almost never in manipulation experiments. F. Rosei et al. wrote a review about "*Properties of large organic molecules on metal surfaces.*" [88], in which they describe biphenyl, decacyclene, HtBDC, PVBA, C₆₀, Pc, and the porphyrin and "lander" derivatives, that have built-in rotational freedoms of the so-called legs⁴. If these molecules were called flexible, the molecules presented in this section could be claimed to have no structure at all. There is still a big gap between these stiff small molecules and the molecules studied in biology. Large dendrimers are mostly in this gap. In chapter 3 chemisorption was presented as a method to assemble molecules with repulsive intermolecular interactions. Section 4.1 shortly introduced the concept of alkyl-chain substitution as method to assemble flat molecules on graphite, which will be further discussed in chapter 5. In the present section, a way to immobilise single physisorbed macromolecules, like the 4.2 kg/mol dendrimer seen in figure 4.5, is presented. The preparation and monolayer formation of linear *n*-alkanethiols is well known (see also the short overview in chapter 3). H. Tokuhisa et al. successfully made mixed monolayers of chemisorbed PAMAM dendrimers and chemisorbed *n*-alkanethiols to image them with the AFM [109]. The interspersed alkanethiols were shown to support the PAMAM dendrimers to a more prolate shape than the rather oblate forms of a pure PAMAM monolayer. Our group adapted this idea to stabilise and support *single, physisorbed* dendrimers [93]. At low concentrations, single dendrimers can be embedded in a monolayer of alkanethiols. One example is presented below, others were shown in [93]. *Single*, physisorbed molecules are difficult to image with scanning probe microscopy, because the interaction with the tip is usually too large in relation to the interaction with the substrate [110]. The molecules are moved laterally during the scanning process, or even picked up by the tip,

³ The formation of biphenyl from two iodobenzenes, an Ullman reaction.

⁴ See list of abbreviations on page v for the full names.

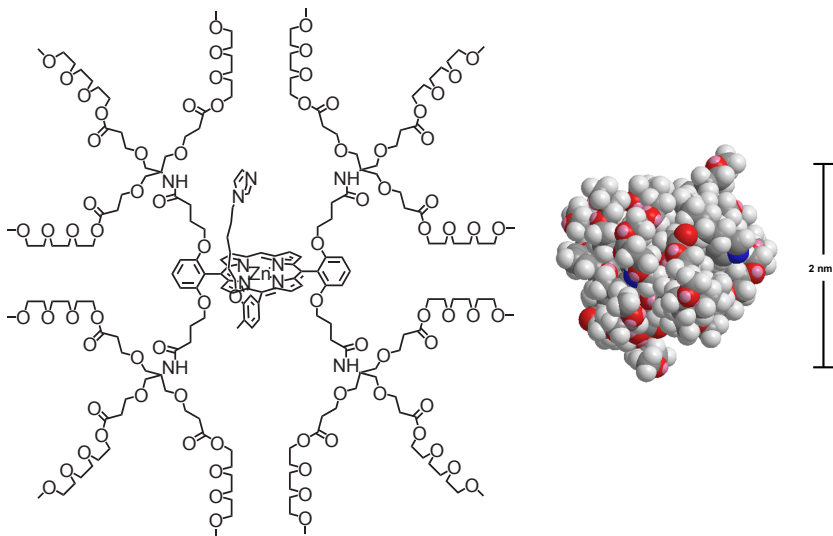


Figure 4.5: Formula and expected dimension of the first generation porphyrin dendrimer synthesised by P. Weyermann

preventing high resolution images. Embedding the macromolecules in layers of alkanethiols can immobilise them, but it can not prevent the intramolecular flexibility. And this flexibility prevents high-resolution images of non-flat macromolecules, because parts of the molecules are moved by the scanning process – the molecules are imaged as blurred “blobs”. The first and second generation of the porphyrin dendrimer presented in figure 4.5 were synthesised by P. Weyermann to study the influence of the poly(ethyleneglycol) shell around the porphyrin in comparison to the natural protein shell, in respect of electrochemical and catalytical activity [96]. The STM samples were prepared by dipping a freshly prepared gold substrate in a dilute ethanolic solution of the dendrimer, see the experimental section 2.1.2 for details.

4.2.1 Results and discussion

Physisorbed molecules show a large lateral mobility. Even very large molecules can be moved or removed by an STM tip, which prevents measurements at room temperature in air. To decrease the available energy for these movements, measurements at low temperatures are necessary. The dendrimer

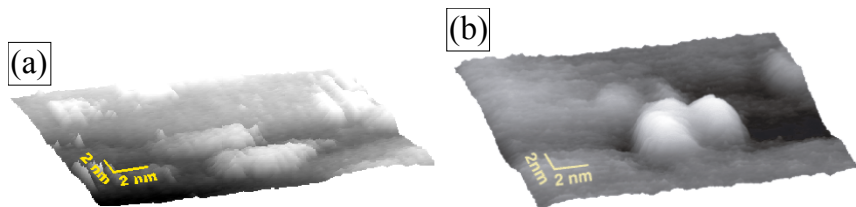


Figure 4.6: (a) Small scale image of few first generation porphyrin dendrimers on a pure gold surface at 4 K. The dendrimers appear very flat and spread. (b) Low temperature image of the same scale, showing a cluster of the dendrimers, embedded in a monolayer of HDT. The dendrimers appear more spherical. Parameters: (a) $U_{\text{bias}} = 700$ mV, $I_t = 8$ pA; (b) $U_{\text{bias}} = -2.5$ V, $I_t = 3$ pA.

could be imaged at 4.2 K, but appeared very flat. Figure 4.6 shows two pseudo-3D images: (a) without and (b) with a monolayer of 1-hexadecanethiol (HDT). The sample shown in figure 4.6 (b) was prepared with the new technique of embedding the dendrimer in a monolayer of HDT, by dipping the substrate in a dilute solution containing both, the dendrimer and the HDT. The supporting effect of the HDT can directly be seen. Without the support of the alkanethiol layer, the dendrimers showed a height-to-width ratio of about 1:8. The dendrimers embedded in HDT showed a height-to-width ratio of 1:5. This value has to be used carefully, because the two images were recorded at very different bias voltages. But the general trend of the more spherical molecules was observed for all voltages. A cartoon of the “support” obtained with a monolayer of HDT is shown in figure 4.7 for the second generation porphyrin dendrimer. For more examples of this immobilisation technique, see [93]. The embedded molecules are also stabilised laterally, so that they can be imaged at room temperature in air, without being wiped away immediately. The first generation of the porphyrin dendrimer aggregates in small clusters of a few molecules, as can be seen in figure 4.8. While the dendrimers could be imaged at room temperature, they were still wiped away from the scanning area, so that each sequential scan showed less molecules. Only at low temperature, the molecules could be imaged for a longer time (hours to days) in a stable way. The Au(111) surface shows the typical triangular step-edges of mono-atomic height. The surface also shows the ‘holes’, roughly circular depressions of a depth of one gold layer, that are formed upon adsorption of alkanethiols. For further discussions of this surface restructuring, see [67] and references therein.

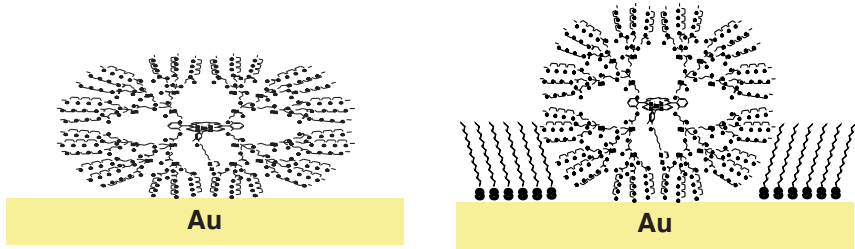


Figure 4.7: Scheme of the support of a monolayer of HDT on gold, with a second generation porphyrin dendrimer.

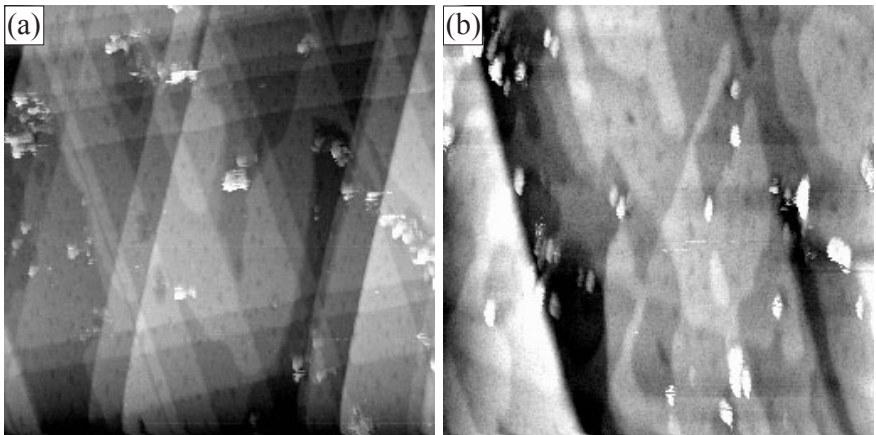


Figure 4.8: Two representative images of the first generation porphyrin dendrimer embedded in a monolayer of HDT on gold. The dendrimers show a tendency to cluster in small numbers. The gold surface shows the typical holes, that are formed upon adsorption of a monolayer of alkanethiols. Parameters: $U_{bias} = 700$ mV; $I_t = 10$ pA; 100 nm \times 100 nm.

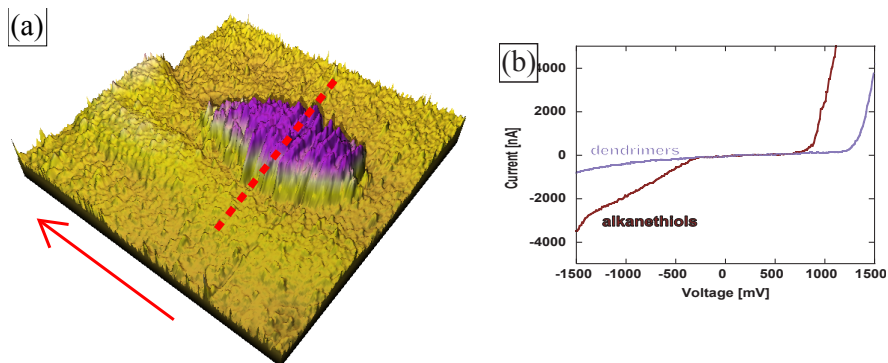
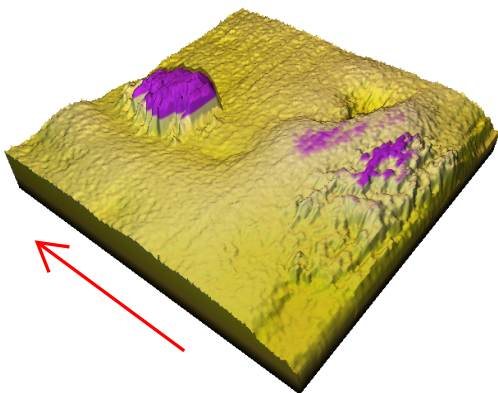


Figure 4.9: (a) STM (topography) image of the two porphyrin dendrimers before the manipulation. The dashed red line indicates where the STM tip was moved during the recording of the tunnelling spectra. The red arrow indicates the slow scan axis. The colour-scale is designed to display the purple porphyrin dendrimer on the gold surface. Low z -values are displayed in dark yellow, changing to bright yellow with increasing z , and turning into purple for highest z -values. Parameters: 4.2 K; $U_{bias} = 750$ mV; $I_t = 4$ pA; size = $10 \text{ nm} \times 10 \text{ nm}$; z -scale ≈ 2 nm. (b) Two tunnelling spectra: (red) above the alkanethiols and (blue) above the dendrimer.

The width of a single dendrimer embedded in HDT was 1.5 nm, which is slightly smaller than the diameter of the dendrimer including the whole PEO chains. It is not expected that the imaged molecular orbitals extend to the outermost branches.

A cluster of two dendrimers was selected for closer investigation at 4.2 K. After recording a small scale STM image (figure 4.9 (a)), several tunnelling spectra (current versus voltage curves) were measured. The curves measured at tip positions above the dendrimer showed a diode-like characteristic. Only at positive voltages, the dendrimer displays a high conductivity. In other words, only the LUMOs were accessible with the tunnelling electrons in the tested range of bias voltages. In Figure 4.9 (b) an STS recorded above the monolayer of HDT is included for comparison. To record the spectra, the tip was moved along the dashed red line in figure 4.9 (a) while the spectra were recorded as follows. The tip was moved to the location of the next spectrum, after a short time the feedback loop was switched off, in order to keep the tip at a constant distance above the surface, the voltage was ramped from -1.5 V to $+1.5$ V, and the resulting tunnelling current was recorded. Two typical spectra, one above the alkanethiols and one above the dendrimer are

Figure 4.10: STM image of the two dendrimers separated. The moved dendrimer on the bottom right appears flatter and more spread out. The red arrow indicates the slow scan axis of this image. The colour scale is applied in z , and does not colour all of the flat-lying dendrimer purple, as is seen on the right border of the image. Parameters: 4.2 K; $U_{bias} = 750$ mV; $I_t = 4$ pA; size = 10 nm \times 10 nm; z -scale ≈ 2 nm.



shown in figure 4.9 (b).

This procedure of moving the tip along the dashed line, while ramping the bias voltage up and down, moved the dendrimer at the right side by about 2 nm, as can be seen in the sequential STM image shown in figure 4.10. The dendrimer on the right looks much flatter and more spread out. The place where it was before the manipulation, next to the dendrimer on the left, shows a small depression. This confirms that the dendrimers are indeed embedded between the alkanethiols, directly in contact with the gold, and not lying on top of the alkanethiol layer. The moved dendrimer on the right of figure 4.10 looks much flatter and spread-out, comparable to those measured without the surrounding support of HDT (see above). The STM image in figure 4.10 was recorded with the slow scan axis from bottom right to top left, as indicated with the red arrow. The mere scanning at 4 pA was enough to move the dendrimer back into its former place. Figure 4.11 (with the slow axis from top left to bottom right, as indicated) shows the two dendrimers after the complete reversion of the manipulation. The dendrimers in the HDT were not moved at low temperature by the scanning process at 4 pA. But the dendrimer, that had been pushed onto the monolayer of HDT, was easily moved and “snapped” back into its place between the HDT.

The whole procedure of recording tunnelling spectra along the dashed red line in figure 4.11 was repeated, and the movement of the dendrimer was reproduced, as shown in figure 4.12 (a)⁵. The pushing back of the molecule

⁵ The reproduction with another sample failed, most probably because the parameters could never be prepared as ideal again.

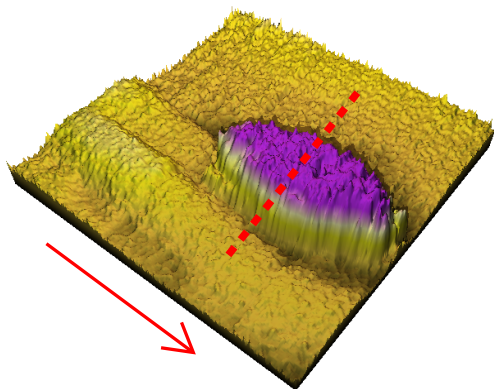


Figure 4.11: Both dendrimers are in contact again. The red arrow indicates the slow scanning direction of this image, while the red line indicates the positions of the tip in the manipulation *after* this image. Parameters: 4.2 K; $U_{bias} = 750$ mV; $I_t = 4$ pA; size= 10 nm \times 10 nm; z-scale \approx 2 nm.

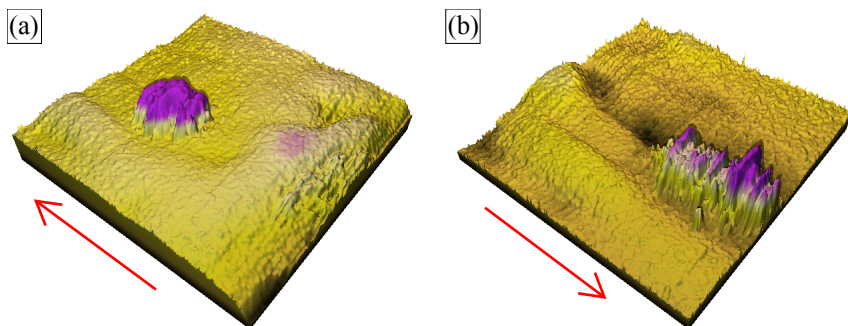


Figure 4.12: The manipulation experiment was successfully repeated once more. Parameters: 4.2 K; $U_{bias} = 750$ mV; $I_t = 4$ pA; size= 10 nm \times 10 nm; z-scale \approx 2 nm.

was also repeated a second time, which is shown in figure 4.12 (b). The procedure was reproduced three times with the same molecules.

This is a mechanical manipulation of a single macromolecule of much larger size than *any* reported so far in literature. It will be a long time, before pushing a molecule of a mass of 4.2 kg/mol will become routine work. These experiments provide an interesting starting point for future work in this field, showing, that even the interaction with such flexible and large molecules can be controlled at the nanometre scale.

5. SELF-ASSEMBLY BY WEAK INTERACTIONS (PHYSISORPTION)

In the two decades of the existence of SPM, flat and stiff molecules have been measured almost exclusively, with nearly no examples of large and flexible molecules, due to the difficulties of the measurements. Large and/or flexible molecules are very interesting since they can be designed to have almost any desired function. The question of how to address these molecules, or how to form self-assembled monolayers with them is discussed in this chapter. Alkanes are one class of very flexible molecules, and their adsorption on graphite has been studied experimentally [101] and theoretically [111]. It is known, that alkane chains assemble preferably in an all-*trans* conformation with the carbon plane either parallel or perpendicular to the surface, as illustrated in figure 5.1. Both forms have been observed experimentally, their relative stability seems to depend on the other functionalities of the molecules. The spacing between the chains was found to be 426 pm for the chains lying with the carbon plane perpendicular to the graphite, compared to 420 pm and 480 pm in the two directions in the three-dimensional crystal. It was found, that pure alkanes prefer the perpendicular (fig. 5.1 red) arrangement. If headgroups are attached to the alkanes, that separate the alkanes by more than these 426 pm, the chains assume the parallel pattern (fig. 5.1 green), lying flat on the graphite. The adsorption energy per CH₂ subunit is -12.1 kJ/mol for the flat and -10.4 kJ/mol for the vertical arrangement for pure alkanes [111]. In addition, the *two-dimensional crystallisation energy*, that describes the intermolecular interactions, has to be considered. The ratio between the intermolecular interaction and the adsorption energies lies between 2:5 and 3:5 for alkanes of different lengths. The graphite-alkane interaction can therefore dominate the assembly over the intermolecular interactions. If the ratio would be the other way around, three-dimensional aggregates would be formed instead of two-dimensional layers.

As an interesting example of large and flexible molecules, dendrimers were studied. In contrast to pure alkanes, the Fréchet-dendrons studied in

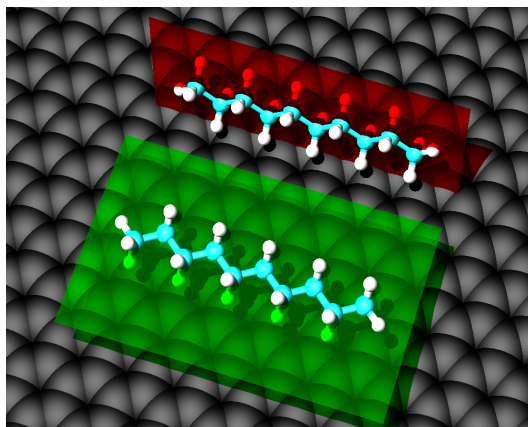


Figure 5.1: An illustration of the two modes of adsorption of all-*trans* alkanes on graphite. With the plane of symmetry through the carbon atoms parallel (green) and perpendicular (red) to the graphite surface.

this chapter have an additional assembly-motif. As expected, the aromatic moieties form π - π bonds with the graphite. The molecule-substrate interaction is therefore stronger, compared to alkanes. The balance between the adsorption energy and the two-dimensional crystallisation energy controls the self-assembly process.

As J. Gimzewski said in the Vega science program about nanotechnology: “*He who can control self-assembly, controls the future.*” [112]. Molecular nano-technology will rely on self-assembly processes. One key example of the importance of self-assembly is, that it is directly responsible for the formation of chiral patterns from achiral molecules adsorbed on surfaces. Chiral domains formed from chiral or achiral molecules were identified with STM [113, 114, 115], coadsorbed achiral molecules were found to express the chirality of an adsorbed layer [116].

In this chapter, STM characterisations of highly flexible, physisorbed (macro-)molecules are presented. Conformational analysis of flexible molecules on graphite surfaces is achieved, and chiral domains formed by achiral molecules are described. Additionally, a delayed transformation of one assembly pattern into another, accompanied by a conformational change is presented. Octyloxy-substituted Fréchet-dendrons are presented as a functional group that allows self-assembly of various molecules and functions.

Parts of this chapter have been published in [94, 117, 53], and will be published in [65, 118, 119]. These studies were done in close collaboration with L. Scherer (synthesis of all the molecules in this chapter, except the DDB-dendrimer and measurements [53, 119]) in the group of E. Constable

and C. Housecroft; I. Widmer (measurements, Diplomarbeit [94]), M. Stöhr (measurements with I. Widmer [117]) in the laboratory of B. Hermann in the group of H.-J. Güntherodt; B. Murer (synthesis of the *S,S*-DDB dendrimer [120]) in the group of D. Seebach.

5.1 A bipy-ligand, expanded with alkoxyated first generation Fréchet-dendrons

To study highly flexible molecules, that can eventually be forced into a flat conformation, the molecule shown in figure 5.2 was synthesised. It was designed as a switchable system, that could be triggered and/or read out with STM. It is a molecule, with several conformational levels at similar energies, that can be studied by STM. Bipy was chosen as a well known ligand with two main conformations: *cis* and *trans* for the interannular C-C bond. The coordination chemistry of bipy is well known with almost every metal ion of the periodic table [121]. The rotation about the central bond is well studied and known to be locked to *cis* when complexed to a metal centre. The free ligand forms a time-averaged *trans* conformation [122]. In this section, a bipy ligand, expanded with two first generation Fréchet-dendrons is studied. Alkyl-chains were added for additional physisorption and increased intermolecular interaction, without any change to the frontier orbitals and therefore to the STM contrast. Figure 5.2 shows the formula and two space-filling representations with the expected dimensions. The huge number of internal degrees of freedom of this molecule is drastically reduced when it is forced into two dimensions, i. e. adsorbed on a surface. Because the alkyl-chains gave little or no contrast at the parameters used in this study, their internal degrees of freedom will be neglected in this discussion, and the chains are assumed to have an all-*trans* conformation. Only the *cis-trans* arrangement at the central bipy, the two *syn-anti* arrangements at the ArOCH₂Ar and the four *syn-anti* arrangements at the ArOR, a total of $2^7 = 128$ conformations, have to be considered.¹ The system provides an interesting playground for conformational analysis and manipulation with its “conformational switches”.

¹ This number is further decreased, by the the fact, that some conformations have a C_2 -symmetry and therefore are counted twice, by this simple exponentiation.

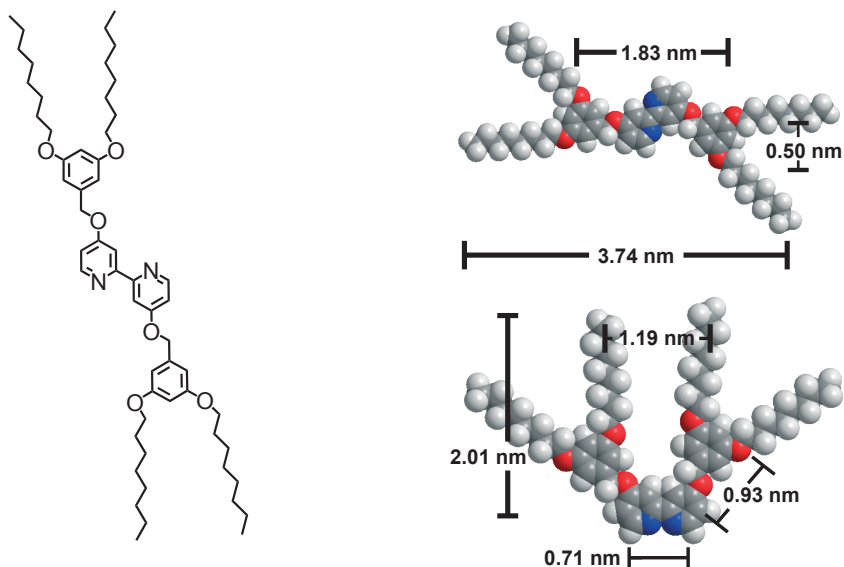


Figure 5.2: Formula of the first generation bipy dendrimer and space-filling representations of the *transoid* and the *cisoid* conformation with expected dimensions.

5.1.1 Results and discussion

5.1.1.1 Domains and their internal structures – conformational analysis with STM

The bipy ligand was dissolved in either dichloromethane or hexane to give 0.2 mM solutions. Up to three droplets of these solutions were put on a freshly cleaved HOPG sample. For further preparation details see the experimental section, on page 11. This procedure yielded ordered domains of monolayer thickness. The molecules formed bright stripes, that are built of close-packed molecules, lying flat on the surface. Immediately after the approach of the scanning tip, the domains could be observed. The ordering was found over all the examined graphite surface. It is concluded that in this case, a *self-assembly* takes place, without the interaction of the measurement, as opposed to some known phenomena e. g. in STM studies at the liquid solid interface, where voltage-pulses have sometimes been used to initiate the ordering. The domains on samples prepared from hexane were always of much

larger size than those prepared from dichloromethane solutions. Using hexane, domains larger than $500\text{ nm} \times 500\text{ nm}$ were usually observed. Domains formed from dichloromethane were rarely larger than $150\text{ nm} \times 150\text{ nm}$. Representative examples are shown in figure 5.3. This difference can be attributed to the fact that hexane (b.p. 342 K, $\Delta_{\text{vap}}\text{H}^\circ = 31.52\text{ kJ/mol}$) evaporates slower than dichloromethane (b.p. 313 K, $\Delta_{\text{vap}}\text{H}^\circ = 28.82\text{ kJ/mol}$). During the slower evaporation of the solvent, the molecules have more time for self-assembly and conformational ordering.

Two sets of three domains with an angular relationship of 6.5° between the two sets were observed. Within each set, three domains at an angular periodicity of 120° were found. This reflects the three-fold symmetry of the surface of the ABA-type graphite (see the experimental section, page 12). Figure 5.3 (c) shows an image of all six domains, indicated with white lines. No domain was found to be more stable than any other. That is to say, no conversion could be observed and no large scale statistics were possible, because many domains could not be identified due to changing resolution and lack of presence of other domains for comparison. The two sets of domains have a different internal structure, as can be seen in figure 5.3 (a).

Conformational analysis with STM. With a series of high-resolution images, these internal structures could be assigned. The fact, that the frontier orbitals, namely the occupied HOMOs (which are imaged when using a negative sample bias, compare [62]), are located on the benzylic rings, adds an additional challenge. This creates highly symmetric patterns, which are difficult to assign with certainty. In figure 5.4 the cluster of filled orbitals at the highest energy is shown for two of the possible conformations. The molecular orbital calculations were done with a semi-empirical PM3 method (see also section 2.3). The conformation² did not change the fact, that a cluster of the highest filled orbitals is located at the benzylic rings. Only the relative energy levels, and the sequence within the cluster slightly changes with the conformation. The next cluster of orbitals is always located at the bipy. As can be seen in figure 5.4, the filled HOMOs extend to the phenol-ether oxygens. This could be observed in the best resolved images, and thus provides a near atomic resolution, by showing the location of the oxygen atoms (see below).

Figure 5.5 (a) shows the boundary between two domains that form an angle of 6.5° . The two domains have clearly a different internal structure,

² All the frontier orbitals of the flat conformations discussed below, and of some energy-optimised 3D conformations were calculated and compared.

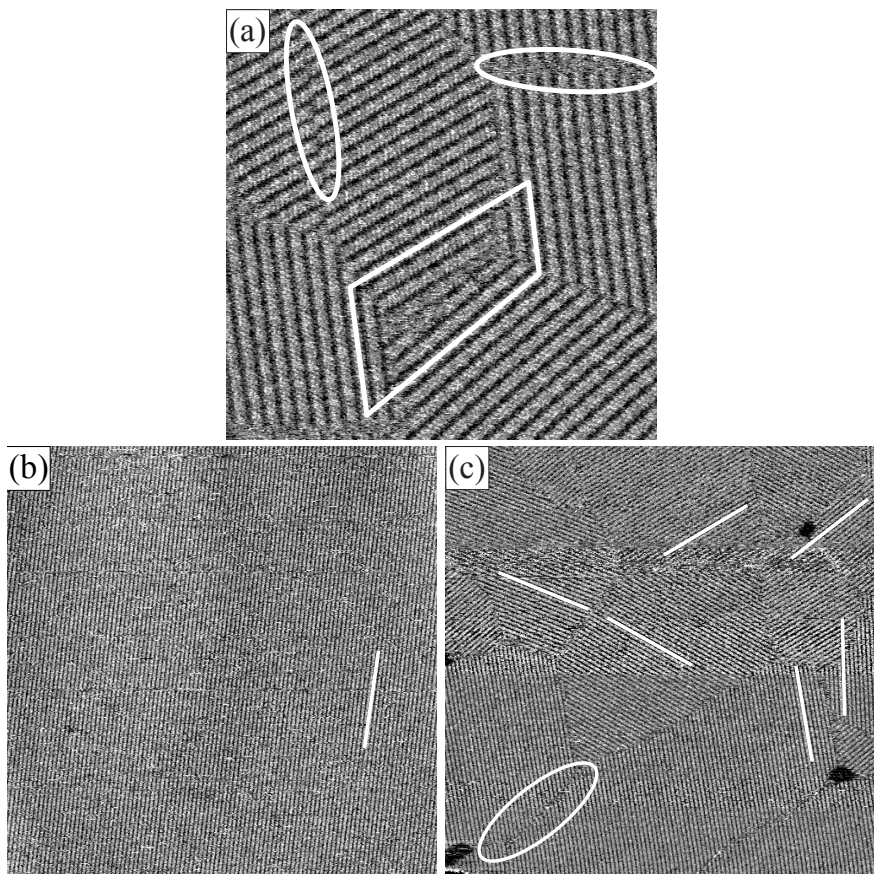


Figure 5.3: (a) A $80 \text{ nm} \times 80 \text{ nm}$ image of a sample, prepared from a dichloromethane solution, showing four domains (marked with a white quadrangle) in three different orientations. Two domain mismatches with half a molecule offset are marked with white ellipses. (b) A large domain formed from a hexane solution. Both (b) and (c) are $180 \text{ nm} \times 180 \text{ nm}$, for direct comparison. Image (c) shows all six orientations of the observed domains. Samples prepared from dichloromethane always showed small domains, sometimes with mismatches (marked with an ellipse). Parameters: (a) $U_{bias} = -700 \text{ mV}$; $I_t = 0.7 \text{ pA}$; size= $80 \text{ nm} \times 80 \text{ nm}$; $z\text{-scale} \approx 0.12 \text{ nm}$; (b) $U_{bias} = -700 \text{ mV}$; $I_t = 0.8 \text{ pA}$; size= $180 \text{ nm} \times 180 \text{ nm}$; $z\text{-scale} \approx 0.15 \text{ nm}$; (c) $U_{bias} = -770 \text{ mV}$; $I_t = 1 \text{ pA}$; size= $180 \text{ nm} \times 180 \text{ nm}$; $z\text{-scale} \approx 0.15 \text{ nm}$.

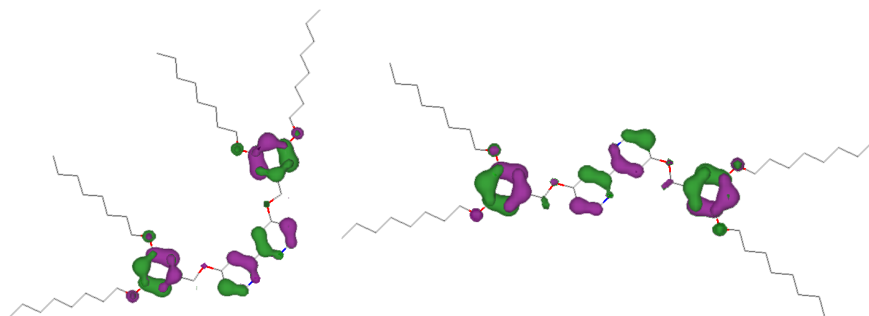


Figure 5.4: Illustration of the 5 filled molecular orbitals at the highest energy (HOMO 0-4) for a *cisoid* and a *transoid* conformation. Calculated semi-empirically with a PM3 method, using HyperChem. Purple and green represent positive and negative signs of the wavefunctions. A cluster of orbitals is located on the phenyl rings and extends to the oxygen. At a slightly lower energy, the orbitals of the aromatic bipy are found.

as is most obvious when the angle α , formed between the row of molecules and a line, drawn through both benzylic protrusions, are compared as in figure 5.5 (c) and (d) (green rhomboids). In the left domain (fig. 5.5 (c)) α is 55° , whereas the right domain (fig.5.5 (d)), shows an α of 38° . By an extensive analysis (details described in the experimental section 2.4 on page 19), the internal conformations of the molecules and the supramolecular arrangement could be assigned. The molecules were fitted on the measurements. The transparent models were fixed and transferred to a printout of a graphite lattice at the same scale. The whole arrangement was rotated and translated to a parallel orientation of the benzyl rings with the graphite, but with an offset of half a hexagon. The aromatic moieties of the molecules were then in the position of the next graphite layer, that was cleaved off prior to the measurement. This is one of the positions with the highest π - π interaction. The 6.5° between the two arrangements arise from a different relative location of the second molecule in a row (using identical positions of the first molecule). Figure 5.5 (b) illustrates the different location in respect to the graphite. The proposed arrangements of the two domains in figure 5.5 are shown in figure 5.6.

An exceptionally high resolution was achieved on another domain, that shows a further variant of arrangement. Figure 5.7 shows the averaged measurement with three molecules superimposed with the measurement in a pseudo-3D representation. As discussed in the experimental section (page

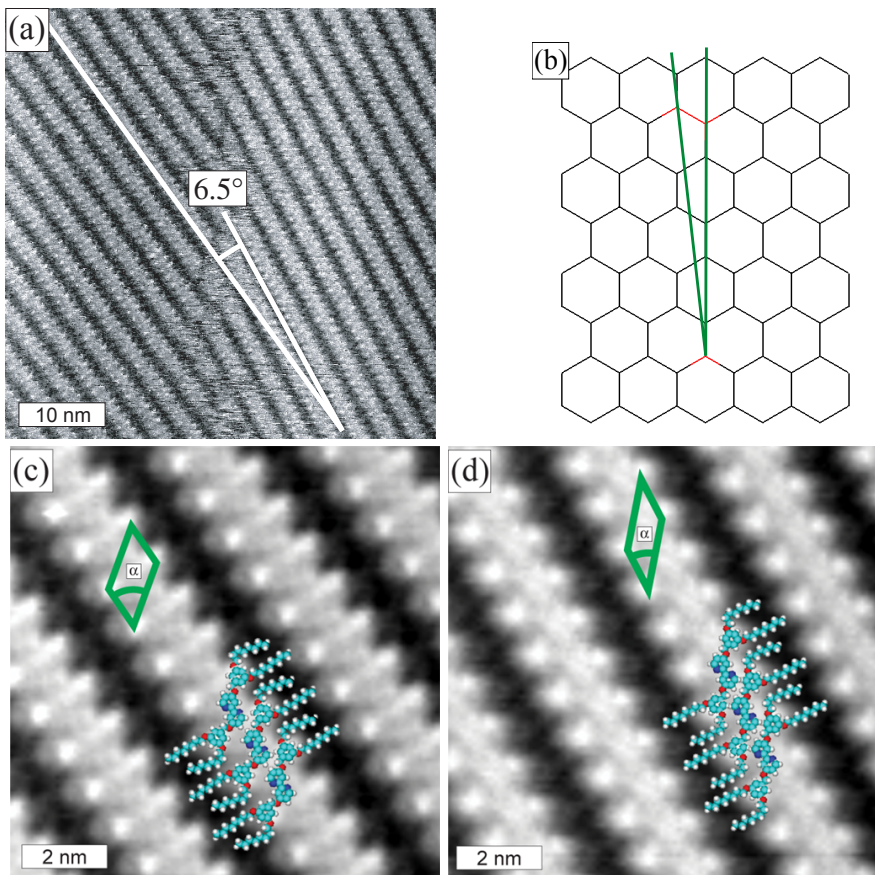


Figure 5.5: (a) A boundary between two domains with different internal structure forming an angle of 6.5° . (b) Illustration of the 6.5° with respect to the graphite lattice. (c) $10 \text{ nm} \times 10 \text{ nm}$ enlargement of the left domain of (a), correlation averaged over 121 positions. Three molecules are overlaid to envisage the organisation, further explanations are given in the text. (d) $10 \text{ nm} \times 10 \text{ nm}$ enlargement of the right domain of (a), correlation averaged over 104 positions, with three molecules, indicating the found arrangement. Parameters: $U_{bias} = -1111 \text{ mV}$; $I_t = 1.5 \text{ pA}$; size= $50 \text{ nm} \times 50 \text{ nm}$; z-scale $\approx 0.15 \text{ nm}$

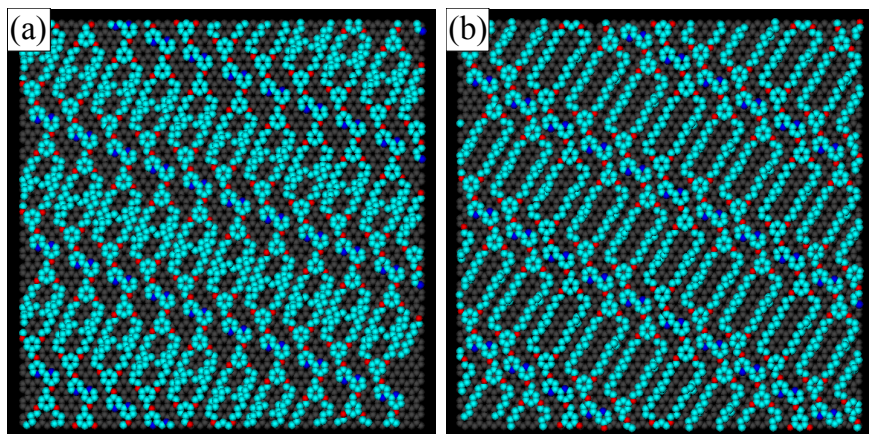


Figure 5.6: Proposed arrangements on graphite for the domains shown in figure 5.5 (c) and (d). Each graphite square is $10 \text{ nm} \times 10 \text{ nm}$ and has the same orientation. The alkyl-chains are only included to show the overall size of the molecules, their orientation was not modelled. (Hydrogen atoms were omitted for clarity.)

17), the STM does not show locations of atoms, but the shapes and locations of molecular orbitals of adsorbed species. A comparison of the orbital plots in figure 5.4 with the STM image in figure 5.7 shows an impressive match. In this image, the lobes of the molecular orbitals, extending to the oxygens of the phenol-ether can clearly be recognised. In this case, the STM gives the exact location of the oxygen atoms and can therefore be claimed to have near atomic resolution, at room temperature in air. Also for this pattern, the molecular arrangement was constructed. Figure 5.8 shows a topview of the measurement (a) and the proposed arrangement on graphite (b). The most noticeable difference is that α is obtuse, if it is defined in the same way as in the previous arrangements. The molecules are tilted towards the right in a stripe, whereas the measurements shown in figure 5.6 are tilted to the left. Only arrangements with the bipy aligned along the stripes, formed by the molecules, were observed. That is to say, the molecules in this arrangement are lying on the other side, forming a *Z*-like rather than an *S*-like shape. Figure 5.9 shows a schematic model of the molecule and explains how the molecule gets an orientation when it is adsorbed on the surface. Performing a simple thought experiment, one can flip a molecule onto its other side (a turn of 180° around the axis between the two phenyls, from *S* to *Z*) but leave it in the same supramolecular arrangement. This molecule

would then have its bipy perpendicular to the direction of the stripe, like in figure 5.9 (c). The α larger than 90° can, with the bipy aligned with the stripe, only be formed by a molecule that lies on its other stereotopic side, thus forming a *Z*-like arrangement opposed to the *S*-like seen above. It is important to note, that the alkyl-chains in figure 5.8 (b)) are drawn all-*trans*, which results in overlapping chains. At exactly the crossing points, a small protrusion is visible in the averaged image 5.8 (a). This may result from the averaging procedure, indicating that the probability of finding a chain there is much larger, than in the other places. The chains are expected to lie flat on the graphite, forming an interdigitating pattern, to reach the lowest energy. However, a certain mobility may still be present.

Out of the 128 conformations mentioned in the introduction of this chapter, only those eight arising from the inner three “conformational switches” were considered, and only two were identified on the surface. No *cisoid* form of the bipy dendrimer could be observed with the free ligand, as expected from x-ray crystallography of bulk crystals of bipy ligands. The four possible *transoid* conformations are shown in figure 5.9. The molecules (b) and (c) have the same conformation, but lie on different faces of the molecule, and are therefore distinguishable. Only the conformations (a), (b), and (c) were found in the measurements, (d) was never observed. In the vast majority of the measurements, only the six domains discussed above, consisting of two arrangements in three orientations were seen. These could be assigned with a high certainty. The domain shown in figure 5.7 and 5.8 could not be securely identified in other measurements. But as the angle in respect to the graphite is the same as in the domain in figure 5.5 (d), it might be present in some of the images with less resolution. The surface coverage is not very different and difficult to measure in the higher resolved, small scale images.

The domain boundaries were usually noisy with very low resolution. Sometimes, the substrate (HOPG) can be seen between domains: very planar areas with no internal structure, or with some noise generated by highly mobile molecules (see fig. 5.3 (c)). If the observed, ordered domains would be multilayers, an ordered structure would be expected to become visible on those lower areas. In this case, a structure similar to the observed stripes with somewhat better resolution would be seen. It is therefore concluded, that the observed ordered layers are true *mono*-layers. In these layers, single molecular defects were often observed.

5.1.1.2 Defects

Domain mismatches between two (identically oriented) domains were observed (see the fig. 5.3, marked with ellipses). Defects were more frequently observed in layers prepared from dichloromethane, which is directly related to the smaller domain size found on samples prepared with this solvent. As mentioned already, this is a consequence of the faster evaporation, therefore, the molecules have less time to assemble themselves and defects are more prone to occur. Single molecular vacancies were observed, which were found to be relatively stable. Even repeated scanning over them did neither “fill” them, nor move them to different locations as had been observed with ZnPcOC_8 in section 4.1. Figure 5.10 shows a single defect and a row of defects. Quite regular patterns of vacancies were observed, in which the vacancies skip every second stripe of molecules and are aligned along the long molecular axis.

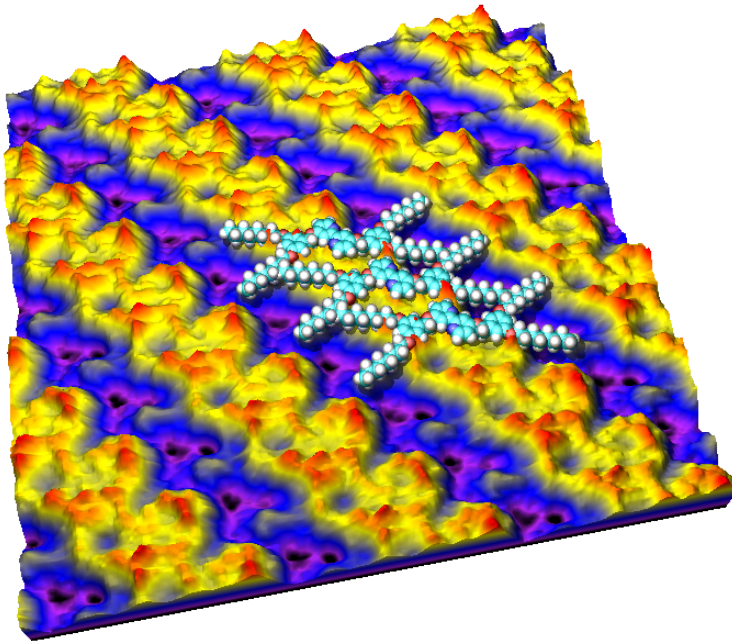


Figure 5.7: Pseudo-3D representation of the third kind of domain of the bipy ligand with a high-contrast colouring. Three superimposed molecular models illustrate the proposed arrangement. The shapes of the HOMOs (compare fig. 5.4) can clearly be recognised. Even the position of the oxygen of the phenol-ether can be identified, because the HOMOs extend to them with small extrusions. The image was correlation averaged over 41 positions in a $30 \text{ nm} \times 30 \text{ nm}$ image. Parameters: $U_{bias} = -900 \text{ mV}$; $I_t = 4 \text{ pA}$; size = $10 \text{ nm} \times 10 \text{ nm}$; z -scale $\approx 0.15 \text{ nm}$

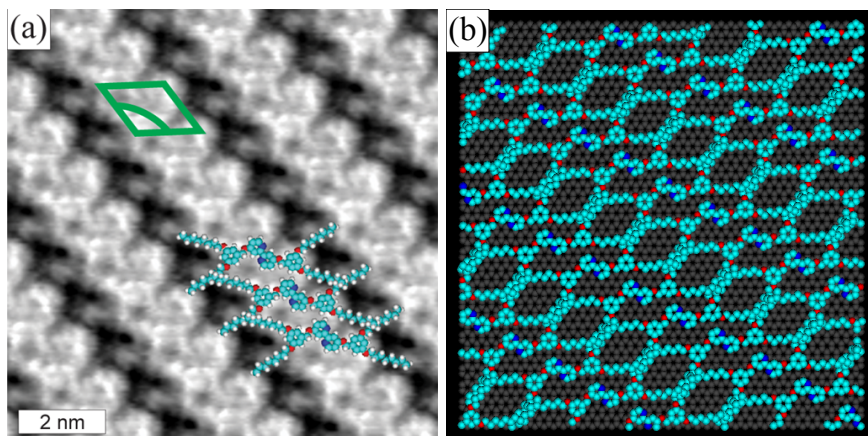


Figure 5.8: The third arrangement found for the bipy ligand. (a) STM image, averaged over 41 positions in a $30 \text{ nm} \times 30 \text{ nm}$ scan. Parameters: $U_{bias} = -900 \text{ mV}$; $I_t = 4 \text{ pA}$; size = $10 \text{ nm} \times 10 \text{ nm}$; z-scale $\approx 0.15 \text{ nm}$ (b) The proposed arrangement on graphite is not aligned with the measurement on the left, but has the same graphite orientation as fig. 5.6, for easier comparison with the other patterns.

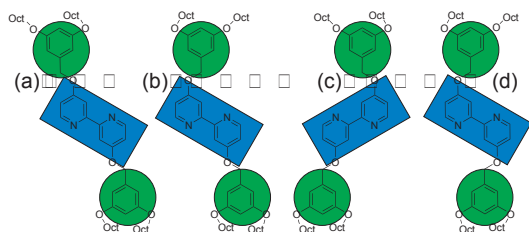


Figure 5.9: An abstraction to explain the stereochemistry, that arises from the adsorption onto a surface. Note, that the conformations (b) and (c) are not superimposable without desorption from the surface. The molecules (a), (b), and (d) have an *S*-like conformation and (c) has a *Z*-like shape.

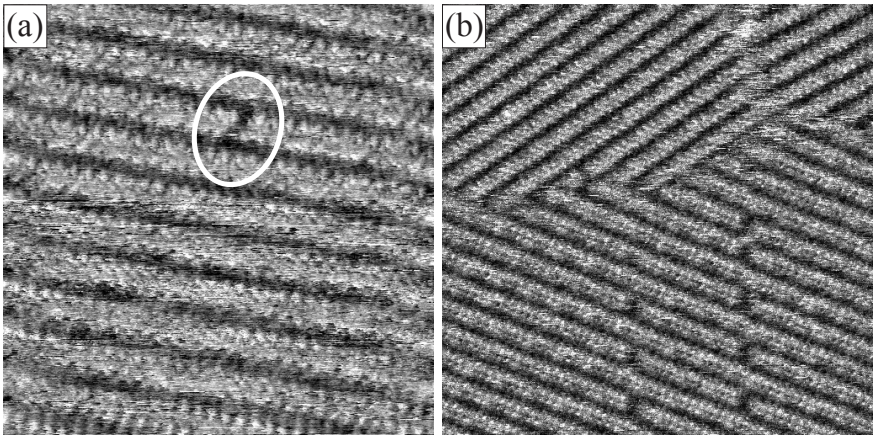


Figure 5.10: Single molecular defects were observed. Sometimes even in ordered rows (b), skipping every second molecular stripe. (a) $U_{bias} = -1040$ mV; $I_t = 0.9$ pA; size= 30 nm \times 30 nm; z -scale ≈ 0.15 nm (b) $U_{bias} = -900$ mV; $I_t = 0.8$ pA; size= 50 nm \times 50 nm; z -scale ≈ 0.17 nm.

5.1.1.3 Protonation

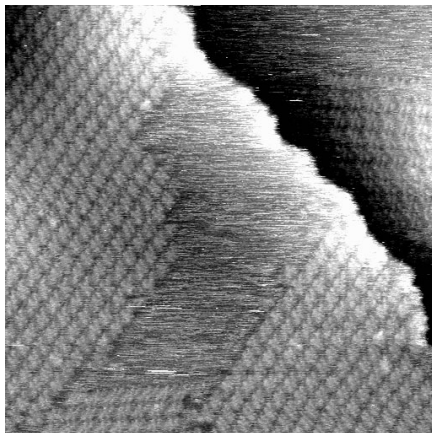
In solution, the free bipy ligand is known to have a time-averaged *transoid* conformation. The obvious way to force it to the *cisoid* conformation is to bind it to a metal ion or a proton. Two approaches were followed to induce protonation, and the respective change of conformation, as described below.

Protonation in liquid After treatment with acetic acid, no different pattern was discernible. The same ordered domain structure as before was seen. It was more difficult to prepare the monolayers, but otherwise no difference could be observed. After complexation with Pd(II) and Cu(II), the molecules could not be imaged with STM on a graphite surface. Slightly different preparation methods were tried, but no domain formation could be observed. It could be recognised, that entities left back after the evaporation of the solvent were on the surface, but as they did not self-assemble, only noise and movements could be observed.

Protonation on the surface Fresh samples were prepared as previously described and shortly measured, to assure that the self-assembly took place. These samples were then brought into contact with dilute aqueous solutions, of either acetic acid or hydrochloric acid, for different time intervals. After this treatment, the droplet of the acid solution was removed by gentle suction applied with blotting paper, and the sample was remounted in the STM. Large areas of several samples were examined in the hope of finding a *cisoid* conformer. No difference could be detected after these acid treatments. Only *transoid* conformations and the molecular stripes discussed above were found. It cannot be excluded that protonation occurred, but it can be concluded, that a vast majority of the molecular layers did not change the arrangement, nor the conformation of the molecules, nor the packing density. To flip into the *cisoid* conformation, the molecules would have to desorb at least half of the molecule. The physisorption energy of half the ligand seems to be larger than the available energy at room temperature under protonating conditions – the molecules could not flip into the *cisoid* conformation, which it is known to adopt preferentially, when the bipy is protonated in liquid. To exclude the hydrophobicity of the molecule as the cause preventing the change of conformation, freshly prepared and checked samples were placed for about 15 sec. in a gentle stream of gaseous hydrochloric acid³. Even these measurements showed a majority of unchanged, *transoid* domains such as those

³ Prepared by placing a few drops of H₂SO₄ on NaCl.

Figure 5.11: A rare observation of the *cisoid* conformation of the first generation bipy dendrimer. Despite the large thermal drift, it is clearly recognisable that no *transoid* conformation can build this arrangement. The ragged line in the top right is a graphitic step edge. Parameters: $U_{bias} = -800$ mV; $I_t = 0.9$ pA; size= 50 nm \times 50 nm; z -scale ≈ 0.2 nm.



discussed above. With the treatment of gaseous HCl, on rare occasions, domains that could be assigned a *cisoid* conformation were observed. Figure 5.11 shows such a measurement. Despite the thermal drift, a *transoid* conformation could be excluded. For one reason, no *transoid* molecule fits, when tested with the method of analysis used above and always considering the interpolated measurement between two sequential images. And for another reason, the periodicity of *two* protrusions (instead of *one*) along the stripes seems only realistic with a *cisoid* arrangement. There is no known reason, why identical *transoid* molecules should behave differently with a periodicity of two molecules.

5.2 Variations of the alkoxyated second generation Fréchet-dendrimer

The four derivatives of the second generation of the octyloxy-substituted Fréchet-dendrons displayed in figure 5.12 were studied. Using the second generation, more degrees of freedom are introduced: four additional Ar–OCH₂Ar groups can adopt two possible conformations on the surface. The expected dimensions for some of the conformations are shown in figure 5.12 (e) and (f).

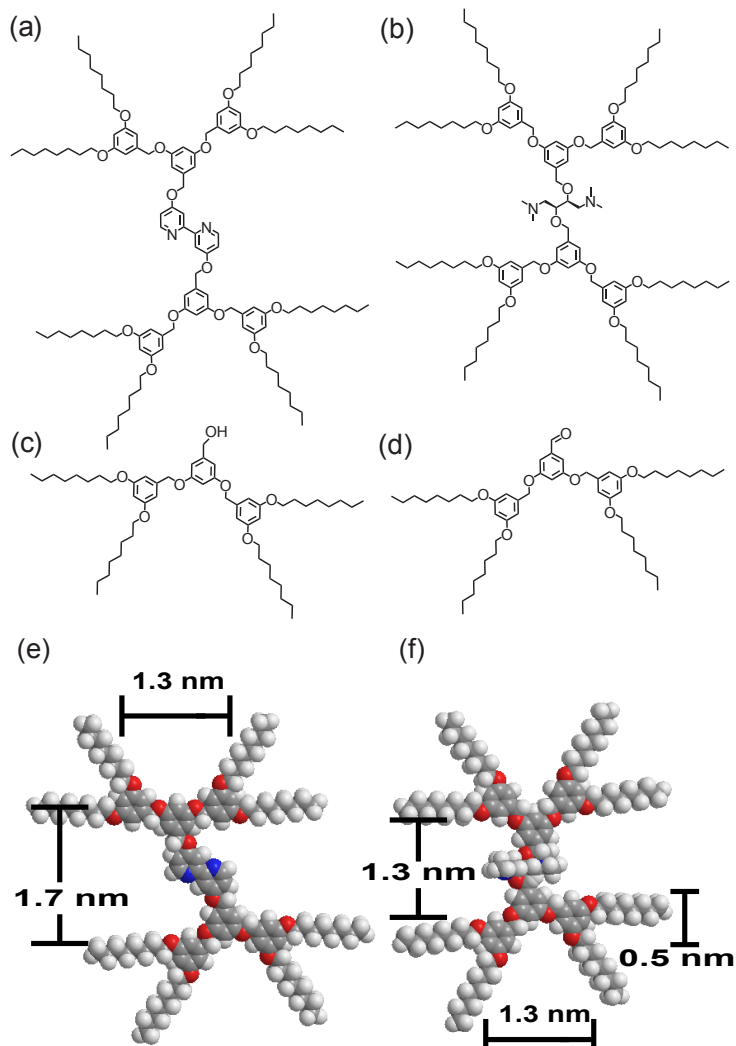


Figure 5.12: (a) and (b): bipy and DDB, expanded with two alkoxyated second generation Fréchet-dendrons. (c) and (d): alcohol and aldehyde derivative of the dendron. Space-filling representations with estimated sizes for one conformation of the second generation bipy dendrimer (e) and one conformation of the *S,S*-DDB dendrimer (f). The alcohol and aldehyde are of the same size as the dendron dimensions indicated in (f).

5.2.1 A bipy-ligand, expanded with two alkoxyated second generation Fréchet-dendrons

The structural formula of the second generation bipy-dendrimer is shown in figure 5.12 (a). It was expected to form lamellar domains similar to the first generation dendrimers (see above). For steric reasons, the *cisoid* conformation is less likely to occur. The samples were prepared by “solution casting” from 0.2 mM solutions, as done with the first generation.

5.2.1.1 Results and discussion

While the first generation bipy-dendrimer was the most “reliable” molecule, studied in this thesis, the second generation was much more difficult to characterise on a surface. The interaction energy of the alkyl-chains with the graphite should be doubled, because the number of chains is doubled. But the closest packing is not covering the surface as densely anymore, so that some of the two-dimensional crystallisation energy is lost. This should be more than compensated by the additional π - π interactions between the four additional phenyls and the graphite. For the larger molecules, the mismatch between the bond lengths and angles of the dendrimer, and the graphite becomes more noticeable. It was much more challenging to get stable images of the second generation dendrimer. Only relatively small, ordered domains were found, such as shown in figure 5.13. It is absolutely necessary to scan with very low tunnelling currents. The achieved resolution was somewhat lower than for the first generation. Nevertheless, two different conformations could of the molecule be distinguished. Using averaged images of two neighbouring domains two conformations were distinguished. Figure 5.14 shows these measurements with overlaid molecular models to display the different conformation and orientation. A conformation analysis was performed, similar to the first generation. Only the two domains shown in figure 5.14 were sufficiently resolved to allow a definite association with a conformation. No reason is known, why those two conformations should be more stable than most of the other possible conformations, but those two are the only ones that could be identified. It can not be excluded, that the others were formed, or even measured. It may be solely due to the instability of the measurements, that only these two conformations could be identified. The alkyl-chains were not modelled, and therefore overlap with neighbouring molecules in this simple picture. The chains are expected to lie flat and straightened in an interdigitating pattern. A lot less two-dimensional crystallisation energy can be gained, compared to the lamellar domains of the

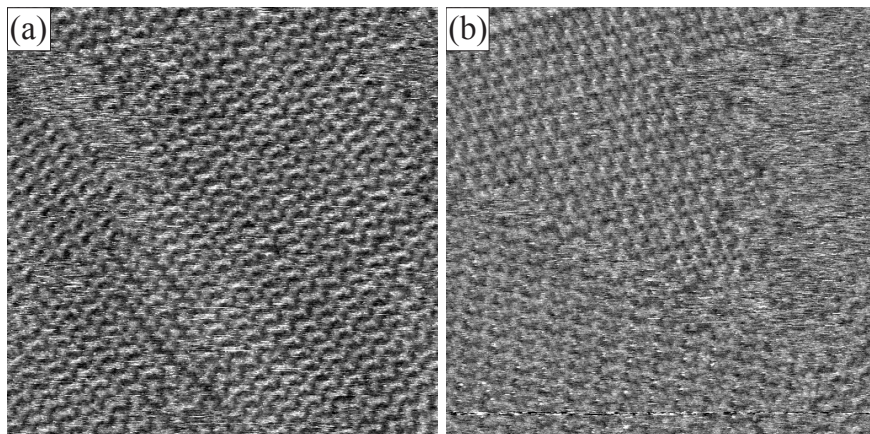


Figure 5.13: Two images showing the relatively small domains formed by the second generation bipy dendrimer. Different orientations with different internal structures can be recognised. Parameters: (a) $U_{bias} = -750$ mV; $I_t = 0.65$ pA; size= 60 nm \times 60 nm; z-scale ≈ 0.15 nm; (b) $U_{bias} = -750$ mV; $I_t = 0.65$ pA; size= 50 nm \times 50 nm; z-scale ≈ 0.15 nm.

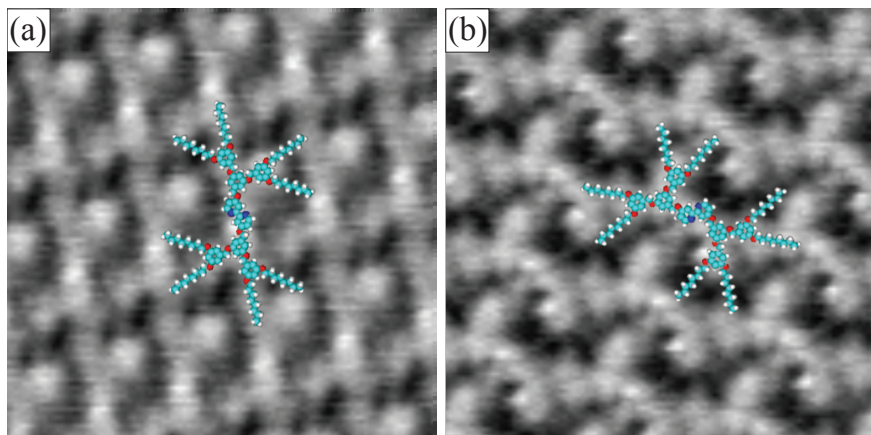


Figure 5.14: Averaged images of the two domains seen in fig. 5.13 (b), with one molecular model of each of the corresponding conformations. The relative orientation here reflects the orientation found on the sample. The alkyl-chains were not modelled, and are drawn in an all-*trans* conformation, that would overlap with the neighbouring molecules. Some chains will probably be folded back between the molecules. Parameters: $U_{bias} = -750$ mV; $I_t = 0.65$ pA; size= 10 nm \times 10 nm; z-scale ≈ 0.15 nm (a) averaged over 48 and (b) over 70 positions.

first generation, because in this case, the molecules do not form lamellar domains. The alkyl-chains are not aligned in stripes between stripes of the aromatic centre. Some of the chains seem to be folded back between the aromatic centres of the molecules.

The central region of the molecules around the bipy seems to have a preferred conformation. The inner part of the second generation molecules, that is their first generation part, shows the same two conformations that were found for the first generation (compare to fig. 5.9 on page 61). Interestingly, no molecules were found displaying a *Z*-like conformation, that is with a bipy that is lying “on the other side”. The question arises, whether a pure lamellar phase could be formed with a second generation molecule comprising a different centerpiece. To address the possibility that a smaller centre could help to prevent a back-folding of the chains, and therefore increase the stability of the monolayers, by increasing the total two-dimensional crystallisation energy another dendrimer, having a smaller centre, was measured.

5.2.2 A chiral DDB derivative, expanded with two alkoxyated second generation Fréchet-dendrons

An apolar, dendritically expanded derivative of *S,S*-1,4-bis(dimethylamino)-2,3-dimethoxybutane (*S,S*-DDB) has been synthesised by P. Murer in the group of D. Seebach, to study its catalytic properties. No x-ray characterisation was possible because the dendrimer does not crystallise. The *S,S*-DDB was covalently bound in a dendrimer, that mimics an inverse micelle, and its synthesis is described in [123, 124]. T. Butz (group of D. Seebach) found, that with the *S,S*-DDB dendrimer as chiral modifier, the catalysis of the addition of methanol to methylphenyl chains to 2-phenylpropionic acid methylester proceeds significantly more enantioselectively than with pure *S,S*-DDB [120]. The second generation of the *S,S*-DDB dendrimer was studied with STM in the scope of the diploma thesis of I. Widmer and this PhD thesis. Despite its flexibility, it is found to lie flat on a graphite surface.

This dendrimer was dissolved in dichloromethane or hexane, and a droplet of the 0.2 mM solution was put on a freshly cleaved HOPG substrate to study its assemblies with STM.

5.2.2.1 Results and discussion

Without any further external influence, the molecules assembled in regular domains, that is to say, they were observed from the first scan line, and no

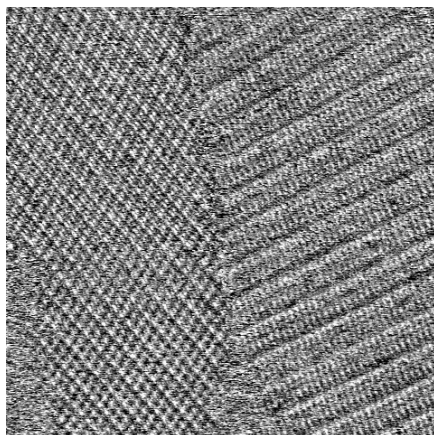


Figure 5.15: A boundary between two differently oriented domains of the DDB dendrimer. Parameters: $U_{bias} = -700$ mV; $I_t = 0.65$ pA; size = 140 nm \times 140 nm; z -scale ≈ 0.2 nm.

domain-formation in unordered regions was observed after scanning repeatedly over them.

Domains and superstructures All observed DDB-dendrimers were organised in lamellar domains, similar to the first generation bipy-dendrimer. Already the first scan line after the approach of the STM tip showed the ordered domains. The *S,S*-DDB dendrimers appeared as bright stripes, that could be resolved down to submolecular resolution. Three orientations of these domains were observed, with an angle of 120° between them (figure 5.15). The space between the domains is filled with highly mobile molecules. The DDB-dendrimer formed monolayers of a stability similar to those of the second generation bipy-dendrimer, therefore, very “soft” scanning parameters had to be applied. Applying more than about 1 pA results in the destruction of the layers.

Two different superstructures were observed on the stripes. At a periodicity of two molecules perpendicular to the stripes, the protrusions were higher. The superstructures become most obvious when an image is heavily fourier-filtered (lowpass), as figure 5.16 (b). Along the stripes, every fifth and sixth molecule was imaged slightly higher. In the past, similar patterns have been observed due to a lattice mismatch of some (rigid) layer on top of a substrate with a slightly different periodicity, similar to a Moiré-pattern. One example of such a superstructure, caused by the lattice mismatch of alkanes on graphite was observed by J. Rabe in [101]. As explained in the introduction to this chapter and in [101, 114], the adsorption energy for long

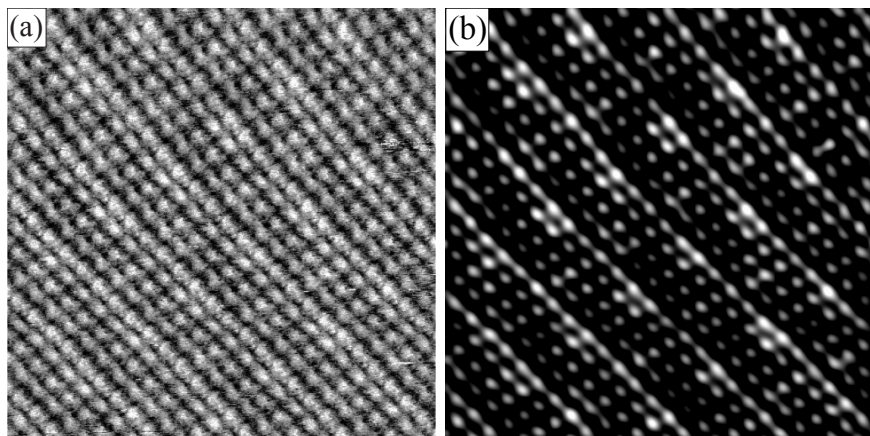


Figure 5.16: (a) A domain of the DDB-dendrimer showing both the superstructures, and (b) an extremely lowpassed version of the same image, to show the superstructures more clearly. Every fourth stripe (half of every second molecule) appears higher; and every fifth and sixth molecule along those stripes appear higher. Parameters: $U_{bias} = -700$ mV; $I_t = 0.9$ pA; size = 30 nm \times 30 nm; z -scale ≈ 0.15 nm, measured by I. Widmer

alkanes on graphite is larger than the 2D crystallisation energy by a factor of about two. The DDB-dendrimer has a higher interaction with the graphite due to the π - π overlap of the benzylethers with the graphite. In addition to this, the alkyl-chains cannot form a packing as dense as in the 3D-crystal or in a pure alkane layer. Therefore, an incommensurability can be excluded as the cause of the superstructure. The superstructures were not always observed as regularly as in figure 5.16, but often they showed mismatches and faults. Many measurement did not show any superstructure at all. This is a further clue, that the superstructure is caused by different molecular conformations rather than lattice mismatches between the molecules and the graphite (see below).

Defects On rare occasions, single molecular vacancies in the monolayers were observed. One is shown in figure 5.17. Domain mismatches with half a molecule offset between the domains were also observed (not shown).

Conformational analysis Each DDB molecule showed two triangular protrusions, consisting of three benzene rings each. The aromatic moieties of the molecule are expected to be in the positions where the atoms of the next

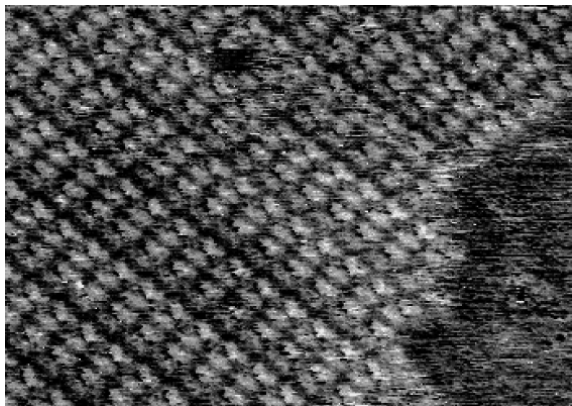


Figure 5.17: A domain of the DDB-dendrimer with a single molecular vacancy.

Parameters: $U_{\text{bias}} = 700 \text{ mV}$,
 $I_t = 1.1 \text{ pA}$, $34 \text{ nm} \times 24 \text{ nm}$,
 $z\text{-scale} \approx 0.2 \text{ nm}$; measured by
I. Widmer and M. Stöhr.

graphite layer, which was cleaved off prior to measuring, used to be. Due to the overlap of the π -orbitals of the molecule with the substrate a higher conductance results, which is imaged as protrusion. The alkyl chains could not be imaged in the range of the applied tunnelling parameters (namely in the T Ω range). To image the alkyl chains, much lower tunnelling resistances would be needed, at which the STM tip destroys the domains and moves the molecules around. In addition, a chemically modified tip, able to interact with the chains, might show more contrast in such a case. The aliphatic centre of the molecule was not seen with the applied scanning parameters. In some images, a small deformation of one protrusion can be seen. This might be the case, when the lone pair of the nitrogen overlaps with the graphitic π -orbitals, that is to say, the methyl groups point upwards and away from the graphite. Using averaged images, a higher resolution was achieved. One molecule shows clearly six protrusions, which can be assigned to the benzene rings. Figure 5.18 shows an example, where the conformation of the molecule could be assigned. By fitting different conformations⁴ of the molecule, the conformation could be determined. Different domains with different internal structure were observed. Figure 5.19 shows a pseudo-3D representation of a domain, that clearly shows the superstructure discussed above. The conformation of the molecules forming this structure could be successfully elucidated. The structure is built from molecules displaying two different conformations that alternate every second row of molecules. Figure 5.20 (b) shows the same measurement in a topview representation, overlaid with two molecular models.

⁴ All probable conformations resulting from flipping the benzylether bridges were tested.

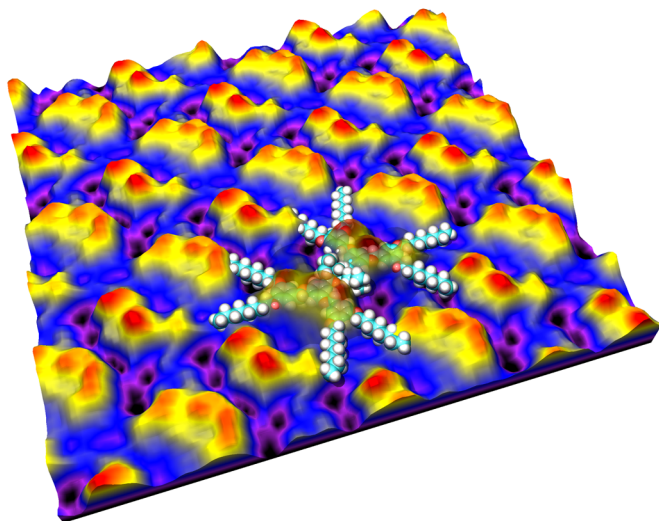


Figure 5.18: A pseudo-3D representation of an averaged STM image with a high-contrast colouring, overlaid with a molecular model showing the conformation. Parameters: averaged over 246 positions in a 50 nm \times 50 nm image. $U_{bias} = -700$ mV; $I_t = 1$ pA; size= 10 nm \times 10 nm; z-scale \approx 0.2 nm. The semitransparent image was combined with the molecular model with POV-Ray.

Stereochemistry Studying the DDB-dendrimer, only domains with a ∇ -like conformation were observed. Never was a ∇ -like conformation measured. At first sight, it is not surprising, that the chiral molecules should display one preferred chirality on the surface. This preference is easily explained with the fact that the molecules lie on that side, in which the central part can point away from the surface. In this way, the maximal π - π overlap between the benzyl-ethers and the graphite is obtained (see formula in figure 5.12 (b) (page 65)). But even with the stereo-centres forcing a central *S*-shaped conformation, if both the conformational switches directly connected to it would point inwards, a ∇ -like conformation would result. Even though this conformation was never observed with the bipy centre, it remains an interesting fact, that it was also not observed with the DDB centre. Up to today, the other enantiomer could not be successfully synthesised by a commercial company or any collaborator. Hopefully, the near future will provide the answer to these questions. It will be a very interesting study to

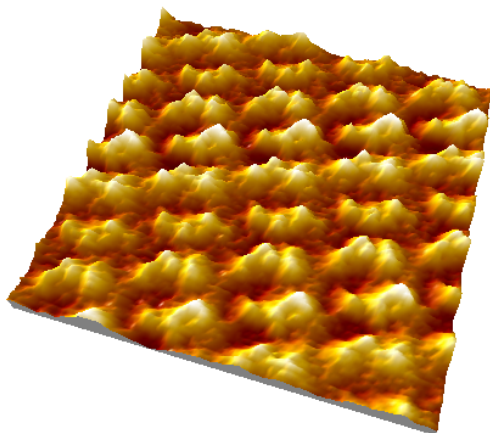


Figure 5.19: A pseudo-3D representation of a domain of the DDB dendrimer, that has the superstructure discussed above. Every second molecule seems to be different. Parameters: $U_{bias} = -730$ mV; $I_t = 1$ pA; size= 10 nm \times 10 nm; z-scale \approx 0.1 nm averaged over 21 positions.

see which patterns the other enantiomer of the DDB dendrimer will form. Also very promising seems to be the study of a racemic mixture. Another question related to this topic is what single, alkoxyated Fréchet-dendrons will do on a surface without a centre, that forces them into lamellar domains. The examinations of the DDB dendrimer show, that the second generation of the Fréchet-dendrons still form a lamellar phase on a surface, even if a small enough centre is used. The function of the centre in the chirality of the arrangement and the question of the arrangement *without* centre will be answered in the next section.

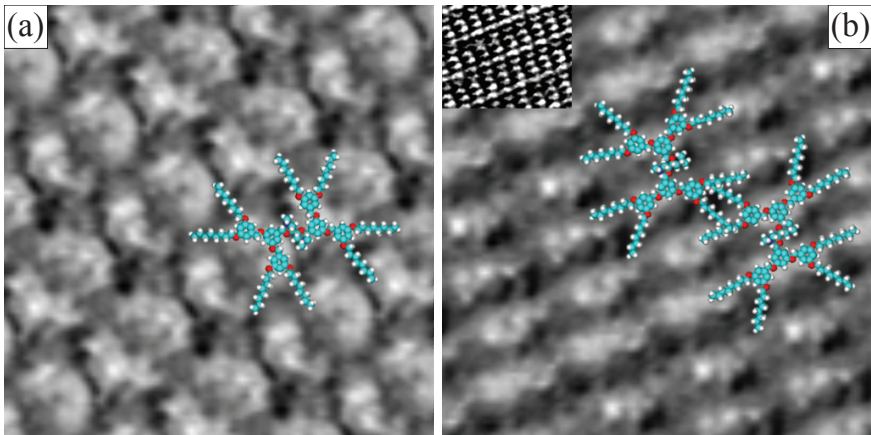


Figure 5.20: Two averaged images with overlaid molecular models. (a) A structure formed by molecules that have all the same conformation, and therefore no superstructure. (b) A measurement with molecules of different conformations. The dendrimers have two conformations in an alternating pattern. Every second row shows the same conformation. The inset at the top left shows a lowpassed section of the image ($20 \text{ nm} \times 16 \text{ nm}$) to display the superstructure. Parameters: (a) averaged over 109 positions in a $50 \text{ nm} \times 50 \text{ nm}$ image $U_{bias} = -700 \text{ mV}$; $I_t = 1 \text{ pA}$; size= $10 \text{ nm} \times 10 \text{ nm}$; z -scale $\approx 0.12 \text{ nm}$. (b) averaged over 127 positions of a $40 \text{ nm} \times 40 \text{ nm}$ image $U_{bias} = -730 \text{ mV}$; $I_t = 1 \text{ pA}$; size= $10 \text{ nm} \times 10 \text{ nm}$; z -scale $\approx 0.1 \text{ nm}$.

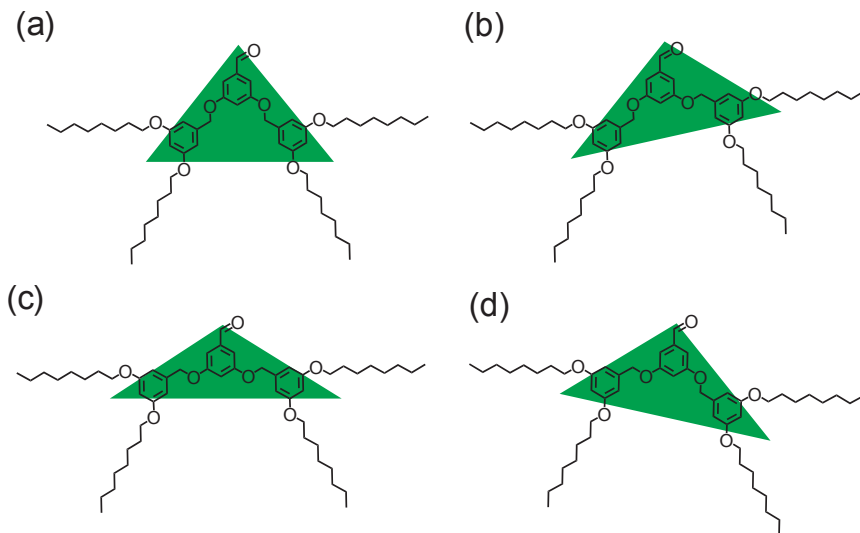


Figure 5.21: The four conformations arising from the two ArOCH₂Ar bridges. The green triangles are a simple abstraction of the contrast, observed in STM images.

5.2.3 Aldehyde derivative of the alkoxyated second generation Fréchet-dendron: a time-delayed molecular rearrangement, accompanied by a conformational change on a graphite surface probed by STM

As already discussed, the alkoxyated Fréchet-dendrons are nonpolar amphiphiles. The formula of the aldehyde derivative studied in this section is shown in figure 5.12 (d) (on page 65) and figure 5.21. These amphiphiles can form supramolecular aggregates, as most amphiphiles do. The dendrimers studied in the previous sections have alkane chains on both ends, and can, therefore, only form lamellar phases or patterns derived directly from them. The aldehyde of a single dendron, however, can also form a disk-like or even an inverse micellar phase. A carboxylic acid derivative of a similar Fréchet-dendron, with longer alkyl chains, was observed to form a disk-like phase on a graphite surface [125]. Figure 5.21 shows the four conformations arising from the ArOCH₂Ar bridges, resulting from the combination of the two conformations that each bridge can adopt on a graphite surface. The STM samples of the aldehyde derivative, studied in this section were prepared like

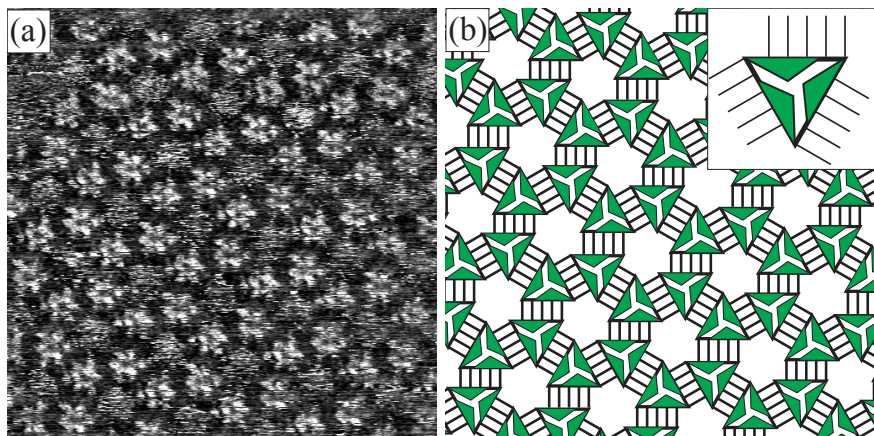


Figure 5.22: (a) A representative image of the “nano-edelweiss” pattern, formed by the aldehyde shortly after the preparation. The structure is a disk-like phase, built from trimers. (b) An abstraction of the pattern. The inset shows an enlargement of a single trimer. The trimers have a rotational orientation and also the resulting hexagonal pattern is chiral. Parameters: $U_{bias} = -700$ mV; $I_t = 1.1$ pA; size= 30 nm \times 30 nm; z -scale ≈ 0.12 nm

all the molecular layers of this chapter. Up to three droplets of a 0.2 mM hexane or dichloromethane solution were put onto a freshly cleaved graphite surface. After evaporation of the solvent, the samples were mounted in the room temperature STM in ambient air.

5.2.3.1 Results and discussion

The “nano-edelweiss” Immediately after the preparation and the approach of the STM tip, a pattern as shown in figure 5.22 (a) was observed, that evoked the expression “nano-edelweiss”. No voltage pulses or prolonged scanning was necessary to observe the pattern, formed by a self-assembly process. The aldehyde self-assembles into a disk-like pattern, similar to the one observed by P. Wu et al. for the acid derivative [125]. What remained undiscussed in [125] was the irregularity of the structure and its chirality (see below). A detailed analysis of this “flower” pattern shows, that the trimers are not identical. All the four different conformations presented in figure 5.21 were found in the measurements. No large scale ordering was found, that is to say, no real periodicity was observed. All conformations were observed,

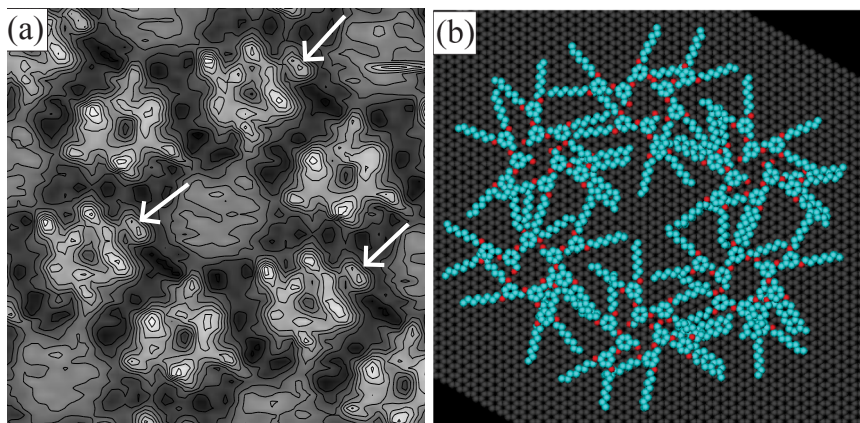


Figure 5.23: (a) An averaged image of the trimeric arrangement. Contour lines are displayed to show the double peaks (marked with white arrows), indicating where two conformations were averaged. (b) Molecular models derived from the measurement in (a), transferred onto a graphite lattice. The different conformations are displayed by two molecules in the same place. The alkanes are not modelled, and their arrangement is discussed in the text. The abstraction in figure 5.24 shows a better model than the chains in the model in (b). Parameters: averaged over 66 positions in a $200\text{ nm} \times 200\text{ nm}$ image; $U_{bias} = -800\text{ mV}$; $I_t = 0.8\text{ pA}$; size = $10\text{ nm} \times 10\text{ nm}$; $z\text{-scale} \approx 0.12\text{ nm}$.

but there was a slight preference for the asymmetric ones ((b) and (d) in figure 5.21). It was probably this irregularity of the pattern, that reminds one on a first look of the flower edelweiss.⁵ This irregularity means, that the correlation averaging procedure used above, has to be employed with care. It is still possible to increase the resolution, but in some locations, several conformations are averaged. This can be recognised as double peaks of a lesser height, as seen in figure 5.23 (a). Contour lines are drawn to show the double peaks. As above, the conformations were printed on transparencies and fitted onto the measurement. The overall pattern is rather irregular, and does not fit on graphite, as the patterns of the lamellar phases discussed in the previous sections do. It was not possible to align all the aromatic rings with the graphite, so that they are in the place of the next graphite layer. A proposed arrangement on graphite is shown in figure 5.23 (b). In the observed lamellar phases, the molecules were always arranged to give

⁵ L. Ramoino, who pointed out this resemblance at the first sight of the pattern, is acknowledged for the expression.

the largest π -interaction with the graphite, and if possible a orientational ordering of the alkyl-chains on the graphite. Here, however, the rotational ordering is not reflecting the graphite lattice. Some molecules can be fitted to be aligned with the graphite, but not all (without changing the pattern found in the measurement). The ratio of adsorption energy to two-dimensional crystallisation energy seems to be shifted in favour of the crystallisation energy (in opposition to the lamellar phases discussed above).

Chiral domains, formed with a unit cell of seven molecules. Neglecting the irregularities, the trimers form a chiral, but periodic pattern. Each trimer has a rotational orientation, as can be seen in the inset of figure 5.22 (b). These chiral triangles are arranged in a pattern of hexagons that also show a rotational order. Built from triangles oriented clockwise, the hexagons show a counterclockwise orientation, and vice versa. This can best be seen, when the edges pointing towards the centre are studied. In each trimer, the triangles (representing the three phenyl-rings) do not point directly towards the centre, but either to the left or to the right of it. The same is observed for the triangles formed by the trimers. Each trimer-triangle points either to the left or to the right of the centre of the hexagon. Figure 5.24 (c) shows an abstraction of a hexagon of trimers. Both chiralities were observed. Figure 5.24 shows two averaged images from two domains of different chirality, enlarged from a single STM image. The fact that the molecules do not point towards the centre of the trimer results in a hollow centre, where bare graphite is visible. This rotated structure could be the result of a non-classical hydrogen bond. In the pattern derived from the averaged measurements, an aromatic hydrogen lies very close to the oxygen of the aldehyde, and the C-H \cdots O atoms lie in a straight line. Due to the drift, the angle between the two domains of different chirality was difficult to measure, but was found to be around 15°.

At low resolution, the flower pattern discussed above can be mistaken for a trigonal pattern. The centre of the hexagons is roughly of the same size as a single trimer. In highly resolved images (or in the averaging process) it is clearly recognisable, that no trimer is located in the centre. The central part of each hexagon is very noisy. That the noise is random noise is confirmed by the smooth structure that results upon averaging, seen e. g. in figure 5.23 (a). Nevertheless, the central part is neither as flat, nor as low (in z) as the blank graphite, that was observed at sub-monolayer coverages between the ordered domains. The noisy centre reminds of the mobile phases discussed in the previous chapter. The obvious speculation is, that one or several

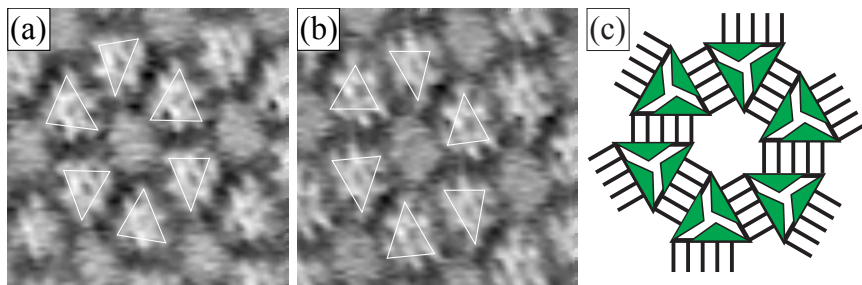


Figure 5.24: Two averaged enlargements of an STM image displaying both chiralities. (a) A hexagon with a counterclockwise orientation. (b) A hexagon from the other domain, showing a clockwise orientation. Thermal drift elongates both images in one direction (top left to bottom right). The white triangles are drawn to show the orientation. (c) An abstraction of a hexagon, forming a clockwise orientation. The angle between the domains in (a) and (b) was about 15° . Parameters: (a) averaged over 12 and (b) over 16 positions. $U_{bias} = -700$ mV; $I_t = 0.9$ pA; size = 13.9 nm \times 13.9 nm; z-scale ≈ 0.16 nm

molecules are trapped in the hexagon, but are highly mobile. Rotation and translation inside the hexagon prevent molecular resolution. The fact that these molecules are not “crystallised” like those, that form the hexagon around, can probably be explained as follows. As already drawn in the abstracted models, the trimers form two-dimensional analogues of inverse micelles (see inset of figure 5.22). They form a centre, consisting of the aromatic region of the molecules and display the alkyl-chains towards the outside. In order to maximise the two-dimensional crystallisation energy, the alkyl-chains are expected to form interdigitating patterns with the alkyl chains of the neighbouring trimers. As seen in the abstracted images as well as in the measurements, the trimers form roughly equilateral triangles. When these form a hexagon, they display a side parallel to the side of the neighbouring triangle. Like this, the interdigitation reaches a maximum. As can be seen in the abstraction of a hexagon in in figure 5.24 (c), this results in a hexagon formed of alternating aromatics and aliphatics. No (or at most very few) alkyl-chains are left to dangle into the centre of the hexagon. The mobile molecule in the centre simply has no “partner” to form a two-dimensional alkane-crystal. It has no fixed lattice space, and therefore a high mobility at higher speeds than the STM measurements. More conclusive arguments, explaining why exactly *one* molecule is located in the centre, are given two paragraphs below. Neglecting the randomness of the orientation of

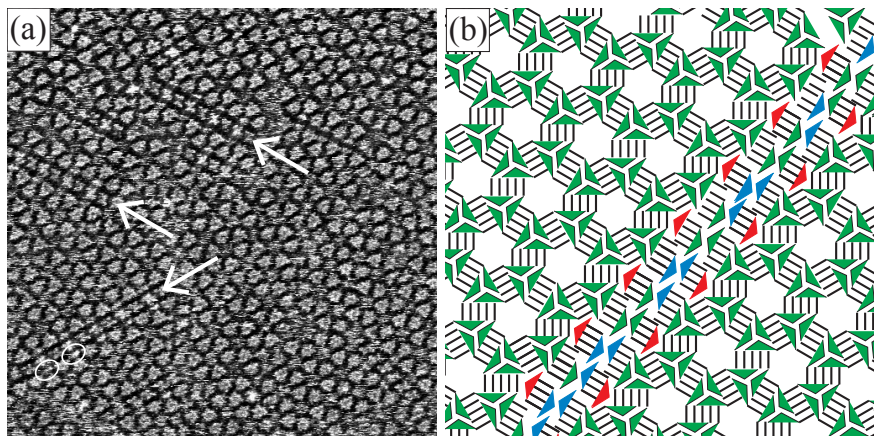


Figure 5.25: (a) A measurement, displaying a trimeric pattern with some embedded rows of dimers (marked with arrows). (b) Abstraction of the pattern. Note, that single molecules (red, white ellipses in (a)) are filling up the pattern, so that a space-filling arrangement results. Parameters: $U_{bias} = -700$ mV; $I_t = 0.9$ pA; size= 80 nm \times 80 nm; z -scale ≈ 0.16 nm

the central molecule and the variations of the conformations, these hexagonal patterns have a unit cell of *seven* molecules. This unit cell comprises two trimers and one centre.

Rows of dimers The domains formed from the hexagons were always rather small. Some domains were interrupted with a different molecular pattern. Single rows of dimers were observed embedded in the hexagonal pattern of trimers. Figure 5.25 shows a measurement with such a row of dimers and an abstract model of the arrangement. These rows of dimers were observed in three orientations, as expected for such a pattern on graphite. Some measurements even showed two rows in parallel with only one row of trimers between them. The single molecules, that complete the space-filling pattern in two dimensions are neither part of the dimers nor of the hexagons (marked red in fig. 5.25 (b)). They are located in the centre of half a hexagon. They have less space available, and, what seems more important, they have a “partner” available to form an interdigitating alkane-grid available. One molecule of the row of dimers extends its alkyl-chains towards this molecule, and the molecule is fixed in its location and can therefore be imaged with STM. These molecules have their aromatic region towards the half-hexagon,

which is a further indication, that no alkyl-chains are extended towards the centre of the hexagons. However, despite those single rows of dimers, no lamellar phase could be observed on freshly prepared samples.

Conversion into a lamellar phase. The hexagonal pattern, consisting of trimers and one mobile molecule in the centre, was not stable over time. After about one hour, the disk-like phase changed into a lamellar phase. The conversion could be followed by STM. A domain, consisting of dimers, appeared from outside of the observed window in the measurement, and spread over all the observed area. The dimers formed a lamellar phase, similar to those formed from the DDB-dendrimers. It is worth emphasising, that the conversion always started outside of the measured range and spread to areas much larger than it. This was noted, when the scan range was enlarged, after the observation of the conversion, and when locations millimetres (!) away from the previously measured area where measured. Figure 5.26 shows a series of sequential images to document the transformation.

The newly formed domain is built from dimers, that is to say, the lamellae are built of two molecules that are close together with a larger separation to the next neighbours. Because the two molecules of a dimer do not face each other directly, but are closer together with a lateral offset, this pattern also displays an orientation, similar to the one observed in the lamellae formed from the DDB-dendrimer. The two triangles formed by the aromatic parts of the molecules can either face the left or the right side of the other, forming a pattern resembling a ∇ - or a \triangleleft -like form. The pattern is not formed from simple rows, but clearly from dimers, that compensate their dipole moments. Figure 5.27 shows an averaged measurement and a model of the proposed arrangement. The lamellar phase was analysed and the molecular conformation was determined. It is interesting, that only *one* conformation of the molecules was found. The rows of dimers all consist of molecules in the same conformation. Probably due to the chemical composition of the STM tip, in figure 5.27 (a), even the alkyl-chains are resolved. They can be recognised in the raw measurement, and appear even clearer in the averaged enlargement that is shown. This means, that even the alkyl-chains have the same conformation for each molecule. The one chain, that points towards the next neighbour in the row, is bent to lie as parallel as possible to the rest of the chains in the lamella. This corresponds nicely to the crystal structure published by B. Rheiner et al.⁶ [126]. The lamellar phase was observed to

⁶ Note, that the publication claims to show the x-ray structure of an alcohol, although the C-O bond length corresponds to an aldehyde.

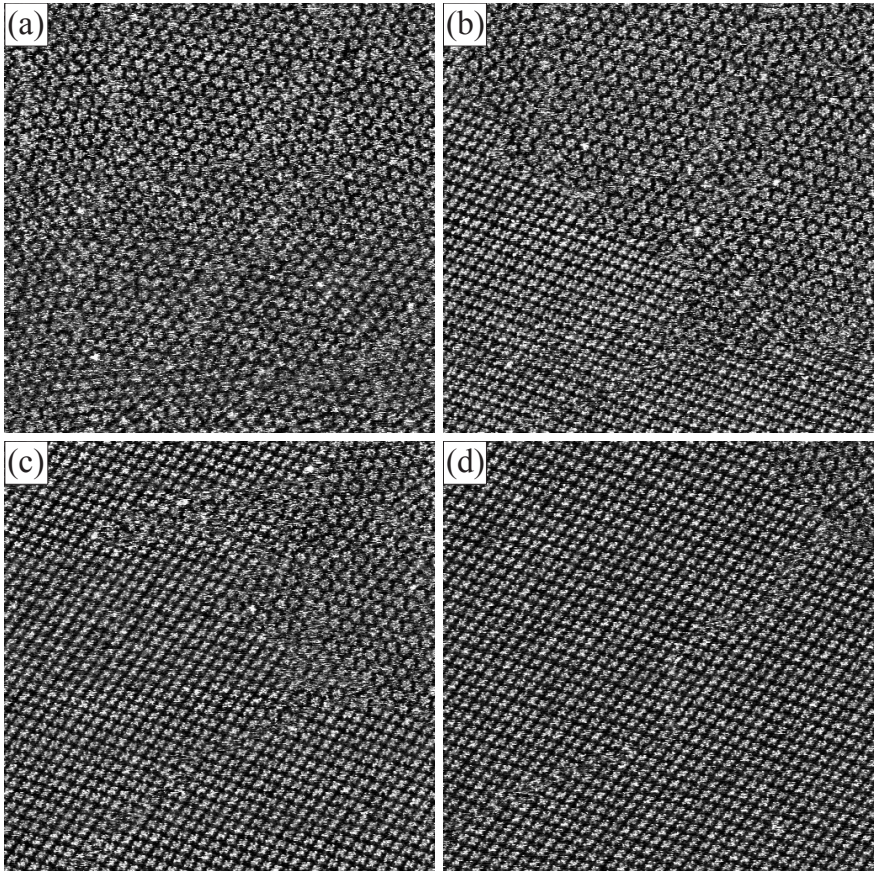


Figure 5.26: Four sequential images, that show the conversion of the irregular, disk-like phase into the regular lamellar phase. About 1 hour after the preparation, the flower pattern, built from trimers, was changed into a stripe pattern, built from dimers. Parameters: $U_{bias} = -700$ mV; $I_t = 0.9$ pA; size= 100 nm \times 100 nm; z-scale \approx 0.15 nm

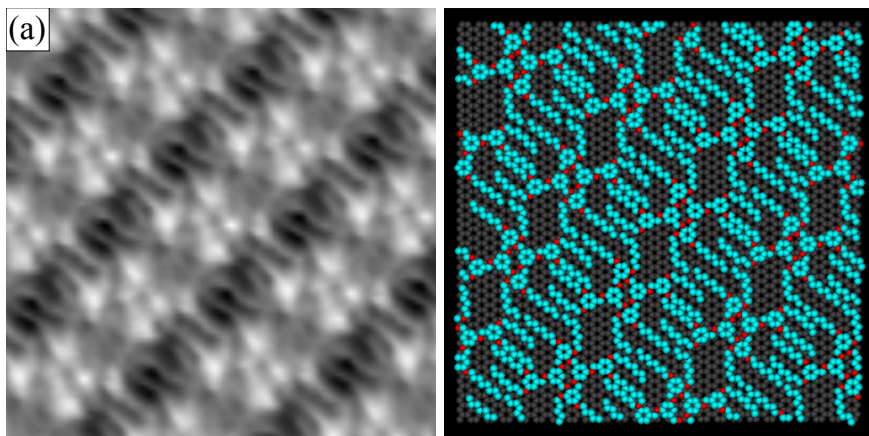


Figure 5.27: (a) The dimeric form, arranged in a lamellar phase, after about 2 h. Averaged over 82 positions in an $50 \text{ nm} \times 50 \text{ nm}$ image. Parameters: $U_{bias} = -700 \text{ mV}$; $I_t = 0.82 \text{ pA}$; size = $10 \text{ nm} \times 10 \text{ nm}$; $z\text{-scale} \approx 0.2 \text{ nm}$. (b) A model of the proposed arrangement.

be stable over several days.

Thanks to the observed spontaneous conversion, the question of the mobile centre of the hexagons could be answered. The surface coverage was calculated for both arrangements. By comparison of the coverage, it could be established, that exactly one molecule must form the mobile centre of the hexagons. The assumption, that no huge flow of molecules (a molecular tsunami?) takes place during the conversion, was used. The newly formed domain was always much larger than the small, hexagonal domains, which it was converted from. The lamellar domains were very well ordered, up to $400 \text{ nm} \times 400 \text{ nm}$ could be observed without any irregularity. On a larger scale, the molecules were not recognisable anymore at the technical resolution of 512×512 pixels that was available, therefore no end of the domain could be found. Only in one occasion, a domain mismatch was observed. Only three samples were studied so far, but all these showed domains formed from a ∇ pattern. Even at different macroscopic places (millimetres apart), only this chirality could be found. This could be attributed to the low number of tested samples. So far, therefore the statistical data available is not significant. Nevertheless, we are confident, that the ongoing research of this topic will settle the question of the existence of the other chirality. There is no

known reason, why only one chirality should be formed. So far, it can be concluded, that only very few initiators trigger the conversion, and that the conversion really “flows” over the surface, rearranging the molecules.

Further discussion of the conversion. From the observations made, the hexagonal phase seems to be metastable. Only after about one to one and a half hour, the conversion could be observed. The hypothesis, that inverse micelles formed in solutions of hexane are imprinted directly in two-dimensional analogues on the graphite, could be disproved. Measurements from dichloromethane solutions show the same metastable trimeric domains, that are converted into a dimeric domain after a delay. The fact that the conversion was only observed after a long time, and that the resulting domains were very large, leads to the conclusion that only very few initiators start the conversion. The obvious proposition, that the rows of dimers, that are found in the trimer phase, initiate the conversion could never be confirmed. The embedded rows of dimers proved stable over the observed time, and were even converted into the lamellar domain with a different orientation, as can be seen in figure 5.26. Another self-evident idea for a possible trigger, was the temperature. Freshly prepared samples are slightly cooler than their environment, due to the evaporation of the solvent. Since this should be levelled after much less time than one hour of measurement, this cannot be a plausible explanation for a trigger. Additionally the low thermal drift that was observed during the measurements indicates, that at least the temperature of the STM and the sample were almost homogeneous. If a trigger temperature would be reached over a homogeneously warm sample, many more initiators would be expected. The STM itself could be excluded as a trigger, because shortly after the conversion was observed, a manual offset of more than a millimetre was made. A place of the sample was measured, that was too far away to be influenced by the previous measurements, and the conversion was already complete there. The search for the initiators of this conversion certainly needs more experiments, to narrow the possibilities. An incredible loss of entropy accompanies the observed conversion. It is in a similar range as the entropy loss of most self-assembly processes. Is it time-delayed self-assembly? A short list of entropy-losses, occurring in the self-assembly process, will be given. First, four different conformations of the molecules are converted into only *one*. Second, the “seventh molecule” with many degrees of freedom is fixed into *one* conformation and *one* lattice space. This is directly comparable to self-assembly processes taking place

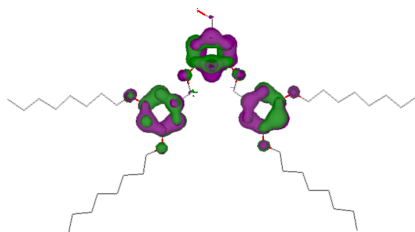


Figure 5.28: The calculated HOMOs (HOMO 0-5) for the alcohol derivative of the alkoxyated Fréchet-dendrimer. Again, at the highest energy a cluster of filled orbitals is found on the aromatics, extending to the oxygens. The colours purple and green denote the sign of the wavefunctions.

on a surface, after vapour-phase deposition. Third, many small domains of different chirality are converted into one large domain with only one chirality.

Many questions still remain unanswered. A few will be discussed in the outlook, and one will be answered in the next section: can the metastable hexagonal pattern, formed by trimers, be stabilised into a stable arrangement? Or in other words, is it possible to stop the conversion?

5.2.4 Alcohol derivative of the alkoxyated second generation Fréchet-dendrimer

In an attempt to fix the trimeric flower pattern, described above, the alcohol derivative of the dendrons was used. The formula can be seen in figure 5.12 (d) (page 65) or figure 5.28. The preparation of the patterns with the alcohol derivative should result in hydrogen-bonded trimers, similar to those observed for the acid of a similar dendron [125]. The structure of the HOMOs was found to be the same as for the aldehyde, as shown in figure 5.28. The STM samples were prepared in the same manner. One or two droplets of a 0.2 mM solution were put onto a freshly cleaved graphite substrate. After the evaporation of the solvent, hexane or dichloromethane, the sample was mounted in the STM.

5.2.4.1 Results and discussion

Again, as for the aldehyde derivative, the structures *self*-assembled without any further external interaction. The expected hexagonal pattern could be observed from the first scanline onwards. Also with the alcohol derivative, the formed pattern was chiral. Both chiralities could be found. Figure 5.29 (b) shows a boundary between two domains of different chirality. The observed trimeric pattern was stable over days, and no transformation into any other phase was observed. Astonishingly, single rows of dimers, embedded in the trimeric pattern, were observed. One is shown in figure 5.29 (a). This

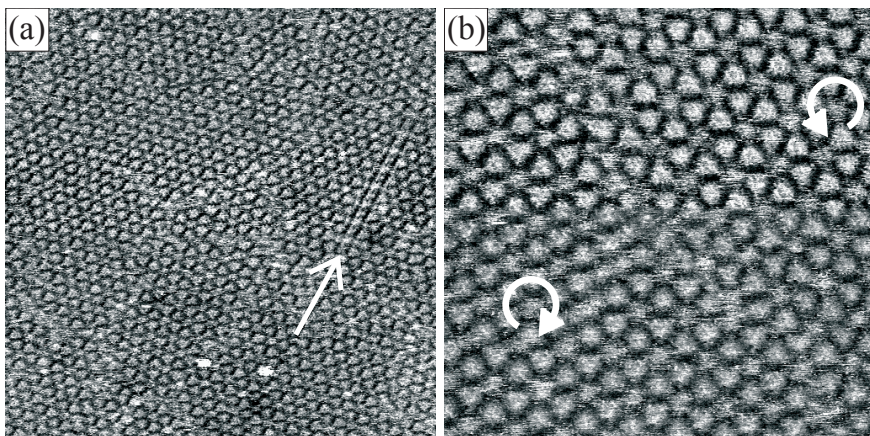


Figure 5.29: (a) A monolayer of the alcohol derivative of the second generation Fréchet-dendron. Many domains and a row of dimers (marked with an arrow) can be seen. (b) At a smaller scale, the two different orientations can be recognised. The boundary between the two domains is running from top left to bottom right. Parameters: (a) $U_{bias} = -700$ mV; $I_t = 1.5$ pA; size= 100 nm \times 100 nm; z-scale \approx 0.12 nm; (b) $U_{bias} = -400$ mV; $I_t = 0.8$ pA; size= 50 nm \times 50 nm; z-scale \approx 0.12 nm.

is a further indication, that the transformation of the aldehyde is not triggered by these rows of dimers. The fact that the flower pattern remained stable with the alcohol means, that it was possible to stop the conversion by increasing the energy barrier height. Additional energy would have to be spent to break the three hydrogen bonds, forming a trimer.⁷

Upon closer examination, the trimeric pattern looks slightly different from the pattern formed from the aldehyde. The little hole in the centre of each trimer seems less pronounced or missing. This is no surprise, as the alcohol groups are expected to form a central six-membered ring, consisting of O and H atoms bridged by hydrogen bonds. Figure 5.30 shows a pseudo-3D representation of an averaged image of the hexagonal pattern of the alcohol. No depression in the centre of the trimers is seen, indicating that not the bare graphite, but the six-fold ring of hydrogen-bonds is observed. The rather high tunnelling current of 10 pA, that could be applied, indicates also an additional stability in respect to the pattern formed from the aldehyde derivative. Although the resolution achieved was slightly lower,

⁷ The additional energy barrier height is even less than the three hydrogen bonds, because the non-classical hydrogen bonds of the aldehyde are not to be accounted anymore.

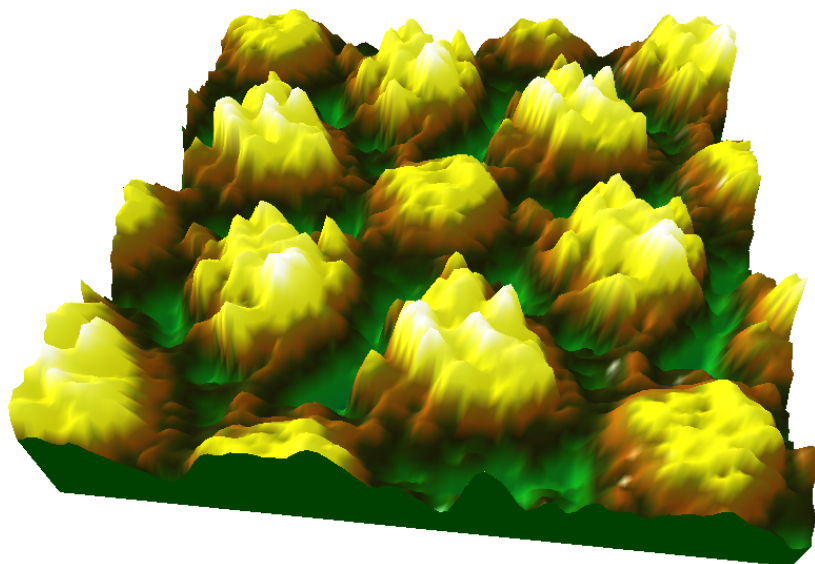


Figure 5.30: A pseudo-3D representation of the hexagonal pattern formed from trimers of the alcohol. The centres of the trimers do not show a depression as the aldehyde does, but are filled with a six-membered ring of the hydrogen-bonded alcohol groups. Parameters: averaged over 63 positions of a $50 \text{ nm} \times 50 \text{ nm}$ image. $U_{bias} = -1000 \text{ mV}$; $I_t = 10 \text{ pA}$; size= $10 \text{ nm} \times 10 \text{ nm}$; z-scale $\approx 0.2 \text{ nm}$.

than with the aldehyde, a conformational analysis could still be performed. Only three of the four possible conformations were observed. This might be due to the low statistics. Again, no real periodicity was found, once the conformations were considered. The domains were rather small (some 10 to about 150 nm).

6. AFM VISUALISATION OF TRIBLOCK-COPOLYMER VESICLES

The STM reaches one of its limits when the molecules or molecular systems are about 100 times larger than those studied in the previous chapters. Usually, only thin films or monolayers of organic molecules are conductive enough to allow successful STM measurements. The atomic force microscope stands in at these limitations. No electrical conduction is necessary and the measured sizes can be as large as several hundred micrometres. The mode of operation of an AFM is shortly explained in section 1.2.1.

In this chapter, a preliminary AFM characterisation of polymeric vesicles is presented. Parts of this chapter will be published in [65]. These studies were done in close collaboration with J. Grumelard (preparation of the vesicles) in the group of W. Meier.

From the perspective of applications, the nanocontainers formed from polymer or lipid vesicles can be included in a more general group containing also the dendrimers 1.1.1 since both systems show a globular structure in solution and both are claimed to be able to encapsulate smaller entities. Whereas the picture of a dendrimer is mostly associated to a lipidic micelle (a so-called unimolecular micelle); the vesicular structures obtained from amphiphilic polymers can be related to their lipidic counterparts, the liposomes. Due to their inner void core and the possibility to manufacture larger superstructures, vesicles are more obvious containers than dendrimers are. Many variations of microcapsules and nanocontainers receive currently much interest. Manipulations such as swelling and shrinking in response to changes in the surrounding media, is studied [127]. Many of these hollow structures are not stable when brought onto a surface, or dried, unless a cross-linked polymerisation freezes their structure. Some even form monodisperse surface micelles [128].

The group of W. Meier synthesises and manipulates amphiphilic triblock copolymers and their superstructures in aqueous media. The used poly(2-methyloxazoline)-b-poly(dimethylsiloxane)-b-poly(2-methyloxazoline)

(PMOXA-PDMS-PMOXA) triblock copolymers form various superstructures in aqueous solutions depending on concentration and other variables. At high concentrations, a cubic phase, that is studied as material for contact lenses, and a lamellar phase were studied. At lower concentrations a vesicular phase, that is examined as nanocontainer was found. The walls of these containers resemble biological membranes. Even membrane proteins can be incorporated and remain functional, providing for instance a way to overcome their impermeability. For a recent review, see the chapter “Nanocontainers” of the *Encyclopedia of Nanoscience and Nanotechnology* [129]. When the polymer is functionalised with methacrylate end-groups, the formed vesicles can be locked in their superstructure through UV-induced free-radical polymerisation and therefore keep their shape and size. These hollow sphere polymers are then very stable and can be dried without change in the structure. As a subproject of this thesis, some non-crosslinked PMOXA-PDMS-PMOXA vesicles were studied on a mica surface. The preparation technique called “solution casting” (see section 2.1.3) that was used to prepare samples of an aqueous solution of vesicles of about 120 nm diameter (measured by TEM). As the vesicles were not polymerised, it was expected that they either reorganise the secondary structure or collapse.

6.0.4.2 Results and discussion

The Vesicles were deposited from aqueous solution onto freshly cleaved mica. A Nanoscope III was used in the tapping mode, with a standard non-contact cantilever from μ -Mash, with a resonance frequency of 150 kHz.

As expected, below the critical vesicle concentration (CVC), that is the lower concentration at which the vesicles are stable, no structure could be observed on the surface. At concentrations of about 0.2 mg/ml, the vesicles could be transferred to the surface. These preliminary studies were done in a dry state, after evaporation of the solvent. Figure 6.1 shows two measurements of the dried vesicles. The vesicles are obviously randomly distributed in a dense packing on the surface. With the evaporation of the water, the vesicles collapsed. This could be derived from the observation that the centre of the circular shapes in figure 6.1 is visibly lower and the shape of the vesicles resembles a deflated ball. The diameter of the vesicles was found to be 136 nm with a very low polydispersity. The apparent height is only a few nanometres, which is a further indication, that the vesicles collapsed upon removal of the solvent. Further studies of vesicles and maybe tubes formed from triblock-copolymers might prove interesting. Immobilisation of

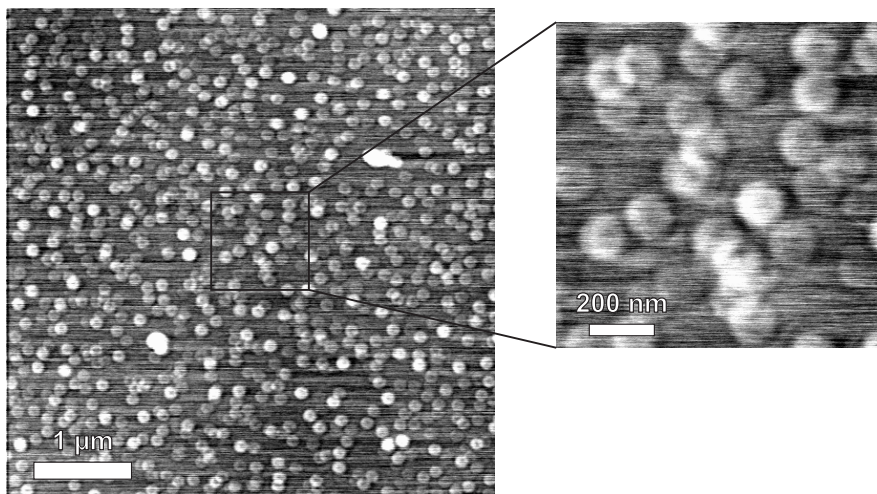


Figure 6.1: The triblock-copolymer vesicles are randomly distributed on mica. The low polydispersity is clearly recognisable. The diameter of the vesicles was found to be 136 nm. The centre of each vesicle shows a depression, that indicates that the vesicles collapsed upon drying.

vesicles on a surface can result in possible future applications, such as sensors for biotechnology. For this purpose it is of key importance to study the behaviour of these self-assembled structures upon adsorption (physisorption) onto different substrates. Further insight gained in these studies might prove effective in the future design of more advanced nanocontainers.

7. CONCLUSIONS AND OUTLOOK

Different “assembly motives”, facilitating self-assembly on surfaces have been investigated with STM.

It could be shown, that self-assembly is best achieved if the ratio of molecule-substrate to intermolecular interactions is fine tuned. Self-assembly is favoured when the molecules adsorb on the substrate by a weak physisorption, that is not very site-selective but fits in several geometries. The π - π interactions between aromatic parts of phthalocyanine or Fréchet-dendrons were shown as examples on HOPG. In order to achieve self-assembled structures, the molecules should adsorb but remain laterally mobile. It was shown, that weak but numerous intermolecular interactions are well suited to assist the assembly. Moreover, alkylation of molecules greatly assists the assembly. Overall shapes of the molecules, that can build a space-filling pattern in two dimensions were shown to be more stable assemblies than molecules, that can not form a space-filling pattern. These results contribute to the understanding of self-assembly processes per se.

Even strongly repulsive intermolecular interactions can be overcome with a strong chemisorption to a substrate. As an example of this, the assembly of chemisorbed oligopyridine complexes on platinum was shown. The surface coverage measured with STM was directly comparable to values calculated from electrochemical experiments. The complexes were shown to be assembled in a wide lattice, that allows a residual mobility, and thus prevent submolecular resolution. One chemical bond to the substrate was too weak to immobilise the molecules completely. Nevertheless, chemisorption is able to couple molecules electrically to a metal substrate, and will be employed in the construction of molecular photovoltaic devices. Physisorption was shown to be important for large molecules. A fullerene-ligand with a free terpyridine was studied on platinum. Thanks to its strong physisorption submolecular resolution is achieved at room temperature in air. This fullerene, that is also strongly bound through chemisorption, might be used as single electron shuttle or in optoelectronic applications.

A short study on the mobility of physisorbed molecules was presented. To gain further insight into the self-assembly processes, it will be interesting to study the molecular dynamics on surfaces in further detail. To manipulate assemblies at the single molecular level, experiments with large dendrimers at low temperatures were performed. A physisorbed dendrimer, embedded in a monolayer of chemisorbed alkanethiols, was pushed out of this layer, and back into it again. Up to date, this is probably the largest molecule, that was ever moved in a controlled manner by an STM tip. This proves, that it is possible to study mobility and interactions of even very large molecules by STM. The detailed study of the balance of intermolecular and molecule-substrate interactions will play a crucial role for successful assembly processes in applications.

Alkoxyated Fréchet-dendrons were used as substituents, that facilitate self-assembly of small molecules on graphite. These nonpolar amphiphiles were shown to have a high tendency to form ordered monolayers, of either disk-like, lamellar, or a related geometry. At room temperature in air, a conformational divergency was studied and characterised with STM. Sub-molecular resolution was achieved on these Fréchet-dendrons, and conformational analysis with STM was introduced. The studied dendrimers can adopt several conformations on a graphite surface, which were analysed with the STM. The conformation of a bipyridine dendrimer was successfully changed after the adsorption by protonation with gaseous HCl. Other variations of the alkoxyated Fréchet-dendrimers revealed, that lamellar assemblies are formed preferentially.

Also a complex, disk-like assembly, formed from aldehydes of the dendron was studied. The pattern was found to be pseudo-periodic with a unit cell of seven molecules, and showed a conformational irregularity. A delayed transformation of this disk-like assembly pattern into a lamellar organisation after about one hour was followed with STM. This transformation was accompanied by a change of conformation of the adsorbed molecules. By using alcohol instead of aldehyde derivatives, the disk-like assembly could be stabilised and the pseudo-periodic pattern remained unchanged over days. On a short term, these results inspire many more experiments: on one hand, it might be tried to trigger the transformation of the disk-like into the lamellar phase by either a controlled change of the environment, or a chemical reaction on the surface. It might be tried to form assemblies of the alcohol (or acid) derivative, that then are oxidised (reduced) to the aldehyde, to initiate the transformation. On the other hand, it might be interesting to stop the transformation by either embedding a different molecule, that

fits selectively inside the hexagons, or by other means. A higher goal will be to reverse the transition, by applying the suitable external parameters. Furthermore, it will prove challenging to find the driving force for this transformation. A higher generation of the alkoxyated Fréchet-dendrimers might form a disk-like shape by themselves.

Another very promising result is the chirality of the layers formed with the alkoxyated Fréchet-dendrimers. The irregular pattern with a unit cell of seven molecules showed orientational ordering. Both resulting chiralities could be observed. Also the lamellar phase, in which the pattern converted into, showed chirality. It remains to be tested, if the initiators that start the conversion might be further reduced in numbers or chosen to initiate only one chirality, so that only *one* orientation results on a macroscopic surface. It will also prove interesting to see, if the *R,R*-DDB dendrimer will form $\nabla\Delta$ - or $\Delta\nabla$ -like patterns, and what pattern enantiomeric mixtures of the dendrimer will form. All the information gained in these studies might find application in heterogeneous catalysis, either by covered catalyst particles, or by chiral modifiers.

Finally, a short characterisation by AFM of polymer vesicles on a mica surface was presented (chapter 6). Vesicles of a diameter of 136 nm could be imaged after they collapsed, due to removal of the solvent. It is interesting to compare the results here obtained with previous light scattering and TEM measurements. While measurements in liquid might provide a playground for manipulation experiments, the further study of the adsorption and immobilisation properties might prove useful for various applications. Immobilisation could be facilitated with the introduction of functionalities able to promote chemisorption. Nevertheless, prior to this, a study of the intrinsic adsorption characteristics of the vesicular aggregates is needed.

APPENDIX

A. SHORT LIST OF OTHER MEASURED MOLECULES

Parts of this chapter have been published in [130], and will be published in [65]. When measuring molecules in air, that were deposited from solution, it is very important to reproduce results with different tips and on different substrate pieces, to eliminate artifacts and contamination or substrate effects. A large amount of time has to be applied to verify the results and observed phenomena. Various different systems were studied in the scope of this thesis. Many of the molecules showed distinguishable patterns, that were reproducible and characteristic. But the interpretation of several systems did not rise above the level of speculations (however reasonable they may be). Theoretical investigations will be necessary for a complete interpretation of many of them. Some of the measured molecules are presented in table A.1.

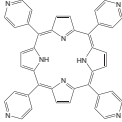
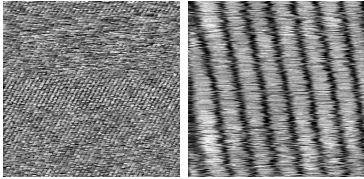
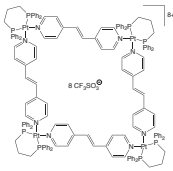
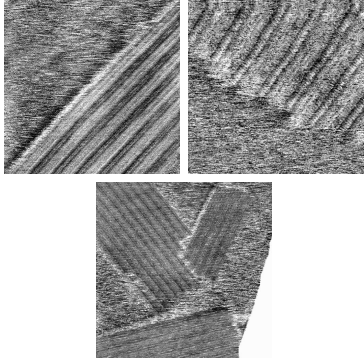
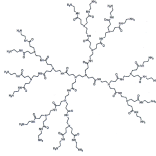
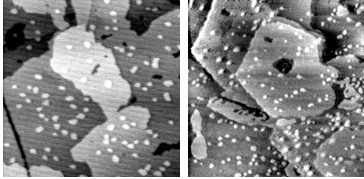
Formula	Comments	Measurements
	<p>Tetra-Pyridyl-Porphyrin could not be imaged, except after addition of a silver salt. Then, the striped pattern seen on the right was observed. Sizes: (left) 25 nm × 25 nm, (right) 5 nm × 5 nm.</p>	
	<p>Six different Fujita-squares were measured on HOPG. Most showed striped patterns. Some with very high resolution. A self-assembly process definitely took place, but the molecular arrangement could not be solved. Hopefully a theoretical study will solve the puzzle. Note, that these squares can be assembled in a flat orientation by use of a secondary template effect. Chloride ions adsorbed on a gold surface allow the assembly. Sizes: (left) 40 nm × 40 nm, (right) 50 nm × 50 nm, (bottom) 100 nm × 100 nm.</p>	
	<p>Different generations of commercial PAMAM dendrimers were measured on gold surfaces. Due to the strong chemisorption, PAMAM dendrimers of different generations could be imaged as single molecules, either embedded in monolayers of HDT or on pure gold surfaces. Sizes: (left) 80 × 80 nm, (right) 120 nm × 120 nm.</p>	

Table A.1: Further studied systems.

A.1 Artifacts and unresolved patterns

As mentioned above, measurements in ambient air have to be checked rigorously against artifacts and effects produced by contaminants. At the low concentrations that have to be used, even very slight contaminations of the solvent can be seen, if the contamination is not expelled by the assembly process. Effects like the solubility of glass in ultra-pure water become a factor of great importance. This section shows a small collection of striped patterns, that could be caused by Moiré-patterns such as discussed in [54]. It might be, that the patterns are caused by adsorbed molecules, but the assembly is not dominated by any characteristic of the studied molecules. The measurement becomes therefore useless to gain information about the molecule. Figure A.1 shows a small collection of stripes measured with different molecules. Note, that sometimes, the same molecules give a nice resolution of a pattern, that is characteristic and reproducible, but with other samples all that can be seen are stripes.

Sometimes, even stranger patterns, that resemble the hard borders of Moiré-patterns, described in [54] were seen. Figure A.2 shows a small collection of those. These measurements are included for completeness. Careful studies are necessary when measuring in ambient air. The amazing fact, that even impurities can be beautiful, is shown in figure A.3.

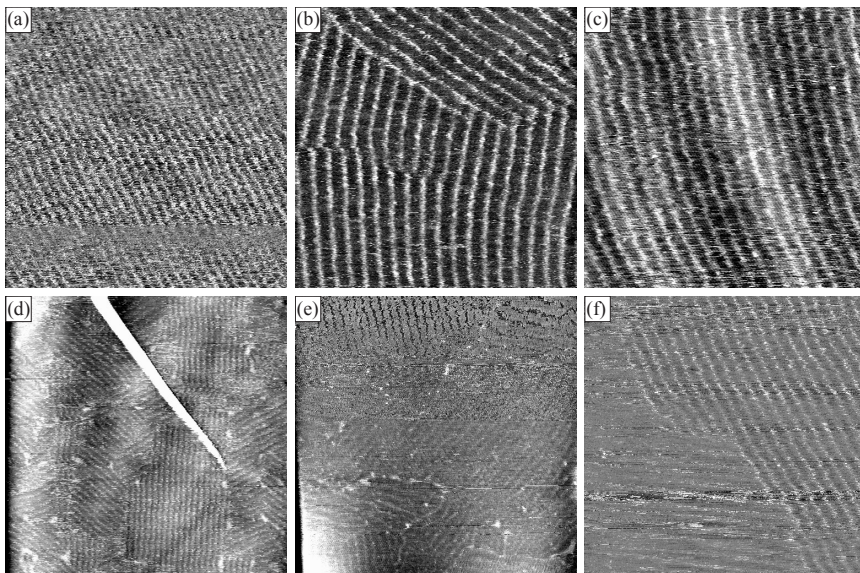


Figure A.1: Various striped patterns, that could not be shown to have any characteristic of the measured molecule. (a), (b), and (c) are different Fujita-squares on graphite, synthesised in the laboratory of C. Schalley in the group of F. Vögtle, (d) and (e) are knotanes on graphite, synthesised by the group of F. Vögtle, and (f) is a tetrapyrrolylporphyrin on graphite. Parameters: (a) $U_{bias} = -1770$ mV; $I_t = 1$ pA; size= 200 nm \times 200 nm; z -scale ≈ 0.2 nm; (b) $U_{bias} = -700$ mV; $I_t = 2$ pA; size= 70 nm \times 70 nm; z -scale ≈ 0.15 nm; (c) $U_{bias} = -850$ mV; $I_t = 1$ pA; size= 100 nm \times 100 nm; z -scale ≈ 0.2 nm; (d) $U_{bias} = -639$ mV; $I_t = 1$ pA; size= 250 nm \times 250 nm; z -scale ≈ 0.3 nm; (e) $U_{bias} = -700$ mV; $I_t = 1$ pA; size= 200 nm \times 200 nm; z -scale ≈ 0.2 nm; (f) $U_{bias} = -1700$ mV; $I_t = 0.7$ pA; size= 100 nm \times 100 nm; z -scale ≈ 0.16 nm.

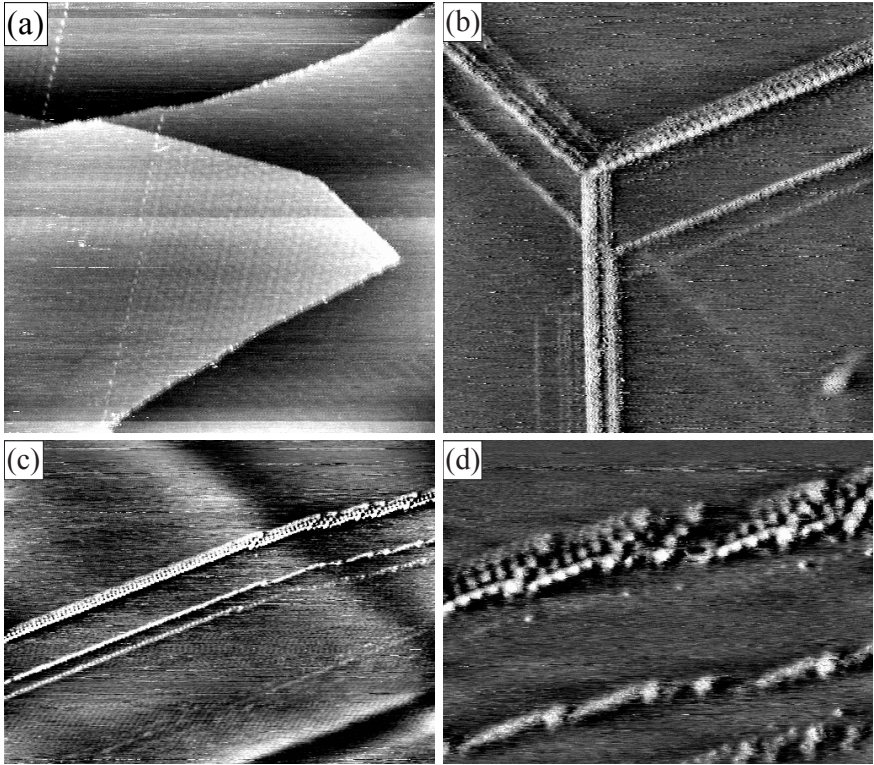


Figure A.2: (a) An image of a Moiré-pattern on graphite terraces that displays very bright last rows. (b), (c), and (d) Three images of a sample prepared with molecular knots. The pattern was also observed with other molecules and does not seem to depend on them. The multiplicity of the stripes could be attributed to a multiple STM tip. Parameters: (a) $U_{bias} = -700$ mV; $I_t = 1$ pA; size= 200 nm \times 200 nm; z-scale ≈ 0.2 nm; (b) $U_{bias} = -864$ mV; $I_t = 1.2$ pA; size= 100 nm \times 100 nm; z-scale ≈ 0.3 nm; (c) $U_{bias} = -770$ mV; $I_t = 20$ pA; size= 200 nm \times 200 nm; z-scale ≈ 0.3 nm cut to 200 nm \times 150 nm; (d) $U_{bias} = 770$ mV; $I_t = 20$ pA; size= 60 nm \times 60 nm; z-scale ≈ 0.3 nm cut to 60 nm \times 45 nm.

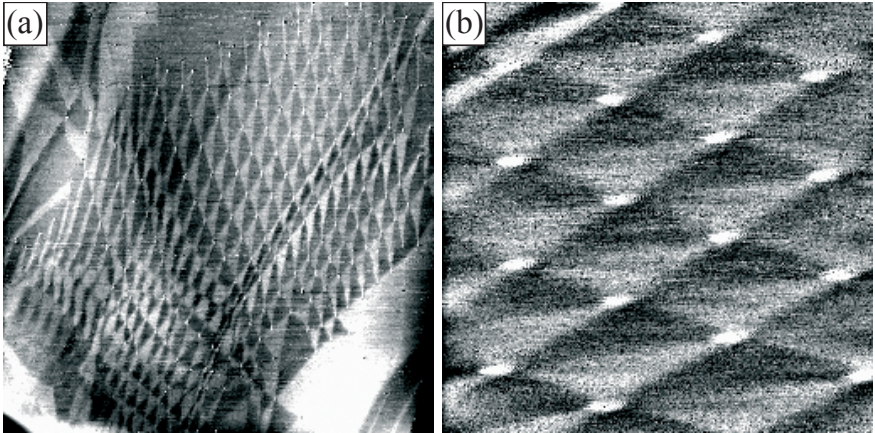


Figure A.3: Two images of “pure” graphite. The pattern could never be reproduced after this measurement. Parameters: (a) $U_{bias} = 610$ mV; $I_t = 360$ pA; size= 1000 nm \times 1000 nm; (b) $U_{bias} = 900$ mV; $I_t = 100$ pA; size= 170 nm \times 170 nm.

B. MEASUREMENTS BY COLLABORATORS

B.1 Oligopyridine complexes on platinum

The oligopyridine complexes, discussed in chapter 3, were synthesised by Y. Zimmermann and studied electrochemically by E. Figgemeier. Figure B.1 (a) shows the cyclic voltammogram, that was used to calculate the surface coverage of the mono-ruthenium complexes on platinum. The area under

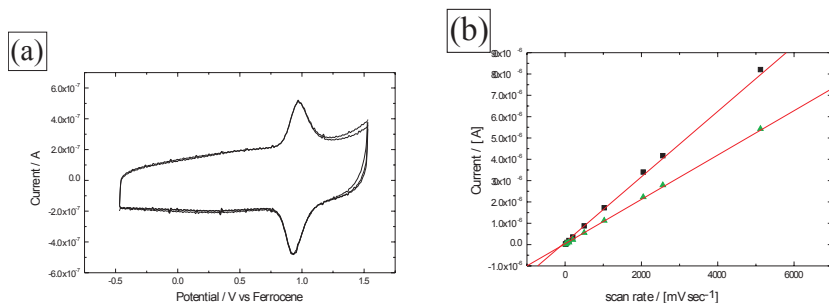


Figure B.1: (a) Cyclic voltammogram of a monolayer of $[\text{Ru}(\text{terpy})(\text{terpypy})]^{2+}$ on platinum. (b) The dependence of the peak current from the speed of the voltage change for a dimer. Measured by E. Figgemeier

the oxidation and reduction peaks is proportional to the charge used for the conversion. With a known area of the measured electrode, this knowledge allows the calculation of the surface coverage. Typical for the measurement of a monolayer, the peak has a nearly ideal form and the difference between the oxidation and the reduction peaks is minimal. (b) Shows the linear dependence of the peak current from the scan rate. This dependence is linear for surface bound molecules. For molecules in solution, the peak current would depend from the square root of the scan rate, see also [63].

C. LIST OF PUBLICATIONS

C.1 Papers

- L. Merz, J. Hitz, U. Hubler, P. Weyermann, F. Diederich, P. Murer, D. Seebach, I. Widmer, M. Stöhr, H.-J. Güntherodt, B. A. Hermann, STM investigation on single, physisorbed dendrimers. *Single Molecules* (2002), 3(5-6), 295-299.
- I. Widmer, U. Hubler, M. Stöhr, L. Merz, H.-J. Güntherodt, B. A. Hermann, P. Samori, J. P. Rabe, P. B. Rheiner, G. Greiveldinger, P. Murer, Hourglass-shaped dendrimers on surfaces: a comparison of different scanning-tunnelling-microscopy approaches. *Helvetica Chimica Acta* (2002), 85(12), 4255-4263.
- E. Figgemeier, L. Merz, B. A. Hermann, Y. C. Zimmermann, C. E. Housecroft, H.-J. Güntherodt, E. C. Constable, Self-Assembled Monolayers of Ruthenium and Osmium Bis-Terpyridine Complexes - Insights of the Structure and Interaction Energies by Combining Scanning Tunneling Microscopy and Electrochemistry. *Journal of Physical Chemistry B* (2003), 107(5), 1157-1162.
- Caroline Safarowsky, Leo Merz, Alexander Rang, Peter Broekmann, B. A. Hermann, Christoph A. Schalley, Second-Order Templatation: Ordered Deposition of Supramolecular Squares on Chloride-Covered Cu(100) Surfaces. *Angewandte Chemie, International English Edition* (2004), 43(10), 1291-1294. German version.
- E. C. Constable, B. A. Hermann, C. E. Housecroft, L. Merz, L. Scherer, Monitoring Conformational Diversity in Self-Organised Monolayers with Scanning Tunnelling Microscopy at Near Atomic Resolution. *Chemical Communications* 2004, 928-929.

- E. C. Constable, B. A. Hermann, C. E. Housecroft, L. Merz, L. Scherer, full paper about G1 and G2 of the bipy dendrimer, *manuscript in preparation*.
- L. Merz, I. Widmer, M. Stöhr, H.-J. Güntherodt, P. Murer, D. Seebach and B. A. Hermann, publication of section 5.2.2. *to be published*.
- L. Merz, L. J. Scherer, C. E. Housecroft, E. C. Constable, H.-J. Güntherodt, and B. A. Hermann, publication of section 5.2.3, *Manuscript in preparation*.
- I. Widmer, D. Ammann, L. Merz, H.-J. Güntherodt, and B. A. Hermann, Discussion of Static and Dynamic Behaviour of Self-Ordered Molecular Layers of a Model-System: Octyl-Substituted Zinc-Phthalocyanine Molecules on Graphite, *Manuscript for Acc. Chem. Res. in preparation*.

C.2 Posters

- B. A. Hermann, L. Merz, D. Ammann, U. Hubler, H.-J. Güntherodt, Y. C. Zimmermann, E. Figgemeier, C. Housecroft, E. C. Constable, P. Weyermann, F. Diederich, P. Murer, G. Greiveldinger, P. B. Rheiner, T. Sifferlen, D. Seebach: *Local Switching and Read-out of Supramolecular Functional Assemblies by Scanning Probe Methods*, Kick-off meeting of the NRP47, Bern 2000.
- L. Merz, U. Hubler, J. Hitz, B. A. Hermann, and H.-J. Güntherodt; P. Weyermann and F. Diederich; G. Greiveldinger, P. B. Rheiner, P. Murer, T. Sifferlen, and D. Seebach: *Macromolecules on the move: Imaging and manipulation of dendrimers by STM*, Edgar Lüscher Seminar, Serneus Feb 2001.
- L. Merz, D. Ammann, U. Hubler, B. A. Hermann, and H.-J. Güntherodt, Y. Zimmermann, E. Figgemeier, C. Housecroft and E. C. Constable: *A Comparative STM Study of Oligopyridine Ruthenium(II) Complexes*, Twannberg 2001 Workshop on Nanoscience, Twannberg October 16-19 2001.
- L. Merz, U. Hubler, J. Hitz, B. A. Hermann, and H.-J. Güntherodt; P. Weyermann and F. Diederich; G. Greiveldinger, P. B. Rheiner, P. Murer, T. Sifferlen, and D. Seebach: *STM Investigations of Macromolecules and Molecular Assemblies*, Spring School on Single Molecules

in Physics, Chemistry and Biology, of the VW-Stiftung Priority Program "Physik, Chemie und Biologie mit Einzelmolekülen", Hofgeismar 8.-12. April 2002.

- L. Merz, I. Widmer, M. Stöhr, H.-J. Güntherodt, and B. A. Hermann, T. Müller and C. A. Schalley, Self-Organisation of Molecular "Squares" Imaged with STM, Twannberg 2002 Workshop on Nanoscience, Twannberg September 30 - October 4 2002.
- I. Widmer, U. Hubler, M. Stöhr, L. Merz, H.-J. Güntherodt, P. Samori, J. Rabe, D. Seebach, and B. A. Hermann, A Comparison of Different STM Approaches on Hourglass-Shaped Dendrimers, Twannberg 2002 Workshop on Nanoscience, Twannberg September 30 - October 4 2002.
- I. Widmer, M. Stöhr, L. Merz, U. Hubler, H.-J. Güntherodt, P. Samori, J. Rabe, D. Seebach, and B. A. Hermann, Investigation of an Hourglass-Shaped Dendrimer with STM, Frühjahrstagung des Arbeitskreises Festkörperphysik der DPG, Dresden 24.-28. March 2003.
- L. Merz, I. Widmer, M. Stöhr, D. Ammann, U. Hubler, B. A. Hermann, L. Scherer, Y. C. Zimmermann, E. Figgemeier, C. E. Housecroft, E. C. Constable, G. Widmer, P. Nielaba, P. Weyermann, F. Diederich, P. Murer, D. Seebach, Local Switching and Read-out of Supramolecular Functional Assemblies by Scanning Probe Methods, Kick-off meeting of the second phase of the NRP47, Bern 2003, (Awarded 1st prize of the poster award).
- L. Merz, M. Stöhr, I. Widmer, H.-J. Güntherodt, B. A. Hermann, G. Widmer, P. Nielaba, P. Murer, D. Seebach, Arrangement of Hourglass-Shaped Dendrimers on HOPG, STM '03, Eindhoven July 21.-25. 2003.

REFERENCES

- [1] Seebach, D. *Angew. Chem., Int. Ed.* **1990**, *29*, 1320-1367 see also *Angew. Chem.*, *102*, 1363-1409.
- [2] Lehn, J.-M. *Acc. Chem. Res.* **1978**, *11*, 49-57.
- [3] Lehn, J.-M. *Pure Appl. Chem.* **1978**, *50*, 871-892.
- [4] Werner, A. *Zeitschr. f. anorg. Chem.* **1893**, *3*, 267-330.
- [5] Lehn, J.-M. *Supramolecular Chemistry: Concepts and Perspectives*; VCH: D-69451 Weinheim, 1 ed.; 1995.
- [6] Yildiz, A.; McKinney, J. N. F. S. A.; Ha, T.; Goldman, Y. E.; Selvin, P. R. *Science* **2003**, *300*, 2061-2065.
- [7] McNaught, A. D.; Wilkinson, A., Eds.; *IUPAC Compendium of Chemical Terminology*; IUPAC: , 2nd ed.; 1997.
- [8] Buhleier, E.; Wehner, W.; Vögtle, F. *Synthesis* **1978**, *2*, 155-158.
- [9] Tomalia, D. A.; Baker, H.; Dewald, J.; Hall, M.; Kallos, G.; Martin, S.; Roeck, J.; Ryder, J.; Smith, P. *Polym. J. (Tokyo)* **1985**, *17*, 117.
- [10] Hawker, C. J.; Fréchet, J. M. J. *Chem. Commun.* **1990**, 1010-1013.
- [11] Hawker, C. J.; Fréchet, J. M. J. *J. Am. Chem. Soc.* **1990**, *112*, 7638-7647.
- [12] Yeung, L. K.; Crooks, R. M. *Nano Lett.* **2001**, *1*, 14-17.
- [13] Oosterom, G. E.; Reek, J. N. H.; Kamer, P. C. J.; van Leeuwen, P. W. N. M. *Angew. Chem., Int. Ed.* **2001**, *40*, 1828-1849.
- [14] Astruc, D.; Chardac, F. *Chem. Rev.* **2001**, *101*, 2991-3032.

-
- [15] Weyermann, P.; Gisselbrecht, J.-P.; Boudon, C.; Diederich, F.; Gross, M. *Angew. Chem., Int. Ed.* **1999**, *38*, 3215-3219.
- [16] Stiriba, S.-E.; Frey, H.; Haag, R. *Angew. Chem., Int. Ed.* **2002**, *41*, 1329-1334.
- [17] Fischer, M.; Vögtle, F. *Angew. Chem., Int. Ed.* **1999**, *38*, 884-905.
- [18] Tully, D. C.; Wilder, K.; Fréchet, J. M. J.; Trimble, A. R.; Quate, C. F. *Adv. Mater.* **1999**, *11*, 314-318.
- [19] Balzani, V.; Ceroni, P.; Gestermann, S.; Kauffmann, C.; Gorka, M.; Vögtle, F. *Chem. Commun.* **2000**, 853-854.
- [20] Misteli, T. *J. Cell Bio.* **2001**, *155*, 181-185.
- [21] Whitesides, G. M.; Grzybowski, B. *Science* **2002**, *295*, 2418-2421.
- [22] Desiraju, G. R. *Nature* **2003**, *423*, 485.
- [23] Likharev, K. *The Industrial Physicist* **2003**, 20-23.
- [24] Service, R. F. *Science* **2003**, *302*, 556-559.
- [25] Meyer, E.; Hug, H. J.; Bennewitz, R. *Scanning Probe Microscopy – The Lab on a Tip*; Springer Verlag: , 2004.
- [26] Binnig, G.; Rohrer, H.; Gerber, C.; Weibel, E. *Phys. Rev. Lett.* **1982**, *49*, 57-61.
- [27] Binnig, G.; Rohrer, H. *Helv. Phys. Acta* **1982**, *55*, 726-735.
- [28] Binnig, G.; Rohrer, H.; Gerber, C.; Weibel, E. *Phys. Rev. Lett.* **1983**, *50*, 120-123.
- [29] Ringger, M.; Hidber, H. R.; Schlögl, R.; Oelhafen, P.; Güntherodt, H.-J. *Helv. Phys. Acta* **1984**, *57*, 741-742.
- [30] Ringger, M.; Hidber, H. R.; Schlögl, R.; Oelhafen, P.; Güntherodt, H.-J. *Appl. Phys. Lett.* **1985**, *46*, 832-834.
- [31] Leewenhoek, M. *Philosophical Transactions* **1674**, *9*, 23-25.
- [32] Leewenhoek, M. *Philosophical Transactions* **1675**, *10*, 380-385.
- [33] Pasteur, P. *Science* **1881**, *2*, 420-422.

-
- [34] Sautet, P.; Bocquet, M.-L. *Phys. Rev. B* **1996**, *53*, 4910-4925.
- [35] Sautet, P. *Surface Science* **1997**, *374*, 406-417.
- [36] Klink, C.; Olesen, L. *Phys. Rev. Lett.* **1993**, *71*, 4350-4353.
- [37] Crommie, M. F.; Lutz, C. P.; Eigler, D. M. *Science* **1993**, *262*, 218-220.
- [38] Fiete, G. A.; Hersch, J. S.; Heller, E. J.; Manoharan, H. C.; Lutz, C. P.; Eigler, D. M. *Phys. Rev. Lett.* **2001**, *86*, 2392-2395.
- [39] Stipe, B. C.; Rezaei, M. A.; Ho, W. *Science* **1998**, *280*, 1732-1735.
- [40] Qiu, X. H.; Nazin, G. V.; Ho, W. *Science* **2003**, *299*, 542-546.
- [41] Ho, W. *J. Chem. Phys.* **2002**, *117*, 11033-11061.
- [42] Bruckner-Lea, C.; Janata, J.; Conroy, J.; Pungor, A.; Caldwell, K. *Langmuir* **1993**, *9*, 3612-3617.
- [43] Conroy, J. F. T.; Caldwell, K.; Bruckner-Lea, C.; Janata, J. *Electrochim. Acta* **1995**, *40*, 2927-2934.
- [44] Binnig, G.; Quate, C. F.; Gerber, C. *Phys. Rev. Lett.* **1986**, *56*, 930-933.
- [45] Meyer, G.; Amer, N. M. *Appl. Phys. Lett.* **x1988**, *53*, 1045-1047.
- [46] Pohl, D. W.; Denk, W.; Lanz, M. *Appl. Phys. Lett.* **1984**, *44*, 651-653.
- [47] Lewis, A.; Isaacson, M.; Harootunian, A.; Muray, A. *Ultramicroscopy* **1984**, *13*, 227-231.
- [48] Hubler, U. *Untersuchungen an Dendrimeren, Kohlenstoff-Nanotubes und Hochtemperatur-Supraleitern mit Rastersondenmethoden*, Thesis, Philosophisch Naturwissenschaftliche Fakultät der Universität Basel, 1999.
- [49] Tománek, D.; Louie, S. G. *Phys. Rev. B* **1988**, *37*, 8327-8336.
- [50] Binnig, G.; Fuchs, H.; Gerber, C.; Rohrer, H.; Stoll, E.; Tosatti, E. *Europhys. Lett.* **1986**, *1*, 31-36.
- [51] Batra, I. P.; García, N.; Rohrer, H.; Salemink, H.; Stoll, E.; Ciraci, S. *Surface Science* **1987**, *181*, 126-138.

-
- [52] Lim, R.; Li, J.; Li, S. F. Y.; Feng, Z.; Valiyaveetil, S. *Langmuir* **2000**, *16*, 7023-7030.
- [53] Constable, E. C.; Housecroft, C. E.; Scherer, L. J.; Hermann, B. A.; Merz, L. *Chem. Commun.* **2004**, 928-929.
- [54] Dalidchik, F. I.; Grishin, M. V.; Kovalesvskii, S. A. *Phys. Low-Dim. Struct.* **2003**, *3/4*, 45-48.
- [55] Hegner, M.; Wagner, P. Procedures in Scanning Probe Microscopy. In ; John Wiley & Sons Ltd: , 1998; Chapter 2:2:4 Ultraflat Au Surfaces, pages 2:2:4 1-7.
- [56] Hegner, M.; Wagner, P.; Semenza, G. *Surface Science* **1993**, *291*, 39-46.
- [57] Güntherodt, H.-J.; Wiesendanger, R., Eds.; *Scanning Tunneling Microscopy I*; Springer Verlag: , 2 ed.; 1992/1994.
- [58] Tersoff, J.; Hamann, D. R. *Phys. Rev. Lett.* **1983**, *50*, 1998-2001.
- [59] Briggs, G. A. D.; Fisher, A. J. *Surf. Science Rep.* **1999**, *33*, 3-81.
- [60] Polytec, P. *Nano Positioning 1998 – PI catalogue*; PI: , 1998 Chapter 4: tutorial piezoelectrics in positioning.
- [61] Woodruff, D. P. *Curr. Opin. Solid State Mater. Sci.* **2003**, *7*, 75-81.
- [62] Qiu, X.; Wang, C.; Zeng, Q.; Xu, B.; Yin, S.; Wang, H.; Xu, S.; Bai, C. *J. Am. Chem. Soc.* **2000**, *122*, 5550-5556.
- [63] Figgemeier, E.; Merz, L.; Hermann, B. A.; Zimmermann, Y. C.; Housecroft, C. E.; Güntherodt, H.-J.; Constable, E. C. *J. Phys. Chem. B* **2003**, *107*, 1157-1162.
- [64] Zimmermann, Y. C. *Polynuclear complexes of new heterodi- and tri-topic ligands*, Thesis, Uni Basel, 2002.
- [65] Hermann, B. A. Habilitation, 2004.
- [66] Ammann, D. “Selbstorganisation von Makromolekülen auf einer Oberfläche – Untersuchungen mit dem STM”, Semesterarbeit, Uni Basel, 2003.
- [67] Schreiber, F. *Prog. Surf. Sci.* **2000**, *65*, 151-256.

-
- [68] Wetterer, S. M.; Lavrich, D. J.; Cummings, T.; Bernasek, S. L.; Scoles, G. *J. Phys. Chem. B* **1998**, *102*, 9266-9275.
- [69] Poirier, G. E.; Pylant, E. D. *Science* **1996**, *272*, 1145-1148.
- [70] Everhart, D. S. Handbook of applied and colloid chemistry. In , Vol. 2, 1 ed.; John Wiley & Sons Ltd: John Wiley & Sons Ltd, Baffins Lane, Chichester, West Sussex PO19UD, England, 2001; Chapter 6, pages 99-116.
- [71] Grätzel, M. *Prog. Photovolt. Res. Appl.* **2000**, *8*, 171-185.
- [72] Baxter, P. N. W. Comprehensive Supramolecular Chemistry. In , Vol. 9; Pergamon: , 1995; Chapter 5 Metal Ion Directed Assembly of Complex Molecular Architectures and Nanostructures, pages 165-211.
- [73] Holliday, B. J.; Mirkin, C. A. *Angew. Chem., Int. Ed.* **2001**, *40*, 2022-2043.
- [74] Constable, E. C. *Chem. Commun.* **1997**, 1073-1080.
- [75] Juris, A.; Balzani, V.; Barigelletti, F.; Campagna, S.; Belser, P.; Von Zelewski, A. *Coord. Chem. Rev.* **1988**, *84*, 85-277.
- [76] Sauvage, J.-P.; Collin, J.-P.; Chambron, J.-C.; Guillerez, S.; Coudret, C.; Balzani, V.; Barigelletti, F.; De Cola, L.; Flamigni, L. *Chem. Rev.* **1994**, *94*, 993-1019.
- [77] Hagfeldt, A.; Grätzel, M. *Acc. Chem. Res.* **2000**, *33*, 269-277.
- [78] Anderson, S.; Constable, E. C.; Dare-Edwards, M. P.; Goode-nough, J. B.; Hamnett, A.; Seddon, K. R.; Wright, R. D. *Nature* **1979**, *280*, 571-573.
- [79] Grassian, V. H.; Muettterties, E. L. *J. Phys. Chem.* **1986**, *90*, 5900-5907.
- [80] Haq, S.; King, D. A. *J. Phys. Chem.* **1996**, *100*, 16957-16965.
- [81] Lees, A. C.; Kleverlaan, C. J.; Bignozzi, C. A.; Vos, J. G. *Inorg. Chem.* **2001**, *40*, 5343-5349.
- [82] Figgemeier, E. private communication,.

- [83] Hudson, J. E.; Abruña, H. D. *J. Phys. Chem.* **1996**, *100*, 1036-1042.
- [84] Wilson, R. J.; Meijer, G.; Bethume, D. S.; Johnson, R. D.; Chambliss, D. D.; de Vries, M. S.; Hunziker, H. E.; Wendt, H. R. *Nature* **1990**, *348*, 621-622.
- [85] Chen, T.; Howells, S.; Gallagher, M.; Yi, L.; Sarid, D.; Lichtenberger, D. L.; Nebesny, K. W.; Ray, C. D. *J. Vac. Sci. Technol. B* **1991**, *9*, 2461-2465.
- [86] Behler, S.; Pan, S. H.; Thommen-Geiser, V.; Lang, H. P.; Güntherodt, H.-J. *Z. Phys. B* **1993**, *91*, 1-2.
- [87] Sakurai, T.; Wang, X.-D.; Xue, Q. K.; Hasegawa, Y.; Hashizume, T.; Shinohara, H. *Prog. Surf. Sci.* **1996**, *51*, 263-408.
- [88] Rosei, F.; Schunack, M.; Naitoh, Y.; Jiang, P.; Gourdon, A.; Laegsgaard, E.; Stensgaard, I.; Joachim, C.; Besenbacher, F. *Prog. Surf. Sci.* **2003**, *71*, 95-146.
- [89] de Wild, M.; Berner, S.; Suzuki, H.; Yanagi, H.; Schlettwein, D.; Ivan, S.; Baratoff, A.; Güntherodt, H.-J.; Jung, T. A. *ChemPhysChem* **2002**, *3*, 881-885.
- [90] Mena-Osteritz, E.; Bäuerle, P. **2003**, was presented at the STM 03 in Eindhoven, Tu-Pos-08.
- [91] Armspach, D.; Constable, E. C.; Diederich, F.; Housecroft, C. E.; Nierengarten, J.-F. *Chem. Commun.* **1996**, 2009.
- [92] Armspach, D.; Constable, E. C.; Diederich, F.; Housecroft, C. E.; Nierengarten, J.-F. *Chem. -Eur. J.* **1998**, *4*, 723-733.
- [93] Merz, L.; Hitz, J.; Hubler, U.; Weyermann, P.; Diederich, F.; Murer, P.; Seebach, D.; Widmer, I.; Stöhr, M.; Güntherodt, H.-J.; Hermann, B. A. *Single Mol.* **2002**, *3*, 295-299.
- [94] Widmer, I. "Messungen von Alkoxy-substituiertem Zinkphthalocyanin und einem hantelförmigen Dendrimer mit dem Rastertunnelmikroskop", Diplomarbeit, Uni Basel, 2002.
- [95] Widmer, I.; Ammann, D.; Merz, L.; Güntherodt, H.-J.; Hermann, B. manuscript for Acc. Chem. Res. in preparation.

-
- [96] Weyermann, P. *Dendritische Porphyrine mit kovalent angebondenen axialen Liganden als neue Modellverbindungen für Haem-Proteine*, Thesis, ETH Zürich, 2000 ETH-Diss. Nr. 13885.
- [97] Xu, B.; Yin, S.; Wang, C.; Qiu, X.; Zeng, Q.; Bai, C. *J. Phys. Chem. B* **2000**, *104*, 10502-10505.
- [98] Liu, Y.; Lei, S.; Yin, S.; Xu, S.; Zheng, Q.; Wang, C.; Wan, L.; Bai, C. *J. Phys. Chem. B* **2002**, *106*, 12569.
- [99] Lei, S. B.; Wang, C.; Yin, S. X.; Wang, H. N.; Xi, F.; Liu, H. W.; Xu, B.; Wan, L. J.; Bai, C. L. *J. Phys. Chem. B* **2001**, *105*, 10838-10841.
- [100] De Feyter, S.; De Schryver, F. C. *Chem. Soc. Rev.* **2003**, *32*, 139-150.
- [101] Rabe, J. P.; Buchholz, S. *Science* **1991**, *253*, 424-427.
- [102] Berner, S.; de Wild, M.; Ramoino, L.; Ivan, S.; Baratoff, A.; Güntherodt, H.-J.; Suzuki, H.; Schlettwein, D.; Jung, T. A. *Phys. Rev. B* **2003**, *68*, 115410-115420.
- [103] Eigler, D. M.; Schweizer, E. K. *Nature* **1990**, *344*, 524-526.
- [104] Meyer, G.; Neu, B.; Rieder, K.-H. *Appl. Phys. A: Mater. Sci. Proc.* **1995**, *60*, 343-345.
- [105] Gimzewski, J. K.; Jung, T. A.; Cuberes, M. T.; Schlittler, R. R. *Surface Science* **1997**, *386*, 101-114.
- [106] Jung, T. A.; Schlittler, R. R.; Gimzewski, J. K.; Tang, H.; Joachim, C. *Science* **1996**, *271*, 181-184.
- [107] Hla, S.-W.; Bartels, L.; Meyer, G.; Rieder, K.-H. *Phys. Rev. Lett.* **2000**, *85*, 2777-2780.
- [108] Heinrich, A. J.; Lutz, C. P.; Gupta, J. A.; Eigler, D. M. *Science* **2002**, *298*, 1381-1387.
- [109] Tokuhisa, H.; Zhao, M.; Baker, L. A.; Phan, V. T.; Dermody, D. L.; Garcia, M. E.; Peez, R. F.; Crooks, R. M.; Mayer, T. M. *J. Am. Chem. Soc.* **1998**, *120*, 4492-4501.
- [110] Nevernov, I.; Kurnikov, I.; Nicolini, C. *Ultramicroscopy* **1995**, *58*, 269-274.

- [111] Yin, S.; Wang, C.; Qiu, X.; Xu, B.; Bai, C. *Surf. Interface Anal.* **2001**, *32*, 248-252.
- [112] Blakemore, C.; Kroto, H.; Gimzewski, J.; Dobson, P.; McGlade, J. "The Next Big Thing: Nanotechnology", The Vega Science Trust Programs, vega.org.uk.
- [113] De Feyter, S.; Gesquière, A.; Grim, P. C. M.; De Schryver, F. C. *Langmuir* **1999**, *15*, 2817-2822.
- [114] Yablon, D. G.; Giancarlo, L. C.; Flynn, G. W. *J. Phys. Chem. B* **2000**, *104*, 7627-7635.
- [115] Berner, S.; Brunner, M.; Ramoino, L.; Suzuki, H.; Güntherodt, H.-J.; Jung, T. A. *Chem. Phys. Lett.* **2001**, *348*, 175-181.
- [116] De Feyter, S.; Grim, P. C. M.; Rücker, M.; Vanoppen, P.; Meiners, C.; Sieffert, M.; Valiyaveetil, S.; Müllen, K.; De Schryver, F. C. *Angew. Chem., Int. Ed.* **1998**, *37*, 1223-1226.
- [117] Widmer, I.; Hubler, U.; Stöhr, M.; Merz, L.; Güntherodt, H.-J.; Hermann, B. A.; Samorí, P.; Rabe, J. P.; Rheiner, P. B.; Greiveldinger, G.; Murer, P. *Helv. Chim. Acta* **2002**, *85*, 4255-4263.
- [118] Merz, L.; Weyermann, P.; Diederich, F.; Güntherodt, H.-J.; Hermann, B. A. to be published.
- [119] Scherer, L. *Titel to be announced*, Thesis, Uni Basel, 2005.
- [120] Murer, P. K. *Synthese und Eigenschaften von Dendrimeren mit zwei- und dreifach verzweigten chiralen Bausteinen ausgehend von (R)-3-Hydroxybuttersäure*, Thesis, ETH Zürich, thesis nr. 12001, 1996.
- [121] Constable, E. C. *Adv. Inorg. Chem. Radiochem.* **1986**, *30*, 69-121.
- [122] Constable, E. C. *Metals and Ligand Reactivity – An Introduction to the Organic Chemistry of Metal Complexes*; VCH: Weinheim, 1995.
- [123] Murer, P.; Seebach, D. *Angew. Chem., Int. Ed.* **1995**, *34*, 2116-2119.
- [124] Murer, P. K.; Lapierre, J. M.; Greiveldinger, G.; Seebach, D. *Helv. Chim. Acta* **1997**, *80*, 1648-1681.
- [125] Wu, P.; Fan, Q.; Deng, G.; Zeng, Q.; Wang, C.; Bai, C. *Langmuir* **2002**, *18*, 4342-4344.

-
- [126] Rheiner, P. B.; Seebach, D. *Chem. –Eur. J.* **1999**, *5*, 3221-3236.
- [127] Gao, C.; Leporatti, S.; Moya, S.; Donath, E.; Möhwald, H. *Chem. –Eur. J.* **2003**, *9*, 915-920.
- [128] Maaloum, M.; Muller, P.; Krafft, M. P. *Angew. Chem., Int. Ed.* **2002**, *41*, 4331-4334.
- [129] Benito, S. M.; Sauer, M.; Meier, W. Encyclopedia of Nanoscience and Nanotechnology. In , Vol. X; American Scientific Publishers: , 2004; Chapter Nanocontainers, pages 1–19 Many thanks to the authors for providing a print of their chapter prior to publication.
- [130] Safarowsky, C.; Merz, L.; Rang, A.; Broekmann, P.; Hermann, B. A.; Schalley, C. A. *Angew. Chem., Int. Ed.* **2004**, *43*, 1291-1294.

ACKNOWLEDGEMENTS:

This thesis would not have been possible without the cooperation and support of many collaborators and friends. I'd like to express my gratitude to all of them.

I thank my parents, who financed and supported my whole education for many years. I would like to express my gratitude to my "Doktorvater" Prof. Dr. H.-J. Güntherodt, who gave me the great chance, to do research as a chemist in the Institute for Physics. I thank Prof. Dr. B. Hermann and Prof. Dr. E. Constable for being co-referees and Prof. Dr. E. Meyer for being chairman of the dissertation committee.

Prof. Dr. Bianca Hermann and Dr. Urs Hubler introduced me to the world of STM. I thank them for all the good time we enjoyed together, which included not only research, but also making the institute movie in 2001. Of the collaborators who synthesised molecules, that I was allowed to measure, Lukas Scherer deserves special thanks. – Not only proved his molecules "perfect" for measurement with the STM, but he also corrected large parts of this thesis (over the Christmas holidays!), and the collaboration with him is a great pleasure. Further thanks for fruitful discussions as well as provision of interesting molecules (many different dendrimers, complexes, ligands, fullerenes, molecular knots, squares, vesicles, &c.) are expressed to (in no particular order) Dr. Philipp Weyermann, Dr. Yves Zimmermann, Dr. Peter Murer, Dr. Derk Joester, Julie Grumelard, Dr. Egbert Figgemeier, Prof. Dr. François Diederich, Prof. Dr. Dieter Seebach, Prof. Dr. Ed Constable, Prof. Dr. Catherine Housecroft, Prof. Dr. Wolfgang Meier, Dr. Christoph Schalley, Prof. Dr. Fritz Vögtle.

I thank Samantha Benito for all the support and the critical corrections of my script. Prof. Dr. Ed Constable and Prof. Dr. Bianca Hermann are acknowledged for the corrections of the manuscript.

This research would never have been possible without the scientific staff at the institute for physics in Basel: Jean-Pierre Ramseyer (if you ever look for anything that has existed in the institute in the last 30 years, he will know

where it might be today!), Andi Tonin, Roberto Maffiolini, H. R. Hidber, Heinz Breitenstein, Sylvester Jakob, Werner Roth, and all the others.

I acknowledge everybody of the “Gü-group”, that helped to provide a good atmosphere for research. Especially, Remo Hofer, with his immediate SXM-support; Luca Ramoino for the good discussions, Dr. Regina Hoffmann for the averaging procedure and the discussions, Isa Widmer, “Mr. R. West”, Dr. Meike Stöhr, Damaris Ammann, and Roland Stöckli for the good times in the lab. I thank all of the “Bio-group”, especially Dr. Karin Gfeller, for the moral support and the good catering.

Many thanks belong also to Verónica Cerletti, Senta Karotke, and Christian Schroll, who share a slight addiction to Tichu. I thank Matthias Nold and David Saladin for the good times during the years of study.